

CRTD – Center for Regenerative Therapies Dresden
Technische Universität Dresden
Direktor: Prof. Dr. Federico Calegari

**Incorporation, polarization and maturation
of human photoreceptor transplants
in the mouse retina**

Dissertationsschrift
zur Erlangung des akademischen Grades
Doctor of Philosophy (Ph.D.)

vorgelegt
der Medizinischen Fakultät Carl Gustav Carus
der Technischen Universität Dresden

von

MSc Karen Anja Teßmer
geboren am 06.03.1992 in Bad Nauheim

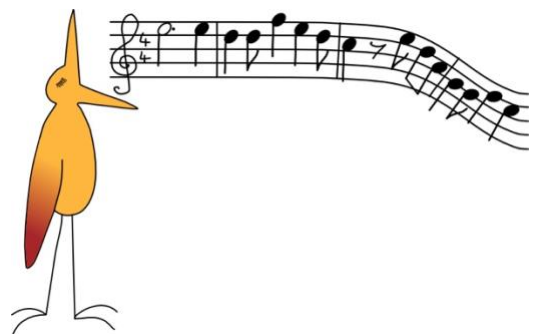
Dresden 2022

1. Gutachter:

2. Gutachter:

Tag der mündlichen Prüfung:

gez.: _____
Vorsitzender der Promotionskommission



Acknowledgements

First and foremost I would like to express my gratitude to Marius Ader for giving me the opportunity to carry out my thesis work in the Ader lab, for creative ideas and an open-minded, communicative environment. Thank you for pushing my optimism and for providing me with every opportunity and more to research, think and grow. Similarly, my deepest thanks belong to Sylvia Gasparini, for taking me on board, teaching me and investing so much time and energy to help me and everyone else succeed. We made a great team and your ease will never cease to astonish me.

No work would be possible without the people behind the scenes and this is true above all for Jochen. Simply a wholehearted thanks for everything – I'm glad to not only call you my colleague but my friend. Thank you also to Klara, Oli, Suse, Nundi and all other members of the Ader lab, past and present, who have filled this journey with a lovely atmosphere, lots of lunch break entertainment and who have helped me many ways and countless times. My gratitude also goes to my students Sneha, Sydney, Nivedha and Trishla for trusting me and helping me advance.

A project like this requires a lot of help from many collaborators, above all the fantastic core facilities at CMCB. My special gratitude goes to Thomas Kurth (EM), whose efforts, enthusiasm for and knowledge of the retina has helped me tremendously. Also, my deepest thanks go to Fabian Rost, for hours and hours of sequencing analysis help, as well as Andreas, Katrin and the entire DcGC team. I would further like to particularly highlight Anne and Katja (Flow), Kathrin, Susanne, Susi and the animal caretakers (VTH), Katrin and Claudia (Stem Cells), and Ellen and Ali (LMF). Thank you also to Madalena and Susanne for all your help with organoid culture, as well as the entire Karl lab for providing us with the possibility to give our organoids a home. Many thanks also go to Miriam Reh and Günther Zeck from Tübingen for the MEA analysis and the fruitful collaboration.

I would further like to thank my TAC members, Mike Karl, Frank Buchholz and Jochen Guck for their valuable feedback.

Last but not least, thank you to the most important people in my life. Pavel, thank you for your constant support and endurance. My friends, near and far, especially Sophie, Carey-Ann, Jana, Constanze and Odila. You have shaped me in more ways than you know and I am forever grateful to have you in my life. Above all, my family – Mama, Papa, Menno, Henni und Frauke – I can't thank you enough for giving me roots and wings and songs and everything in between.

Abstract

Photoreceptors are highly specialized neurons within the eye and the key retinal cells sensing light. They are indispensable for our visual perception and loss of photoreceptors consequently leads to loss of vision, a sense that alone is responsible for more than 30% of the input to our brain. Vision impairment and blindness is a leading cause of disability in the industrialized world and is in many cases ultimately due to a degeneration of the photoreceptors, which cannot be halted or reversed.

Retinal degenerative diseases encompass a heterogeneous group of etiologies, mainly caused by various mutations in a plethora of proteins involved in the visual process. Currently, several therapeutic options are being explored, with so far one gene therapy for a rare inherited blinding condition being clinically approved. However, the gene therapy approach requires not only the presence of remaining photoreceptors but the tailoring of the therapy to each individual mutation.

An alternative, more generally applicable approach is to restore vision through photoreceptor replacement therapy. As such, research on mouse-to-mouse photoreceptor transplantations has been carried out for many years, though with mixed results. In the last decade, it has however also become possible to generate large quantities of human photoreceptors through retinal organoid technology, allowing to instead transplant human cells. While promising, this field is still in development and principal conditions for successful photoreceptor transplantation have yet to be defined.

Here, human-to-mouse photoreceptor transplantations were performed and assessed with the aim to receive insights into retinal cell replacement technology with specific focus on photoreceptor maturation, polarization and functional integration. Using a cone-degeneration host line, large-scale incorporation of human photoreceptor grafts into the murine retina was shown for the first time. It was found that for human photoreceptors, the choice of developmental stage strongly affects incorporation and maturation capacity. Furthermore, the results demonstrate the necessity of adequate graft-host interaction for successful transplant maturation and function, suggesting that photoreceptor replacement strategies might benefit from transplantation in earlier rather than late stages of retinal degeneration.

Taken together, this thesis lays important groundwork for the further development of human photoreceptor replacement strategies to treat retinal degenerative disease.

Zusammenfassung

Photorezeptoren sind hochspezialisierte Nervenzellen im Auge und entscheidende Zellen für die Wahrnehmung von Licht. Sie sind für unsere visuelle Wahrnehmung unverzichtbar, und der Verlust von Photorezeptoren führt folglich zum Verlust des Sehvermögens, eines Sinnes, der allein für mehr als 30% des Informationsflusses in unser Gehirn verantwortlich ist. Sehstörungen und Blindheit gehören zu den häufigsten Ursachen für Behinderungen in Industrieländern und sind in vielen Fällen letztlich auf eine Degeneration der Photorezeptoren zurückzuführen, welche nicht aufgehalten oder rückgängig gemacht werden kann.

Die degenerativen Erkrankungen der Netzhaut sind bedingt durch eine heterogene Gruppe von Ursachen, und werden hauptsächlich durch verschiedene Mutationen in einer Vielzahl von Proteinen verursacht, die am Sehprozess beteiligt sind. Derzeit werden mehrere therapeutische Optionen erforscht, wobei bisher nur eine Gentherapie für eine seltene erbliche Erblindungskrankheit klinisch zugelassen wurde. Der gentherapeutische Ansatz erfordert jedoch nicht nur die Präsenz verbleibender Photorezeptoren, sondern auch die Anpassung der Therapie an jede einzelne Mutation.

Ein alternativer, allgemeiner anwendbarer Ansatz besteht darin, das Sehvermögen durch eine Photorezeptor-Ersatztherapie wiederherzustellen. In diesem Zusammenhang wird seit vielen Jahren an der Transplantation von Photorezeptoren von Maus zu Maus geforscht, allerdings mit gemischten Ergebnissen. Im letzten Jahrzehnt ist es jedoch auch möglich geworden, große Mengen menschlicher Photorezeptoren mit Hilfe der Netzhaut-Organoid-Technologie zu erzeugen, sodass vermehrt menschliche Zellen transplantiert werden können. Dieser Forschungszweig ist vielversprechend, befindet sich aber noch in der Entwicklung, und die wichtigsten Bedingungen für erfolgreiche Transplantation von humanen Photorezeptoren müssen noch definiert werden.

In dieser Arbeit wurden Photorezeptortransplantationen von Mensch zu Maus durchgeführt und bewertet, um Einblicke in die Technologie zum Ersatz von Netzhautzellen zu erhalten. Der Schwerpunkt lag dabei auf der Reifung, Polarisierung und funktionellen Integration der Zellen. Unter Verwendung einer Wirtslinie mit Zapfendegeneration wurde zum ersten Mal demonstriert, dass menschliche Photorezeptortransplantate in großem Umfang in die murine Netzhaut eingebaut werden können. Es konnte gezeigt werden, dass die Wahl des Entwicklungsalters menschlicher Photorezeptoren die Inkorporations- und Reifungskapazität stark beeinflusst. Darüber hinaus verdeutlichen die Ergebnisse die Notwendigkeit einer adäquaten Transplantat-Wirt-Interaktion für eine erfolgreiche Reifung und Funktion des

Transplantats. Dies deutet darauf hin, dass Photorezeptor-Ersatzstrategien von einer Transplantation in früheren Stadien der Netzhautdegeneration profitieren könnten.

Zusammengefasst legt diese Arbeit wichtige Grundlagen für die weitere Entwicklung menschlicher Photorezeptor-Ersatzstrategien zur möglichen Behandlung degenerativer Netzhauterkrankungen.

Publications

Published:

Gasparini*, S. J., **Tessmer***, K., Reh, M., Wieneke, S., Carido, M., Völkner, M., Borsch, O., Swiersy, A., Zuzic, M., Goureau, O., Kurth, T., Buskamp, V., Zeck, G., Karl, M. O., & Ader, M. (2022). Transplanted human cones incorporate into the retina and function in a murine cone degeneration model. *The Journal of Clinical Investigation*, 132(12). <https://doi.org/10.1172/JCI154619>

Herbig*, M., **Tessmer***, K., Nötzel, M., Nawaz, A. A., Santos-Ferreira, T., Borsch, O., Gasparini, S. J., Guck, J., & Ader, M. (2022). Label-free imaging flow cytometry for analysis and sorting of enzymatically dissociated tissues. *Scientific Reports*, 12(1), 1–17. <https://doi.org/10.1038/s41598-022-05007-2>

Accepted:

Tessmer*, K., Borsch*, O., Ader, M., & Gasparini, S. J. (accepted). Micromanipulator-Assisted Subretinal Transplantation of Human Photoreceptor Reporter Cell Suspensions into Mice. In *Brain Organoid Research* (Vol. 189). SPRINGER NATURE.

In Preparation:

Schmidtke, K., Gasparini, S. J., **Tessmer**, K., Adhikari, T., Michalke, L., Carido, M., Luft, S., Ader, M. Developmental stage of hiPSC-derived RPE affects monolayer formation post transplantation.

* these authors contributed equally

Table of Contents

ACKNOWLEDGEMENTS.....	I
ABSTRACT.....	III
ZUSAMMENFASSUNG	V
PUBLICATIONS	VII
TABLE OF CONTENTS	IX
LIST OF FIGURES.....	XIII
LIST OF TABLES.....	XIV
GENERAL ABBREVIATIONS.....	XV
GENE AND PROTEIN ABBREVIATIONS.....	XVII
1 INTRODUCTION	1
1.1 THE RETINA AND LIGHT PERCEPTION.....	1
1.1.1 <i>General structure of the eye.....</i>	1
1.1.2 <i>General structure of the retina</i>	1
1.1.3 <i>General photoreceptor structure</i>	3
1.1.4 <i>Phototransduction.....</i>	4
1.1.5 <i>Signal transmission to the brain.....</i>	6
1.1.6 <i>Major differences between rods and cones</i>	7
1.1.7 <i>The role of Müller glia in photoreceptor support and light perception</i>	9
1.2 RETINAL DEGENERATION DISEASES AND TREATMENT OPTIONS	11
1.2.1 <i>Retinal degeneration diseases</i>	11
1.2.2 <i>Therapeutic approaches to treat retinal degeneration diseases.....</i>	12
1.3 CELL REPLACEMENT AS TREATMENT APPROACH FOR RETINOPATHIES	14
1.3.1 <i>Transplantations of rodent retinal tissue and cells.....</i>	14
1.3.2 <i>Transplantations of human retinal tissue and cells</i>	17
1.4 AIM OF THIS THESIS	22
2 CHARACTERIZATION OF CRX-MCHERRY HUMAN RETINAL ORGANIDS AS PHOTORECEPTOR CELL SOURCE	23
2.1 AIMS	23
2.2 CHARACTERIZATION OF CRX-MCHERRY REPORTER-EXPRESSING CELLS	23
2.2.1 <i>Crx-mCherry expression overlaps with endogenous CRX expression and increases over time</i>	23
2.2.2 <i>Crx-mCherry organoids contain an outer and an inner nuclear layer.....</i>	24
2.2.3 <i>Crx-mCherry⁺ cells express early and mature rod and cone markers</i>	25
2.2.4 <i>Crx-mCherry⁺ cells do not express proliferation markers.....</i>	27
2.3 ENRICHMENT AND CHARACTERIZATION OF CRX-MCHERRY ⁺ DONOR CELLS	28
2.3.1 <i>Enrichment of Crx-mCherry⁺ cells by FACS.....</i>	28
2.3.2 <i>Characterization of Crx-mCherry enriched cells by single cell sequencing</i>	29
2.3.3 <i>Characterization of D200 Crx-mCherry-enriched cells by immunocytochemistry ...</i>	30
2.4 SUMMARY.....	31

3	TRANSPLANTATION OF HUMAN CRX-MCHERRY⁺ GRAFTS AGED D100, D200 AND D300 INTO CPFL1 MICE.....	33
3.1	AIMS	33
3.2	CRX-MCHERRY ⁺ CELLS OF ALL AGES CAN BE TRANSPLANTED AND SURVIVE IN THE MURINE RETINA	33
3.2.1	<i>Human grafts can be identified by RCVRN staining</i>	34
3.2.2	<i>D100 Crx-mCherry⁺ transplants are larger than D200 and D300 grafts</i>	34
3.2.3	<i>Graft volume increase over time is not due to in vivo proliferation.....</i>	36
3.3	GRAFT MORPHOLOGY DIFFERS WITH DONOR AGES	37
3.3.1	<i>Human grafts can adopt an intraretinal position.....</i>	37
3.3.2	<i>Graft positioning changes over time</i>	37
3.3.3	<i>Qualitative differences in graft morphology between donor ages</i>	38
3.4	GRAFT MATURATION.....	41
3.4.1	<i>D200 but not D100 or D300 grafts develop large quantities of inner segments</i>	41
3.4.2	<i>Inner segment development is associated with close proximity to the host retina</i>	42
3.5	HUMAN IDENTITY OF INTRARETINAL GRAFTS.....	43
3.5.1	<i>Intraretinal Crx-mCherry⁺ grafts are largely a result of true morphological incorporation</i>	43
3.5.2	<i>Rare indications of potential human-to-mouse material transfer</i>	45
3.6	SUMMARY	47
4	IN DEPTH CHARACTERIZATION OF TRANSPLANTED D200 CRX-MCHERRY⁺ CELLS	49
4.1	AIMS	49
4.2	EARLY POST TRANSPLANTATION DYNAMICS IN GRAFT POSITIONING AND GRAFT-HOST INTERACTIONS	49
4.2.1	<i>Intraretinal and proximal D200 grafts interact with the host retina while isolated and distal clusters show only little interaction.....</i>	49
4.2.2	<i>Incorporation of D200 grafts is first evident at 8 weeks post transplantation</i>	50
4.2.3	<i>Host Müller glia extend processes into the graft before host bipolar cells.....</i>	51
4.2.4	<i>MG staining in D200 grafts originates from host MG.....</i>	51
4.3	INCORPORATING D200 GRAFTS POLARIZE AND FORM STRUCTURES OF MATURE PHOTORECEPTORS	53
4.3.1	<i>Grafts and host form an outer limiting membrane (OLM)-like structure.....</i>	53
4.3.2	<i>Inner segment formation occurs where an OLM is formed.....</i>	54
4.3.3	<i>Incorporating grafts form outer segment-like structures</i>	55
4.3.4	<i>Incorporating grafts form synaptic structures</i>	57
4.3.5	<i>Transplanted Crx-mCherry⁺ cells become enriched for cones</i>	58
4.3.6	<i>Higher levels of mature photoreceptor markers in ex vivo compared to in vitro cones.....</i>	60
4.4	INCORPORATION AND MATURATION CAPACITY DEPEND ON THE HOST ENVIRONMENT	63
4.4.1	<i>Graft morphology and maturation in C57BL/6JRj recipients resembles that in Cpf1 hosts.....</i>	63
4.4.2	<i>Graft morphology and maturation in highly degenerated rd1 and tgCR host lines differs strongly from the outcome in models with an ONL</i>	63
4.5	SUMMARY	67
5	FUNCTIONAL ASSESSMENT OF TRANSPLANTED CRX-MCHERRY⁺ CELLS	69
5.1	AIMS	69
5.2	HIGH-LEVEL FUNCTION	69
5.2.1	<i>Light-Dark Box</i>	69
5.3	TISSUE-LEVEL FUNCTION	71
5.3.1	<i>Multi-electrode array assessment of D200+26w grafts in Cpf1 mice</i>	71

5.3.2	<i>Isolation of cone-mediated RGC response through photopic light stimulation and L-AP4 addition</i>	71
5.3.3	<i>Graft-containing retinal portions exhibit cone-mediated light responses</i>	72
5.4	SUMMARY	74
6	DISCUSSION AND FUTURE PERSPECTIVES	75
6.1	HUMAN GRAFTS CAN MORPHOLOGICALLY INCORPORATE INTO THE MODERATELY DEGENERATED MOUSE RETINA	75
6.2	INTRARETINAL GRAFTS MOSTLY REPRESENT TRUE INCORPORATION EVENTS, NOT MATERIAL TRANSFER	76
6.3	GRAFT MATURATION DEPENDS ON GRAFT-HOST INTERACTION	77
6.4	ESTABLISHMENT OF GRAFT-HOST INTERACTION AND GRAFT INCORPORATION	78
6.5	D200 CRX-MCHERRY ⁺ CELLS ARE THE PREFERABLE DONOR POPULATION COMPARED TO D100 AND D30080	81
6.6	CONES SHOW PREFERENTIAL SURVIVAL POST GRAFTING	81
6.7	FUNCTIONAL ANALYSES OF TRANSPLANTED ANIMALS	82
6.8	FUTURE CLINICAL TRANSLATION	85
6.9	MAJOR CONTRIBUTION TO OTHER WORK	88
7	FINAL CONCLUSION	89
8	MATERIALS AND METHODS	91
8.1	STUDY APPROVAL	91
8.2	MATERIALS	91
8.2.1	<i>Materials and Chemicals</i>	91
8.2.2	<i>Cell Line</i>	92
8.2.3	<i>Mouse Lines</i>	92
8.2.4	<i>Antibodies</i>	93
8.3	METHODS	95
8.3.1	<i>Cell culture</i>	95
8.3.2	<i>Transplantations</i>	96
8.3.3	<i>Functional analyses</i>	98
8.3.4	<i>Immunohistochemistry and Immunocytochemistry</i>	100
8.3.5	<i>Imaging and image processing</i>	103
8.3.6	<i>Statistics</i>	106
8.3.7	<i>Single cell sequencing</i>	107
8.3.8	<i>Bioinformatic analysis</i>	108
9	BIBLIOGRAPHY	111
10	APPENDIX	128
10.1	APPENDIX 1: ERKLÄRUNGEN ZUR ERÖFFNUNG DES PROMOTIONSVERFAHRENS	128
10.2	APPENDIX 2: BESTÄTIGUNG ÜBER EINHALTUNG DER AKTUELLEN GESETZLICHEN VORGABEN	129

List of Figures

FIGURE 1. SCHEMATIC STRUCTURE OF THE HUMAN EYE AND RETINA.....	2
FIGURE 2. SCHEMATIC DEPICTION OF PHOTORECEPTOR STRUCTURE AND FUNCTION.	4
FIGURE 3. ARTISTIC REPRESENTATION OF MÜLLER GLIA MORPHOLOGY AND INTERACTIONS.	9
FIGURE 4. MATERIAL TRANSFER OCCURRING IN MOUSE-TO-MOUSE TRANSPLANTATIONS.....	16
FIGURE 5. CRX-MCHERRY CO-LOCALIZATION WITH CRX AND INCREASE OVER TIME.	24
FIGURE 6. MÜLLER GLIA IN D150 CRX-MCHERRY ORGANIDS.	25
FIGURE 7. CRX-MCHERRY ⁺ CELLS EXPRESS EARLY ROD AND CONE MARKERS.....	25
FIGURE 8. CRX-MCHERRY ⁺ CELLS EXPRESS MATURE PHOTORECEPTOR MARKERS.....	26
FIGURE 9. DECREASE IN KI67 ⁺ CELL NUMBER DURING ORGANOID MATURATION.	27
FIGURE 10. PERCENTAGE OF CRX-MCHERRY ⁺ CELLS BEFORE AND AFTER FACS ENRICHMENT.	28
FIGURE 11. TRANSCRIPTOME ANALYSIS OF HRO CRX-MCHERRY ⁺ CELLS BY SINGLE CELL SEQUENCING.	29
FIGURE 12. ASSESSMENT OF D200 SORTING FOR CRX-MCHERRY BY ICC.	30
FIGURE 13. EXPERIMENTAL SETUP AND TIMELINE.	34
FIGURE 14. GRAFT VOLUMES IN D100, D200 AND D300 TRANSPLANTS.	35
FIGURE 15. TRANSPLANTED CRX-MCHERRY ⁺ CELLS ARE NEGATIVE FOR THE PROLIFERATION MARKER KI67.....	36
FIGURE 16. QUANTIFICATION OF GRAFT SUBTYPES BY POSITIONING.....	38
FIGURE 17. GENERAL MORPHOLOGY OF D100 GRAFTS.....	39
FIGURE 18. GENERAL MORPHOLOGY OF D300 GRAFTS.....	40
FIGURE 19. GENERAL MORPHOLOGY OF D200 GRAFTS.....	40
FIGURE 20. INNER SEGMENTS IN IHC AND EM AND THEIR QUANTIFICATION IN D100, D200 AND D300 GRAFTS.....	41
FIGURE 21. INNER SEGMENT DEVELOPMENT IN PROXIMAL AND DISTAL GRAFTS.....	42
FIGURE 22. HUMAN IDENTITY OF INTRARETINAL GRAFT CLUSTERS.....	44
FIGURE 23. NANOGOLD LABELING OF HUMAN NUCLEI IN EM.....	45
FIGURE 24. POTENTIAL OCCURRENCES OF HUMAN-TO-MOUSE MATERIAL TRANSFER.	46
FIGURE 25. ISOLATED GRAFTS INTERACT LESS WITH HOST MÜLLER GLIA AND BIPOLAR CELLS.	50
FIGURE 26. GRAFT SIZE AND POSITIONING IN D200 EARLY TIMELINE SAMPLES.....	51
FIGURE 27. EARLY INTERACTION WITH HOST MÜLLER GLIA AND BIPOLAR CELLS IN D200 GRAFTS.....	52
FIGURE 28. HOST MG NUCLEI ARE PRESENT IN D200 GRAFTS.	53
FIGURE 29. INTRASPECIES OLM FORMATION IN INTRARETINAL D200 GRAFTS.....	54
FIGURE 30. IS GENERATION CORRELATES WITH OLM FORMATION.	55
FIGURE 31. POTENTIAL OUTER SEGMENT FORMATION IN D200 GRAFTS.	56
FIGURE 32. FORMATION OF SYNAPTIC STRUCTURES WITHIN HUMAN GRAFTS.	58
FIGURE 33. SINGLE CELL TRANSCRIPTOME ANALYSIS OF EX VIVO AND IN VITRO CRX-MCHERRY ⁺ CELLS.	59
FIGURE 34. DIFFERENCES IN FUNCTIONAL GENE EXPRESSION BETWEEN IN VITRO AND EX VIVO CONES.....	61
FIGURE 35. D200 GRAFTS IN C57BL/6JRJ HOSTS.	63
FIGURE 36. QUALITATIVE COMPARISON OF GRAFT MORPHOLOGY IN CPFL1, TGCR AND RD1 MICE.	64

FIGURE 37. GRAFT INTERACTION AND MATURATION IN TGCR HOSTS AT D200+26W.	65
FIGURE 38. GRAFT INTERACTION AND MATURATION IN RD1 HOSTS AT D200+26W.	66
FIGURE 39. LIGHT-DARK BOX RESULTS OF C57BL/6JRJ AND CPFL1 ANIMALS.....	70
FIGURE 40. LIGHT-DARK BOX RESULTS OF STRONGLY DEGENERATED ANIMALS.	70
FIGURE 41. ROD RESPONSE AFTER FLUORESCENT LIGHT EXPOSURE IN UNTRANSPLANTED CPFL1 RETINA.	72
FIGURE 42. INCREASED OFF RGC ACTIVITY IN TRANSPLANTED CPFL1 RETINAS.	73
FIGURE 43. ABSOLUTE IRRADIANCE AND FULL SPECTRUM OF LIGHT USED DURING MEA STIMULATION.....	100

List of Tables

TABLE 1. MATERIALS AND CHEMICALS.....	91
TABLE 2. PRIMARY ANTIBODY DETAILS.	93
TABLE 3. SECONDARY ANTIBODY DETAILS.	94
TABLE 4. STATISTICAL ANALYSES.....	106

General Abbreviations

AAV	adeno-associated virus
AC	amacrine cell
AMD	age-related macular degeneration
BC	bipolar cell
BRB	blood-retina-barrier
BP	biological processes
C57BL/6Jrj	C57BL/6Jrj mouse model
CC	connecting cilium (PR morphology)
CC	cellular component (GO term analysis)
cc	correlation coefficient
CHM	choroideremia
Cpfl1	cpfl1 mouse model
Crx-mCherry	Crx-mCherry cell line or reporter fluorescence
Cy	cyanine dye
ctrl	control
d	day
D	day, used in conjunction with cell age
DAPI	4', 6-Diamidino-2-Phenylindole
DIC	differential interference contrast
ECM	extracellular matrix
EM	electron microscopy
FACS	fluorescence-activated cell sorting
g	gravitational force
GCL	ganglion cell layer
GFP	green fluorescent protein
h	hour
HC	horizontal cell
hESC	human embryonic stem cell
hiPSC	human induced pluripotent stem cell
hMITO	human mitochondria
HRO	human retinal organoid
HuNu	human nuclei
INL	inner nuclear layer
IPL	inner plexiform layer
IPM	interphotoreceptor matrix
iPSC	induced pluripotent stem cell
IRD	inherited retinal degeneration
IS	inner segment

KU	Kuntz units
L-AP4	l-2-amino-4-phosphonobutyric acid
LCA	leber congenital amaurosis
LDB	light-dark box
MACS	magnetic-activated cell sorting
MEA	multi-electrode array
MF	metabolic function
MG	Müller glia
min	minute
MT	material transfer
mtRNA	mitochondrial RNA
mV	millivolts
μ	micro
OLM	outer limiting membrane
ONL	outer nuclear layer
OPL	outer plexiform layer
OS	outer segment
PBS	phosphate buffered saline
PNA	peanut agglutinin
PR	photoreceptor
rcf	relative centrifugal force
rd1	rd1 mouse model
RGC	retinal ganglion cell
RP	retinitis pigmentosa
RPE	retinal pigment epithelium
rpm	rotations per minute
RT	room temperature
SRS	subretinal space
TEM	transmission electron microscopy
TP, tp	transplantation
tgCR	tgCR mouse model
U	units
w	week
wpt	weeks post transplantation

Gene and Protein Abbreviations

ARR3	Arrestin 3, Cone arrestin
CA10	Carbonic anhydrase-related protein 10
CRALBP	Retinaldehyde-binding protein 1
CRX	Cone-rod homeobox protein
CTBP2	C-terminal binding protein 2
GFAP	Glial fibrillary acidic protein
GFP	Green fluorescent protein
GLAST	Sodium-dependent glutamate/aspartate transporter 1
GS	Glutamine synthetase
GSG1	Germ cell-specific gene 1 protein
HUC	ELAV-like protein 3
HUD	ELAV-like protein 4
IBA1	Allograft inflammatory factor 1
KI67	Proliferation marker protein Ki-67
KU80	ATP-dependant DNA helicase II or DNA repair
MGLUR6	Metabotropic glutamate receptor 6
NRL	Neural retina-specific leucine zipper protein
OPN1L/MW	Long- and medium wave opsin
OPN1SW	Short-wave opsin
PAX6	Paired box protein Pax-6
PKCA	Protein kinase C alpha type
PRPH2	Peripherin 2
RBP4	Retinol-binding protein 4
RCVRN	Recoverin
RDH12	Retinol dehydrogenase 12
RHO	Rhodopsin
RP1	Oxygen-regulated protein 1
RPE65	Retinoid isomerohydrolase
GNAT2	Guanine nucleotide-binding protein G(t) subunit alpha-2
GRK7	Rhodopsin kinase GRK7
IMPG1	Interphotoreceptor matrix proteoglycan 1
PDC	Phosducin
SAG	S-arrestin, rod arrestin
SCGN	Secretagogin
SOX2	Transcription factor SOX-2
TULP1	Tubby-related protein 1
VIM	Vimentin
ZO1	Tight junction protein ZO-1

1 Introduction

1.1 The Retina and Light Perception

1.1.1 General structure of the eye

According to the American writer and philosopher Henry David Thoreau, “The eye is the jewel of the body” (Robertson, 1998). While it may be as beautiful and mesmerizing, fortunately for us it has a much more intricate and biologically sophisticated design and function, adapted for the perception of light and ultimately vision.

From the outside, the mammalian eyeball is protected by the external layer, the sturdy sclera, appearing white, and the transparent cornea in the front, which is continuous with the sclera (Figure 1A). Extraocular muscles attached to the sclera rotate the eyeball in its cavity. Below the cornea lies the anterior chamber containing the aqueous humor and the lens, a biconvex, transparent structure for light refraction. The lens is hinged at the ciliary body, connecting it to the highly pigmented choroid, a vascular tissue and part of the posterior intermediate layer that neighbors the sclera within the entire globe. The amount of light that enters the eye is controlled by the iris, a colored circular muscle on top of the lens, which contracts and relaxes to adapt the size of the opening in its middle, the pupil. Once through the lens, the light traverses the vitreous and is focused onto the retina or neuroretina, the sensory part of the eye that lines the inner surface of the globe and the site of visual perception. Behind it lies the retinal pigment epithelium (RPE), a highly pigmented epithelial monolayer with a plethora of functions, amongst which are the absorption of scattered light and the connection of the retina to the choroid (Figure 1A).

1.1.2 General structure of the retina

The mammalian retina itself, whose function is the conversion of light into a visual signal that is forwarded to the visual cortex, is a densely packed, highly organized structure (Figure 2B). It contains three nuclear and two synaptic layers. From the vitreal, i.e. basal side, the inner retina is constituted by the ganglion cell layer (GCL), the inner plexiform layer (IPL) and the inner nuclear layer (INL) followed by the outer retina, consisting of the outer plexiform layer (OPL) and, on the most apical side, the outer nuclear layer (ONL). Beyond the ONL, inner and outer segments (IS, OS), highly specialized cell compartments of the photoreceptors (PRs) that reside within the ONL, protrude into the subretinal space towards the RPE.

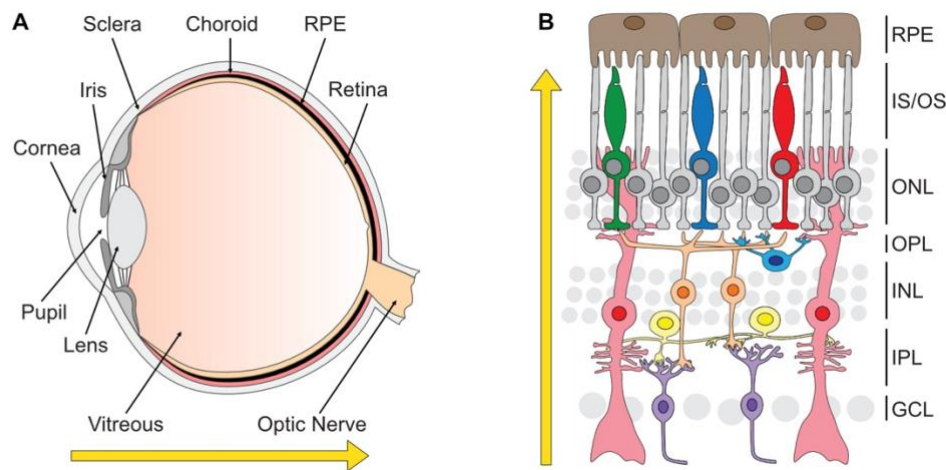


Figure 1. Schematic Structure of the Human Eye and Retina.

A. Schematic structure of the human eyes. **B.** Schematic structure of the human retina, showing nuclear layers and exemplary cell types. Both adapted from (Llonch Armengol, 2018) RPE: Retinal pigment epithelium; IS: Inner segments; OS: Outer segments; ONL: Outer nuclear layer; OPL: Outer plexiform layer; INL: Inner nuclear layer; IPL: Inner plexiform layer; GCL: Ganglion cell layer. Yellow arrow represents light path.

Each layer has a particular function that is defined by the neurons residing in it. The two types of PR, rods and cones, are positioned in the ONL and are the primary cells responsible for conversion of photon energy into a biological signal (Figure 2B, grey, blue, green, red). Through synapses in the OPL, they transmit that information to the secondary neurons, bipolar (BC) and horizontal cells (HC), whose nuclei reside in the INL (Figure 2B, orange and blue, respectively). Amacrine cells (AC, Figure 2B, yellow), also present in the INL, modulate the signal upon its transmission in the IPL to retinal ganglion cells (RGC, Figure 2B, purple), which are the neurons of the GCL whose axons form the optic nerve that transmits the signal to the brain.

In addition to neuronal cells, the retina contains microglia and two types of macroglia, astrocytes in the GCL (not shown) and Müller glia (MG), a type of radial glia. MG nuclei reside in the INL, yet their stem processes span the entire retinal thickness (Figure 2B, pink). MG anatomy and function is described in more detail in section 1.1.7 *The role of Müller glia in photoreceptor support and light perception.*

The composition, distribution and exact function of cell types within the retina differs in a species-specific manner. Most importantly, primate, including human, retinas contain a specialized, cone-rich region in the retinal center, the fovea, the point of highest acuity vision (Kostic & Arsenijevic, 2016; Yan et al., 2020).

As part of the central nervous system, the retina is separated from the systemic circulation through the inner and outer blood-retina-barrier (BRB, not shown). The inner BRB is formed between the vascular plexus, a network of blood capillaries extending from the GCL into the OPL, pericytes and MG. The outer BRB is constructed by the

RPE monolayer, between the neuroretina and the fenestrated vessels of the choroid. Transport of nutrients, oxygen and waste products across the BRB is highly regulated and ensures the relative immune privilege of the retina.

1.1.3 General photoreceptor structure

Rods and cones, the two types of photoreceptors (PR), are highly specialized, asymmetric neurons, whose function is the capture of light and subsequent signal transmission to the secondary neurons. While the details of that task differ between the two, the basic morphology of rods and cones is similar – both have an elongated shape with three main functional compartments: The inner segment (IS), extending apically from the nucleus and perikarium in the ONL, the outer segment (OS), extending out further from the inner segment, and, on the opposite side of the perikarium, the axon, directed towards the OPL with a synaptic terminal at its end (Figure 2A) (Malhotra et al., 2021). In the following, the structure and function of the OS and IS will be described in more detail. For an introduction to the PR synapse and function, refer to section 1.1.5 Signal transmission to the brain.

The OS is the site of photon capture and initialization of the phototransduction cascade, the perception and conversion of light into a biological signal. It is a highly modified primary cilium divided into two main portions that differ strongly in morphology. At the proximal end, the connecting cilium (CC) connects the OS with the IS (Wensel et al., 2021). While the CC is thin and directly surrounded by plasma membrane, the OS contains large stacks of membrane discs, providing compartmentalization and vast membrane area for the phototransduction machinery. The OS discs are formed by evagination of the plasma membrane around the distal cilium and are continuously displaced along it towards the apical side (Burgoyne et al., 2015), where older discs are shed in packets and phagocytosed by the RPE (Kevany & Palczewski, 2010). This shedding allows for the turnover of the entire OS within 10 days in mice and rats, ensuring renewal of phototransduction machinery and hence maximum photosensitivity. In rods, the discs are initially open, but over time their leading edges fuse, resulting in closed membranous discs within the rod cytosol (Wensel et al., 2021). In cones, such a fusion does not take place and the lamellar folds are continuous with each other at all times.

Below the OS and the CC lies the IS, an important support hub for OS function. The high turnover of membranes and phototransduction proteins in the OS requires constant supply which is met through the presence of extensive metabolic and biosynthetic machinery like ribosomes, endoplasmic reticulum and the Golgi complex in the IS (Molday & Moritz, 2015). In addition, the IS contains a high amount of potassium

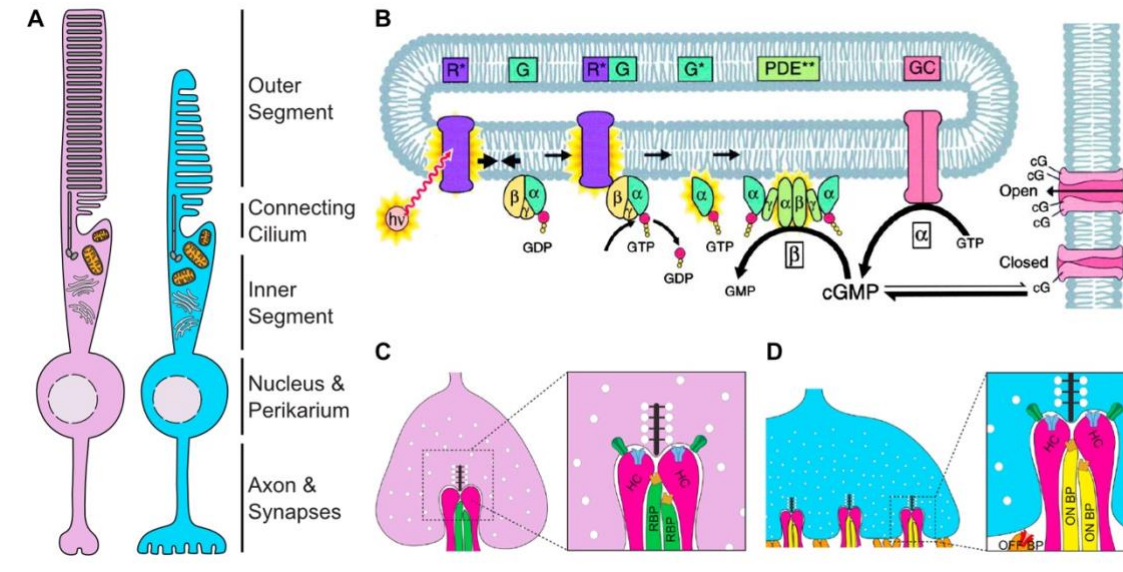


Figure 2. Schematic Depiction of Photoreceptor Structure and Function.

A. Schematic depiction of rod (magenta) and cone (blue) structure, adapted from (Gasparini et al., 2018). **B.** The rod phototransduction cascade upon light exposure, image from (Leskov et al., 2000). **C-D.** Interaction of photoreceptors, bipolar cells and horizontal cells at the rod (**C**) and cone (**D**) synapse, both adapted from (Burger et al., 2021). *hν*: photon; *R*: rhodopsin; *G*: transducin; *PDE*: phosphodiesterase; *GC*: guanylate cyclase; *cG*: cyclic GMP; *HC*: horizontal cell; *RBP*: rod bipolar cell; *BP*: bipolar cell.

channels and sodium-potassium ATPases (NKA) that, together with other ion channels in the OS plasma membrane, maintain the membrane potential at -40 mV in the dark (Baker & Kerov, 2013). As this is an intensely energy-dependent process, IS also contain large clusters of mitochondria for ATP generation directly below the CC (Ingram et al., 2020).

1.1.4 Phototransduction

Light perception in the OS is mediated by a G-protein coupled receptor cascade (Figure 2B). It is initiated by the capture of a photon through the visual pigments, which consist of the chromophore 11-*cis*-retinal bound to an opsin. Upon exposure to light, 11-*cis* retinal is photoisomerized to all-*trans* retinal, which induces a conformational change in the opsin, activating it. The membrane-bound opsin then binds transducin, and the GDP on the transducin α -subunit is exchanged for GTP, releasing the α -subunit. The α -subunit activates phosphodiesterase 6 (PDE6) by releasing the inhibitory PDE γ -subunit, allowing hydrolysis of cGMP, decreasing the intracellular cGMP concentration. This in turn causes closure of cyclic nucleotide-gated (CNG) channels in the plasma membrane. As these CNG channels control influx of Na^+ and Ca^{2+} , the cell becomes hyperpolarized from -40 mV to -70 mV, eventually inhibiting the tonic glutamate release at the synapse.

To return to the “dark state”, the (in)activation of the signaling components must be reverted and the all-trans retinal changed back to its original conformation. The first can be achieved in the photoreceptors themselves and includes opsin inactivation through phosphorylation by a G protein-coupled receptor kinase (GRK) and binding of arrestin, hydrolysis of GTP on the transducin α -subunit, re-establishment of cGMP levels through guanylate-cyclase (GC) activated by guanylyl cyclase-activating protein (GCAP) and opening of the CNG channels, depolarizing the cell. To revert the all-trans retinal back to 11-cis retinal, a process known as the visual cycle, a second cell type is required. Both rods and cones can participate in the classical visual cycle, mediated by the RPE. Cones can additionally make use of the cone visual cycle, mediated by MG.

In the classical visual cycle, after photoisomerization, all-trans-retinal is reduced to all-trans-retinol and exits the photoreceptor. Binding to retinol-binding protein 3 (RBP3, IRBP) in the interphotoreceptor matrix (IPM), the extracellular matrix between the photoreceptor IS, OS and the RPE, allows shuttling into the RPE. There, all-trans retinol is esterified, converted back to 11-cis-retinol by retinoid isomerohydrolase RPE65 (retinal pigment epithelium-specific 65-kDa protein) and oxidized to 11-cis-retinal. IRBP then transports it back to the PR, where it can bind the opsin and be used again in phototransduction.

In the intraretinal cone visual cycle, 11-cis-retinal is photoisomerized to all-trans-retinol and transported to MG. In the MG, isomerization, esterification and hydrolysis to 11-cis-retinol take place in a graded, light-dependent manner, before shuttling back to the cones. The cones are able to oxidize the 11-cis-retinol back to 11-cis-retinal so that the chromophore can be employed again. The cone visual cycle is particularly relevant during extended bright light exposure, when the photoisomerization of 11-cis-retinal exceeds its synthesis in the RPE (Morshedjian et al., 2019; Tsin et al., 2018).

Beyond its important role in the visual cycle, the RPE has key functions in support of phototransduction and the retina per se (Lakkaraju et al., 2020). It is the interface between the choroidal blood supply on its basal side, and the photoreceptor OS on its apical side. The RPE is the prime constituent of the outer blood-retinal barrier (BRB), shielding the retina from the systemic circulation while actively transporting nutrients, metabolites and waste products. It secretes growth factors, neurotrophic factors and immune modulatory factors. Quick spatial buffering of K^+ in the subretinal space, i.e. the volume between the apical side of the RPE and the apical side of the PR, ensures proper PR membrane potential changes, while absorption of scattered light by its strong pigmentation reduces light noise and reduces photo-oxidative stress. The phagocytosis of the distal OS ends allows the continuous recycling of the phototransduction components, and thus PR homeostasis.

1.1.5 Signal transmission to the brain

Before the information about incoming light is forwarded to the brain, it is modulated and interpreted by computation within the retina itself (Baccus, 2007). The first relay station is the OPL synapse, where PRs contact bipolar cell (BC) and horizontal cell (HC) dendrites through PR ribbon synapses positioned in their thickened axon terminals, the rod spherules and cone pedicles (Figure 2C) (Burger et al., 2021). The synapses are primarily situated in invaginations of the PR axon terminal into which HC and BC dendrites extend. On the presynaptic PR side, each invagination is characterized by the presence of an electron-dense, plate-like structure extending vertically from the membrane into the cytoplasm, the synaptic ribbon, namesake of the ribbon synapse. It is the key hub for the machinery required to tonically release glutamate at the synapse. Tethered to the ribbon are hundreds to thousands of synaptic vesicles, ready to be released, as well as Ca^{2+} channels that drive their exocytosis (Heidelberger, 2007). Upon vesicle docking, the glutamate in the synaptic cleft diffuses away from the release site to different targets at varying distance, with diffusion physically encoding a temporal filter (Matthews & Fuchs, 2010).

While murine rod PRs only have three major types of direct synaptic targets, two HCs and the rod ON BC, eleven other BC types exist in mice and receive direct input from cones (Wässle et al., 2009). They all differ in terms of morphology, stratification, i.e. the exact localization of their axons in the IPL strata, receptors, ion channels, intracellular signaling and output (Masland, 2012). As such, BC can be grouped into ON and OFF BC, with ON BC expressing metabotropic glutamate receptor 6 (mGluR6, encoded by GRM6) and OFF BC expressing AMPA and kainate type receptors. Glutamate binding to mGluR6 causes closure of the TRPM1 cation channel (transient receptor potential cation channel subfamily M member 1), so decrease of glutamate under light conditions leads to TRPM1 opening and ON BC depolarization. Binding of glutamate to OFF BC receptor kainate and AMPA cation channels on the other hand opens them. As glutamate levels decrease upon light exposure, OFF BC channels are closed and the cell hyperpolarizes. In addition to directionality of the response, the inactivation kinetics of glutamate receptors differ between cells, allowing further grouping of BC responses into sustained and transient (Awatramani & Slaughter, 2000).

From the BC onwards, additionally modulated by amacrine cells, the signal is passed to RGCs through the BC ribbon synapse, which is not invaginated and contains more numerous yet much smaller ribbons and a lower number of vesicles present and docked than at the PR ribbon synapse (Matthews & Fuchs, 2010). The connections from BC to RGC again distribute the signal to various functional targets with distinct functions

in retinal computation. There is still ongoing debate about the exact number of RGC subtypes, and a recent review has suggested that roughly 40 RGC types exist (Vlasits et al., 2019). However, similarly to BC, they can be classified into two main groups, ON and OFF GC, with transient or sustained temporal response properties for both. In response to an increased illumination of their receptive field, that is the area of the retina whose stimulation produces a change in the RGC output, ON RGC are depolarized while OFF RGC depolarize in response to decreases illumination (M. V. Wyk et al., 2009).

Rods and cones react to changes in light intensity, yet, as described above, it is the following connections and computations that determine how these changes are interpreted. To perform that task, the retina has a spatially distinct layout of specific cell types in a vast array of interconnections and feedback systems. As such, rods for example convey their light response in three pathways. The primary pathway connects rods to rod ON BCs, which relay to All amacrine cells that in turn can modulate cone BC activity. In the secondary pathway rods connect directly to cones via gap junctions and feed into the cone signaling pathway at the level of the OPL. In some mammals, a tertiary pathway exists, in which rods can make direct contact with a subtype of cone OFF BCs (Euler et al., 2014; Soucy et al., 1998; Tsukamoto & Omi, 2014). These complex interconnections are thought to play important roles in allowing continuous signaling over a broad range of light intensities, e.g. modulating color appearance under mesopic conditions (Grimes et al., 2018).

1.1.6 Major differences between rods and cones

While the general structure and much of the intracellular signaling is similar in rods and cones, there are important differences between the two PR types. Morphologically, rods are cylindrical and long, containing up to ~1000 stacked discs in their OS (Figure 2A) (Burgoyne et al., 2015). Cones on the other hand are shorter and have a conical OS shape with lamellar folds. Rods largely outnumber cones, with the human retina containing 120 million rods but only 6 million cones (Molday & Moritz, 2015). Human cones are most abundant in the fovea, the point of highest visual acuity in the retinal and macular center, from which cone density decreases towards the periphery. Along that gradient, also cone shape changes, with the slightly tapered cone OS longest (45-50 μm) at the macular center, decreasing in length and increasing in thickness and taper towards the periphery. In the far most periphery, cone OS are missing completely (Curcio & Hendrickson, 1991). It is important to note that PR distribution differs greatly between species, and while cone-rich regions exist e.g. in

sheep, dogs and pig, a fovea only exists in adult monkeys, apes and humans. Mice do not harbour a fovea or a site of cone-enrichment (Kostic & Arsenijevic, 2016).

Functionally, rods are able to respond to single photons through signal amplification during phototransduction, conferring high sensitivity under low light conditions, the so-called scotopic vision. Due to their reliance on the classical visual cycle, they have slower pigment recycling kinetics and saturate under higher light intensities (Mahroo & Lamb, 2004). Cones on the other hand are less sensitive, requiring 4-7 photons to yield a detectable light response exceeding the noise (Holcman & Korenbrot, 2005). They do not saturate as fast and have quicker recycling kinetics thanks to the cone visual cycle (J.-S. Wang & Kefalov, 2009), making them mediators of daylight vision. In addition, cones allow for higher spatial resolution than rods and are therefore the prime mediators of high acuity vision (Rossi & Roorda, 2010).

The differences in PR functionality are a direct consequence of distinct expression or composition of proteins involved in phototransduction (Lamb, 2022; Reingruber et al., 2020), such as the subunits of PDE6 (rods: PDE6A, PDE6B, PDE6G; cones: PDE6C, PDE6H; (Deng et al., 2018), transducin or guanine nucleotide-binding protein G(t) (rods: GNAT1; cones: GNAT2; (Mao et al., 2013)) and arrestin (rods: SAG; cones: ARR3; Gurevich & Gurevich, 2014). Another main difference between PR types lies in their pigments, the opsins. In contrast to rods, which only contain a single visual pigment type, rhodopsin (RHO), with a peak absorbance at 498 nm (green light), different cone opsin types exist, allowing for color vision (Bowmaker & Dartnall, 1980). In humans, there are three cone opsins with peak sensitivities at $\lambda_{\max} = 420$ nm, 534 nm and 564 nm for short-wave (OPN1SW, blue), medium-wave (OPN1MW, green) and long-wave (OPN1LW, red) cones respectively (Dartnall et al., 1983). There are however large inter-species differences, and mouse cones on the other hand contain an ultraviolet or short and a middle wavelength sensitive cone opsin (Opn1sw and Opn1mw) with $\lambda_{\max} = 360$ nm and 508 nm respectively. Interestingly, the majority of mouse cones co-expresses both, Opn1sw and Opn1mw opsins, while only a small subset of 5% is restricted to UVS opsin expression (Peirson et al., 2018).

Rods and cones also differ in their signal transmission to BC and HC and the signaling pathways employed thereafter (Figure 2C). The rod ribbon synapses are located in the round rod spherule, with only one invagination present, filled with two HC and two ON BC dendrite tips. In contrast, the flat cone pedicles can contain up to 20-45 invaginations, each one contacted by one or two BC and two HC dendrites (Wässle et al., 2003). Additionally, flat contacts outside of the invaginations are made by mainly OFF BC dendrites. As mentioned above, the only BC type receiving direct input from

rods is the rod ON BC, constituting the first relay station in the primary rod pathway. Cones on the other hand make connections with all other BC types, except the rod ON BC.

1.1.7 The role of Müller glia in photoreceptor support and light perception

Müller glia (MG) are the lastborn cell type in the retina yet they have vital roles in retinal functioning (Reichenbach & Bringmann, 2020). They are associated with virtually all retinal cell types and are involved in mechanical tissue maintenance, retinal water, potassium and pH homeostasis as well as neurovascular coupling, to name only a few. Their perikarya are positioned in the INL, but as a type of radial glia, their two stem processes span the entire retinal thickness, contacting all retinal layers and acting as optical fibers (Franze et al., 2007)(Figure 3). At the basal side, MG footplates form the vitreal surface of the retina, produce the basal lamina of the inner limiting membrane and are in contact with the superficial blood vessels of the inner plexus, while also enwrapping the RGC axons. In the IPL and OPL, perisynaptic MG sheaths are involved in neurotransmitter uptake, directly regulating synaptic activity and controlling lateral glutamate spread (Bringmann et al., 2013).

The multitude of roles MG have in the retina include key functions with regards to photoreceptors (PR), like the cone visual cycle described above (section 1.1.4 *Phototransduction*). Morphologically, MG interact with PR throughout their entire cellular length, with dedicated functionality at each location and differing characteristics depending on retinal region (Voigt et al., 2019). In the ONL itself, MG membrane sheaths envelop the photoreceptor perikarya. Towards the subretinal space, MG and PR

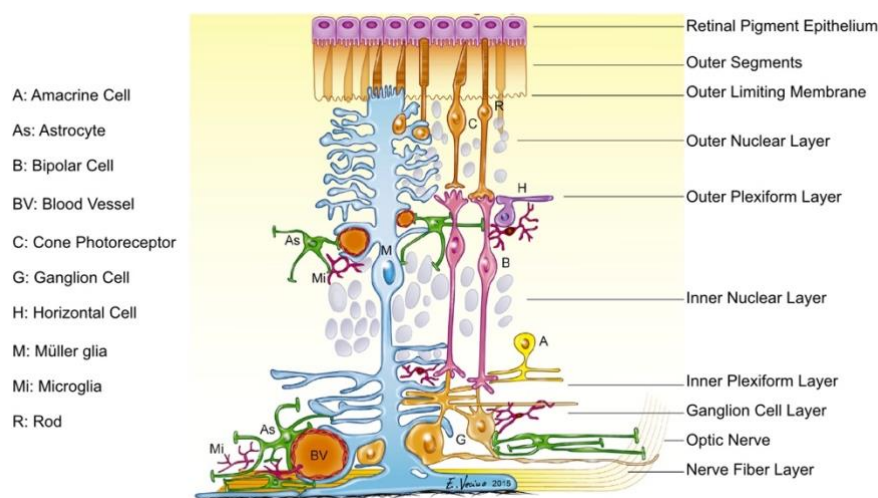


Figure 3. Artistic Representation of Müller Glia Morphology and Interactions.
Adapted from (Vecino et al., 2016)

together as well as MG and other MG seal the neuroretina through a continuous series of heterotypic adherens junctions at the base of the inner segments. The resulting outer limiting membrane (OLM) on the one hand increases the mechanical strength of the retina, and on the other hand acts as a semipermeable diffusion barrier, separating the subretinal from the neuroretinal extracellular space (Omri et al., 2010). Furthermore, it is vital for inner segment formation and homeostasis (Izaddoost et al., 2002; Mehalow et al., 2003; Pellikka et al., 2002). Apical MG microvilli, making up 80% of the cell membrane area (Derouiche et al., 2012), extend onward from the outer stem process between PR inner segments. High sodium-potassium-ATPase activity in the microvilli is used to deposit potassium taken up at the plexiform layers into the subretinal space (Newman & Reichenbach, 1996).

MG not only have crucial functions in retinal homeostasis in health, but also and especially upon injury. Mechanical deformation of the retinal tissue can induce calcium responses, activation of ERK1/2 and upregulation of c-Fos and bFGF in MG (Lindqvist et al., 2010). The MG response to low to moderate damage is characterized by upregulation of intermediate filaments, cellular hypertrophy and absent or moderate proliferation – conservative gliosis, deemed neuroprotective. On the other hand, upon severe damage, the MG adapt a more destructive character – massive gliosis, indicated by MG proliferation and the establishment of a glial scar on the sub- and epiretinal side follow, ultimately damaging the photoreceptors (Reichenbach & Bringmann, 2020).

1.2 Retinal Degeneration Diseases and Treatment Options

1.2.1 Retinal degeneration diseases

Vision is the most dominant of all our senses and its absence has grave personal, societal and emotional consequences. The WHO estimates that every person with an average lifespan will at some point suffer at least one eye condition. While the vast majority of the estimated 2.2 billion people worldwide with vision impairment will experience comparatively mild issues such as refractive errors that can be alleviated or treated, others will be much more severely affected due to irreversible retinal degenerative disease (World Health Organization, 2019). One major reason for blindness is the dysfunction and loss of the central unit of visual perception, the photoreceptors (PR). The causes for PR degeneration are diverse – age-related macular degeneration (AMD) for example is a complex disease developing due to a combination of genetic and environmental risk factors (Fritsche et al., 2014). In 2020, 196 million people were estimated to suffer from AMD alone, with 5.3% (10.4 million) in advanced stages causing moderate or severe distance vision impairment or blindness (World Health Organization, 2019).

Besides AMD, a large array of inherited retinal degeneration (IRD) diseases exists, a collection of conditions based mainly on mutations in more than 280 genes primarily involved in light perception as of June 2022 (*RetNet: Summaries of Genes and Loci Causing Retinal Diseases*, 2022). While each mutation might be comparatively rare, it is estimated that roughly 1 in 1380 individuals worldwide – 5.5 million people – are affected by autosomal recessive IRDs such as retinitis pigmentosa (RP), Usher syndrome, choroideremia (CHM), Leber Congenital Amaurosis (LCA) and Stargardt disease (Hanany et al., 2020). While mutations in the same gene can cause distinct clinical phenotypes, IRD pathologies caused by mutations in different genes can converge into common trajectories, with PRs continuously lost throughout the years, diminishing visual function. The order of PR degeneration varies, allowing grouping of the diseases into those that affect cone viability first, such as AMD, other inherited macular degenerations and cone-rod dystrophy, and those that affect rods first and cones later, e.g. RP. Primary degeneration of cones generally causes diminished visual acuity, loss of central vision and impairment of color vision, while rod degeneration manifests first in night blindness and tunnel vision before subsequent cone damage additionally affects the visual field and acuity (Veleri et al., 2015).

It is important to note that the culprit cell type causing PR degeneration is not always the PR itself and various IRD are instead the result of RPE dysfunction. When

RPE is compromised e.g. with respect to the visual cycle or phagocytosis, PRs die due to lack of support, such as in AMD, LCA mediated by mutations in RPE65, and inherited retinal degeneration mediated by mutations in MERTK, the receptor required to internalize PR OS (Ben M'Barek et al., 2019).

Regardless of its cause, the loss of PR in IRDs is irreversible, as in contrast to other species, the human eye is not capable of regenerating and replacing PR. Particularly in the human retina, gliotic scar formation occurs and neuronal remodeling takes place in response to PR loss (Jones et al., 2003), yet surprisingly, despite a somewhat hostile degenerative environment and deafferentation, the inner retina oftentimes remains, albeit with sometimes extensive changes in structure (Marc et al., 2003).

1.2.2 Therapeutic approaches to treat retinal degeneration diseases

Given the increasingly large health and societal burden of retinal degenerative diseases, therapeutic options are greatly needed. Currently, most IRDs cannot be cured and the main attempts to reduce the risk for developing an IRD are the modulation of environmental factors, e.g. through quitting smoking or changing the diet, or through the treatment with neuroprotective agents, such as vitamin A and docosahexaenoic acid (Duncan et al., 2018). One major exception is the possible treatment of 10-15% of AMD patients with repeated intravitreal injections of an antibody blocking vascular endothelial growth factor, anti-VEGF, which slows down photoreceptor loss and preserves visual function. Another recent success was the FDA approval of in vivo gene augmentation therapy, using an adeno-associated virus (AAV) to introduce a healthy copy of the RPE65 gene into RPE cells of patients with RPE65-associated retinal dystrophy – the first FDA-approved gene therapy for a disease caused by a genetically inherited disease (FDA, 2017). While these treatment options represent important milestones, they are applicable to only a small subset of patients and long-term studies however suggest that they cannot halt photoreceptor degeneration for long (Bainbridge et al., 2015; Ehlken et al., 2014; Jacobson et al., 2015). As further research and development of retinal therapeutics is required, much effort has been invested in identifying potential therapy options in recent years, especially in the areas of gene therapy, optogenetics, visual prosthetics and photoreceptor replacement.

Gene supplementation therapy aims at the introduction of genetic material into target cells to replace mutated genes with their healthy counterparts and restore their function in the cell indefinitely. This is helpful in case of autosomal-recessive disease, where already low expression of wildtype protein is often sufficient to rescue the phenotype. Dominant forms of disease in turn require the causative gene to be silenced

or rendered harmless, e.g. using RNAi technology or gene editing tools (Hartong et al., 2006). Additionally, neuroprotective factors can be (ectopically) expressed, increasing the viability of the target cells or the surrounding tissue (Sahel & Roska, 2013). To introduce the protein machinery and potentially the nucleotides for gene editing, vectors are required. Mostly, recombinant AAVs have emerged as the vector of choice due to their comparatively low immunogenicity, capsid-specific tropisms (Botto et al., 2022). While gene therapy is without doubt the farthest advanced approach to treat retinal degenerative disease, with several clinical trials ongoing (Battu et al., 2022), its large-scale application to retinal degeneration is complicated by a variety of factors, the most important of which is the vast heterogeneity in causative mutations. Even the treatment of mutations within the same gene would require a personalized medicine approach with meticulous tailoring of the product. Replacement of complete genes to integrate different patient cohorts is thus far unfeasible due to the large gene size that mostly exceeds packaging capacity of current vectors. Furthermore, the time window in which gene therapy would be beneficial is limited, as it requires the presence of viable target cells that can be edited to be saved, making the approach one to be useful in early rather than late-stage disease.

A somewhat similar approach that circumvents in particular the last problem is optogenetics, a technology to control biological activity by light. In the context of retinal degeneration treatments, optogenetics mostly refers to the ectopic expression of microbial opsins such as channelrhodopsin or halorhodopsin, light-activated ion channels and pumps, in residual, electrophysiologically competent cells (McClements et al., 2020). Stimulation with high-intensity light of a specific wavelength then allows the hyper- or depolarization of the target cell, yet requires external devices that project such light onto the retina. Targeting of non-degenerating cells increases the time window available for treatment, especially given that the inner retina, despite being remodeled and reduced, retains some functionality throughout most retinal degenerative disease (Marc et al., 2003). Unfortunately, artificially light-sensitive BC or AC cannot correctly mimic the intricate computations within the retina that occur under healthy conditions, allowing only rudimentary perception of light (Sahel & Roska, 2013). Targeting residual photoreceptors without light perception capacity like the dysfunctional cones present in RP (Milam et al., 1998) on the other hand has been found to allow some use of residual networks, potentially allowing for more detailed vision to return (Busskamp et al., 2010). Similar to gene therapy, clinical trials using optogenetic interventions are ongoing (De Silva & Moore, 2022).

A third approach to re-establishing light perception in the degenerated retina is the re-introduction of light-perceiving units. Using a technical approach, visual prosthetic

devices were already available for implantation into the subretinal or suprachoroidal space (Duncan et al., 2018; Ostad-Ahmadi et al., 2021). Despite some setbacks with regards to adverse effects and cost-effectiveness, initial results were promising and conferred improved light perception in RP patients, providing proof of concept for recovery of at least a small degree of visual perception upon reactivation of the inner retinal circuits. Further material and technological developments are likely to improve device sensitivity, biocompatibility and, importantly, the size of the visual field that can be covered (Chenais et al., 2021).

Re-introduction of light-perceiving units into the degenerated retina can however also be achieved with biological material. As such, PR transplantation represents a promising approach to replace lost cells.

1.3 Cell Replacement as Treatment Approach for Retinopathies

The concept behind PR replacement therapy is simple – if vision is lost due to PR degeneration, introduction of functional PR into the retina has the potential to restore it. In cases of PR degeneration as a consequence of RPE loss or dysfunction, transplantation of RPE has already shown beneficial and multiple clinical trials using human stem cell derived RPE are currently ongoing, yet as of now, only a few clinical trials assessing the safety of using PR replacement or cell support therapy exist (Van Gelder et al., 2022). PR replacement is far more complicated as success requires graft cell integration into the host retina, concomitant with establishment of mature, functional PR structures such as light-sensing OS, supporting IS and connections to the host circuitry through synapses. This multi-faceted goal has not yet been achieved and pre-clinical research on PR transplantation in animal models is not only evolving but required before translation of PR replacement therapy into the clinics.

1.3.1 Transplantations of rodent retinal tissue and cells

The first reports of PR transplantations using rodent donor cells date back almost 40 years (del Cerro et al., 1985; Silverman & Hughes, 1989). Already then survival and maturation of rat derived retinal tissue in the host eye could be shown, with indications of functional improvements in case of previously light-damaged retina (del Cerro et al., 1991). Since then, a lot of work has been performed trying to delineate conditions under which the most extensive restoration of visual function could be achieved.

From early on, intraocular transplantation was performed in one of two ways – using dissociated cells (Gouras et al., 1991) or retinal sheets (del Cerro et al., 1985; Kaplan et al., 1997; Radtke et al., 1999). Transplantation of sheets has the advantage that cells retain their attachments and extracellular matrix surroundings, reducing cell

death and allowing for faster recovery post grafting. The preservation of the original polarity, laminar organization and circuitry can however be considered a blessing and a curse, since it improves graft survival, yet the formation of rosettes in the graft is common and the graft inner retinal layers present an obstacle for potential graft PR to host BC connectivity, an issue that has only recently been addressed in more detail (Matsuyama et al., 2021; Yamasaki et al., 2022). The surgically much more challenging procedure additionally complicates the use of small animal models such as mice, hence sheet transplantations are commonly rather performed in large animal models (Shirai et al., 2016) and rats (Ben M'Barek et al., 2019; McLelland et al., 2018; Seiler & Aramant, 1998; Silverman & Hughes, 1989). Single cell suspension transplantations on the other hand are easier to perform in mouse eyes, allow a much more finely tuned selection of donor cells and a better contact between grafted and host cells, making them the method of choice in the present work. Thus, the further introduction will mainly focus on reports and observations made using the single cell suspension transplantation approach.

Intraocular transplantation of rodent PRs and PR precursors cell suspensions labeled by genetically encoded reporters or injected fluorescent tracers resulted in the presence of similarly labelled PR with mature structures in the host retina, interpreted mainly as incorporation of the grafted cells (Young et al., 2000). In 2006, with the help of the Nrl-GFP rod reporter mouse line, the optimal PR donor age to obtain the largest number of what was then thought to be incorporated cells in the host retina, postnatal day (P) 3-6, was identified (MacLaren et al., 2006). It was further shown that populations enriched for rod precursor cells exhibited an even higher propensity for "incorporation" (Eberle et al., 2012; Lakowski et al., 2011) and that its extent also strongly depends on the mouse model and integrity of the retinal environment the cells were brought into (Barber et al., 2013; Pearson et al., 2010). Most studies since have used such early postnatal cell populations, enriched via fluorescence- or magnetic-activated cell sorting (FACS, MACS) leveraging cell type specific reporters or cell surface markers. Importantly, throughout this time, functional improvements in light-induced retinal and brain activity were reported as a result of the transplantation into various mouse models of retinal degeneration (Barber et al., 2013; Pearson et al., 2012; Santos-Ferreira, Llonch, et al., 2016; M. S. Singh et al., 2013).

In 2016 however, the field was shaken up by the discovery of material transfer (MT) reported by our and other labs (Ortin-Martinez et al., 2017; Santos-Ferreira, Llonch, et al., 2016; M. S. Singh et al., 2016), who could show that rather than integrating, the transplanted cells mainly acted as donors, supplying host cells with cytoplasmic material. Since this included their genetically encoded reporter proteins,

endogenous PR acceptor cells were falsely identified as integrated. Experimentally, the distinction between reporter⁺ cells resulting from material transfer and properly integrated cells was enabled by an array of methods, such as the detection of GFP⁺/dsRed⁺ double-positive cells in the host ONL after transplantation of GFP⁺ PR into dsRed⁺ retina, and Y-chromosome probing upon sex-mismatched transplantations (Figure 4).

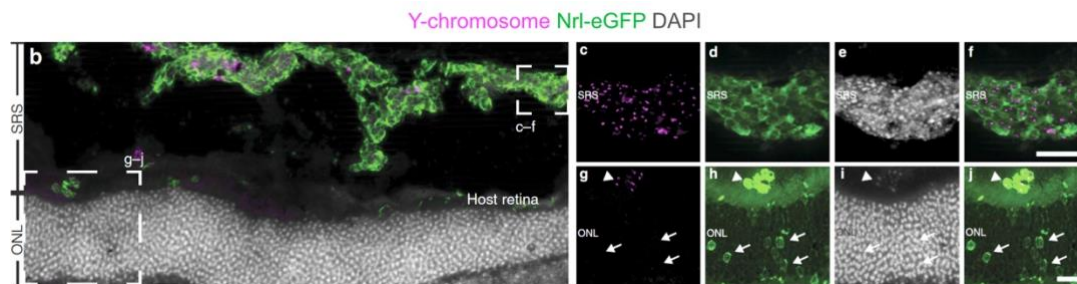


Figure 4. Material Transfer occurring in Mouse-to-Mouse Transplantations.

After transplantation of early postnatal Nrl-GFP labeled male rods into a female wildtype retina, a large, GFP⁺/Y⁺ cluster can be seen in the subretinal space (b-f). Dim GFP⁺ cells within the host retina are however mostly Y⁻ (g), and their GFP⁺ is hence a result of material transfer, not true morphological incorporation. Figure adapted from (Santos-Ferreira, Llonch, et al., 2016).

Further assessment concluded that the amount of properly integrated grafted cells depended strongly on the mouse model used. Of the host lines compared it was highest in the Nrl^{-/-} retina, with a maximum of 23% of GFP⁺ cells within the ONL resulting from incorporation rather than MT, while this fraction was only 1% in wildtype host mice (Santos-Ferreira, Völkner, et al., 2016; Waldron et al., 2018). The structural basis of material transfer was recently uncovered, identifying nanotubes as the main gateway for exchange of mRNA, protein and even organelles such as mitochondria, between donor and host cells (Kalargyrou et al., 2021; Ortin-Martinez et al., 2021). Interestingly, a recent study provided first evidence for material transfer also between cones and rods in the normal, adult retina (Heisterkamp et al., 2022). Importantly, the ability to mediate material transfer is however not restricted to primary retinal cells, as also PR derived from murine embryonic stem cells were found to exchange material with host PR upon transplantation (Waldron et al., 2018).

The high prevalence of material transfer requires a re-interpretation of previous studies, especially with regards to reported improvements in functionality. Cell transplantations were found to improve visual function in mouse models of retinal degeneration, and it was believed that incorporated cells mediated said improvement, as reporter⁺ cells in the ONL were found to contain the protein that was dysfunctional or absent in the mouse host (Pearson et al., 2012). Retrospectively, it is likely that the majority of these cells had rather obtained wildtype protein through MT, supplementing

them and re-instilling the capacity of light perception. While these findings were somewhat disillusioning concerning potential graft maturation after transplantation, they opened another avenue for potential treatment of retinal degenerative disease by cell-mediated supplementation therapies.

1.3.2 Transplantations of human retinal tissue and cells

While rodent-to-rodent transplantations have yielded important insights into the possibilities that human-to-human PR transplantations promise, the human and the rodent retina differ in many aspects, ranging from size to spatial cellular distribution and details of PR function. It is therefore important to adapt pre-clinical research and make use of experimental setups that more closely mimic the human biology, like using human grafts for transplantations into animal models.

As such, human retinal transplantations were first described around 1990, using mostly human fetal retina grafted into rats (Aramant et al., 1990; Ehinger et al., 1991). Promising results with regards to graft survival, maturation and connectivity quickly led to studies transplanting into human RP patients around the millennium, utilizing mainly fetal or post-mortem retinal sheets (Das et al., 1999; Kaplan et al., 1997; Radtke et al., 1999, 2002, 2004, 2008; Seiler & Aramant, 1998). Despite the lack of an immune-suppressive treatment, grafts were mostly well retained and in some cases even an increase in visual function was reported (Radtke et al., 2004, 2008). Despite these encouraging results, the tissue source raised important concerns regarding ethics, supply and safety.

Around the same time, stem cell biology advanced significantly, with the first human embryonic (hESC) and, a little later, human induced pluripotent stem cells (hiPSC) generated in 1998 and 2007 respectively (Takahashi et al., 2007; Thomson et al., 1998). These pluripotent cells were quickly employed for the in vitro differentiation of retinal cells and in 2006 cultivation of hESC-derived neural progenitors with detectable retinal-specific transcripts was first reported (Banin et al., 2006; Lamba et al., 2006). However, mature photoreceptors were not yet obtained with these two-dimensional protocols.

Regardless, the in vitro neural progenitors were employed in transplantation studies in rats and mice, where they were reported to survive for up to 16 weeks with immune suppression using cyclosporine A. While these were promising initial results, the grafted cells mostly remained in the subretinal space without obvious contact to the host retina and the staining for photoreceptor-specific markers remained weak whereas glial and neuronal markers were strongly expressed (Banin et al., 2006). Shortly thereafter, migration of hESC-derived neural progenitors into the murine retina was

reported, with concurrent maturation towards photoreceptor fate in as little as 6 weeks (Lamba et al., 2009). The human cells had been transduced with lentivirus at 5-7 days before grafting, driving GFP under control of the CMV promoter, and thus intraretinal GFP⁺ cells were interpreted as human. Unfortunately, no further proof of human cell identity was shown and given that the proclaimed human cells exhibited murine photoreceptor morphology and the same nuclear size as the surrounding mouse rods, it is much more likely that the GFP⁺ intraretinal cells were instead a result of viral mislabeling or material transfer rather than true integration events.

In the years to follow, two-dimensional human photoreceptor in vitro generation protocols were further improved (Osakada et al., 2008) yet the biggest innovation was published by the Sasai lab in 2011/2012, which provided a new method to generate three-layered murine and human retinal structures (Eiraku & Sasai, 2011; Nakano et al., 2012). The process included the provision of complex extracellular matrix (ECM) components via Matrigel and much more closely mimicked normal development in conjunction with the formation of optic cups than previous approaches. Subsequently, the Gamm lab developed a protocol similarly yielding optic vesicle-like structures by applying a switch from floating to adherent culture, followed by manual lifting of the resulting eye-field rosettes (Ohlemacher et al., 2015). Protocol improvements in human retinal organoid (HRO) formation throughout the years continued to increase the efficiency of HRO induction, PR yield and maturation, and thus enabled the creation of large numbers of human PRs as cell source for transplantation studies (Cowan et al., 2020; Kim et al., 2019; Lowe et al., 2016; R. K. Singh et al., 2021; West et al., 2022; Zerti et al., 2020; Zhong et al., 2014; Y. Zhu et al., 2013).

Current HROs not only contain most retinal cell types, mimicking the native retinal organization, but are also able to mirror in vivo developmental timing and trajectories as well as photoreceptor functionality (Cowan et al., 2020; Llonch et al., 2018; Saha et al., 2022; R. K. Singh et al., 2021). While the plethora of HRO generation protocols in use generally results in similar outcomes, it is important to note that they do contain differing cell ratios and developmental timing as a consequence of the HRO generation method and the cell line used as starting population (Berber et al., 2021; Cowan et al., 2020; Mellough et al., 2019). This warrants the careful characterization of outcomes when using new cell lines, adapting the HRO protocol or using HRO cells for PR replacement research (Capowski et al., 2018; Kruczek & Swaroop, 2020), where, crucially, the use of HRO PRs circumvents ethic and logistic concerns associated with the use of fetal material for research and therapeutic applications.

Given the recent advances in gene editing, it has further become possible to generate patient-specific donor cell lines and rescue the disease-causing mutations.

Autologous transplantation of such lines further reduces the risk for graft rejection and potentially allows for the use of milder immune-suppressive paradigms. While personalized medicine is an appealing prospect, the establishment of super donor lines, e.g. HLA- homozygous lines, that can be grafted into many people on the other hand would provide a more efficient treatment potential with respect to both, time and financing.

Since the availability of in vitro generated human PR, PR transplantation studies have largely shifted to using HRO PRs as donor population. Due to PR replacement being considered a last resort in the treatment of IRDs, and in an attempt to circumvent the complication of material transfer, most research targeted the highly degenerated mouse or rat retina (Barnea-Cramer et al., 2016; Collin et al., 2019; Gonzalez-Cordero et al., 2017; Ribeiro et al., 2021; Zerti et al., 2021; J. Zhu et al., 2017). Commonly, 100,000 to 300,000 donor cells aged day (D) 90-D150 of differentiation were grafted. To reduce xenograft rejection, systemic immune suppression was applied or immune-deficient animals were used as hosts. However, even in eyes without immune modulation about half of the eyes that had received grafts were found to still contain cells after 3 weeks (Gonzalez-Cordero et al., 2017). With immune suppression, that fraction was reported to increase up to 80%, albeit with low remaining cell numbers (Zerti et al., 2021). Morphologically, the human cells mostly remained in the subretinal space, in contact with the residual ONL and/or the remodeled INL, with PR and BC processes extending from one to the other. Overall graft organization however largely remained chaotic and despite expression of PR markers, structured PR polarization was not evident (Gonzalez-Cordero et al., 2017; Ribeiro et al., 2021; Zerti et al., 2021).

To this day, little work on HRO PR transplantation into less degenerated host animals has been performed. Upon grafting into the wildtype rat retina, D120 PR enriched by cell surface labelling against CD73⁺ were found to not only survive for up to 10 weeks, but seemed to intercalate with the host ONL cells (Gagliardi et al., 2018). While expression of both rod and cone opsins was detected, the grafts again seemed unstructured and poorly polarized and a detailed analysis was hampered due to poor graft survival with only two eyes with remaining cells at this later time point. Similarly, transplantation into the cone-rich *Nrl^{-/-}* mouse resulted in largely disorganized subretinal clusters, with single donor cells occasionally moving into the ONL and exhibiting the development of prospective IS and OS, albeit at a very low rate (Gonzalez-Cordero et al., 2017). Here, the authors also investigated the possibility of human to mouse material transfer through assessment of nuclear size, which differs markedly between human and murine cones, and Y-chromosome probing after sex-mismatched transplantations. Gonzalez-Cordero et al. concluded that there was little evidence for such an effect, yet

they did detect some murine cells expressing GFP. L/M-Opsin-promoter driven GFP expression had been introduced into the experimental system by viral labelling of the human donor cells before transplantation and it is important to note that a carry-over of either GFP itself or viral particles inducing GFP expression in murine cells was indeed taking place. Importantly, this did not occur in the retinas that had received control injections of the final wash step from the cells, suggesting that this was not a sufficient control and that the human cells do mediate some exchange of intracellular or viral material with mouse host PR (Gonzalez-Cordero et al., 2017).

With hESC/hiPSC PR survival in the mouse subretinal space established, the focus shifted towards assessment of maturation, integration into retinal circuitry and functionality of the grafted cells. The latter could recently be shown upon transplantation of 500,000 PR aged D120 into the rd1 mouse, a quickly deteriorating model of end-stage retinal degeneration (Ribeiro et al., 2021). Here, the authors reported large cell clusters, which – despite an overall unorganized structure – bore evidence of maturation in the form of peripherin 2 (PRPH2)-positive nascent human outer segments and exhibited a close interaction with the murine INL as evidenced by extension of bipolar cell processes into the graft. Importantly, this resulted in increased light perception of transplanted animals as read out by the behavioral light-dark box (LDB) assay and electrophysiological retinal recordings using multi-electrode arrays (MEA). To control for the possibility of the graft mediating functional improvements by neurotrophic support of the degenerating host rather than proper integration, Ribeiro et al. in parallel transplanted dysfunctional cones, which did not lead to significant changes in light-dependent behavior and retinal electrophysiological responses (Ribeiro et al., 2021).

While single cell suspension transplantations of HRO PR have yet failed to yield well organized, polarized human PR layers, availability of HROs has also enabled the more wide-spread application of hESC/hiPSC-derived retinal sheet transplantations. Due to size considerations, HRO sheet transplantations have mostly been applied to rats and larger animal models, such as non-human primates (Lin et al., 2018; McLelland et al., 2018; Shirai et al., 2016; Tu et al., 2018; Watari et al., 2022; Yamasaki et al., 2022). Similarly to single cell suspensions, extension of host secondary neuron bipolar processes into the grafts was observed, and importantly, visual improvements could be detected by MEA, focal electroretinogram, and cortical recordings from the superior colliculus (Iraha et al., 2018; Lin et al., 2018; McLelland et al., 2018; Tu et al., 2018). Structurally, the problematic presence of a graft inner retinal layer could recently be addressed, allowing for a more direct interaction of graft and host neurons (Yamasaki et al., 2022). One common remaining phenotype observed in all grafted sheets is however the general disorganization and the development of large, intra-graft rosettes,

within which the maturing IS and OS compartments are located. Mostly, as a hallmark of a variety of retinal disorders, rosettes were believed to be a sign of retinal dysfunction and degeneration (Zweifel et al., 2009), unable to sustain light perception due to the physical separation of PR and in particular their OS from the RPE. Yet here, they seem to allow light perception to occur and it will be therefore be vital to examine the longterm survival and functionality of the grafted, rosetting sheets for future applications.

In summary, transplantation of hESC/hiPSC-derived HRO PRs holds great promise as a potential treatment avenue to re-establish vision in patients with IRDs. Given the recent advances in gene editing, it has further become possible to generate patient-specific donor cell lines and rescue the disease-causing mutations. Autologous transplantation of such lines further reduces the risk for graft rejection and potentially allows for the use of milder immune-suppressive paradigms. While personalized medicine is an appealing prospect, the establishment of super donor lines that can be grafted into many people on the other hand would provide a more efficient treatment potential with respect to both, time and financing. However, major challenges before clinical translation still remain, as better knowledge is required on how to enlarge the retinal area covered, how to ensure graft longterm survival, and, how to increase the extent of PR maturation and integration into the host retinal circuitry.

1.4 Aim of this Thesis

Photoreceptor replacement therapy is an exciting potential treatment option for retinal degenerative diseases. Introduction of functional photoreceptors into the dysfunctional retina holds the promise to provide healthy, light-sensing cells, which, upon polarized maturation and integration into the residual host circuitry, have the capacity to re-establish vision. With the recent availability of large numbers of in vitro generated human photoreceptors to use as donor cells, research has been given a tremendous opportunity and task to understand how such a result can be best achieved. While promising results have already been obtained, a systematic comparison of the optimal donor population is still lacking. Similarly, most pre-clinical research on human-to-rodent transplantations utilized end-stage models of retinal degeneration and little is known about human graft performance in other degeneration stages.

The aim of this thesis was therefore to evaluate the outcome of human retinal organoid derived photoreceptor transplantation into the cone photoreceptor function loss 1 mouse model of cone-only retinal degeneration. With particular emphasis on effects mediated by donor cell age, the focus lay furthermore on the possibility to detect and characterize differential outcomes instrumental to ultimately obtaining functional grafts.

2 Characterization of Crx-mCherry Human Retinal Organoids as Photoreceptor Cell Source

2.1 Aims

Since their first isolation, a multitude of human embryonic and pluripotent stem cell (hESC, hiPSC) lines have been created. Together with improvements in human retinal organoid (HRO) culture, they now allow the generation of large numbers of human photoreceptors (PRs). Introduction of cell type specific reporter constructs further allows for the enrichment of select cell types, as has been shown to be beneficial in PR transplantation studies. To obtain large numbers of human PRs through HRO culture and subsequent fluorescence-activated cell sorting (FACS), a previously published photoreceptor-specific reporter hiPSC line was acquired. To ensure that the cell line could be used as donor cell line for PR transplantation studies, this part of the study aimed at characterizing its capacity for HRO formation using the in-house protocol, as well as assessing the specificity of the reporter construct expression.

2.2 Characterization of Crx-mCherry Reporter-expressing Cells

2.2.1 Crx-mCherry expression overlaps with endogenous CRX expression and increases over time

To be able to enrich for human photoreceptors, here, the human induced pluripotent stem cell line Crx-mCherry was used for HRO generation (Gagliardi et al., 2018). Reprogrammed from post-mortem human Müller glia, the Crx-mCherry line contains a reporter construct expressing an mCherry fluorescent reporter protein, fused to a histone 2B fragment for nuclear localization, under the control of the murine Crx promoter. While the Crx-mCherry hiPSC line was already reported to reliably label photoreceptors (Gagliardi et al., 2018), the expression timeline and target specificity of the reporter protein was additionally confirmed by co-staining for endogenous CRX.

The Crx-mCherry reporter primarily labelled cells within the neuroepithelial rim, which were also found to stain positive for CRX (Figure 5A'). Additionally, Crx-mCherry expression was detected in less organized HRO regions such as the core or accessory structures, however also there it was found to co-label with endogenous CRX, confirming that the Crx-mCherry reporter label was indeed consistent with endogenous CRX expression (not shown).

Crx-mCherry expression was found to be induced between day (D) 30 and D60 in culture (Shastri, 2020). The percentage of Crx-mCherry⁺ nuclei continued to increase

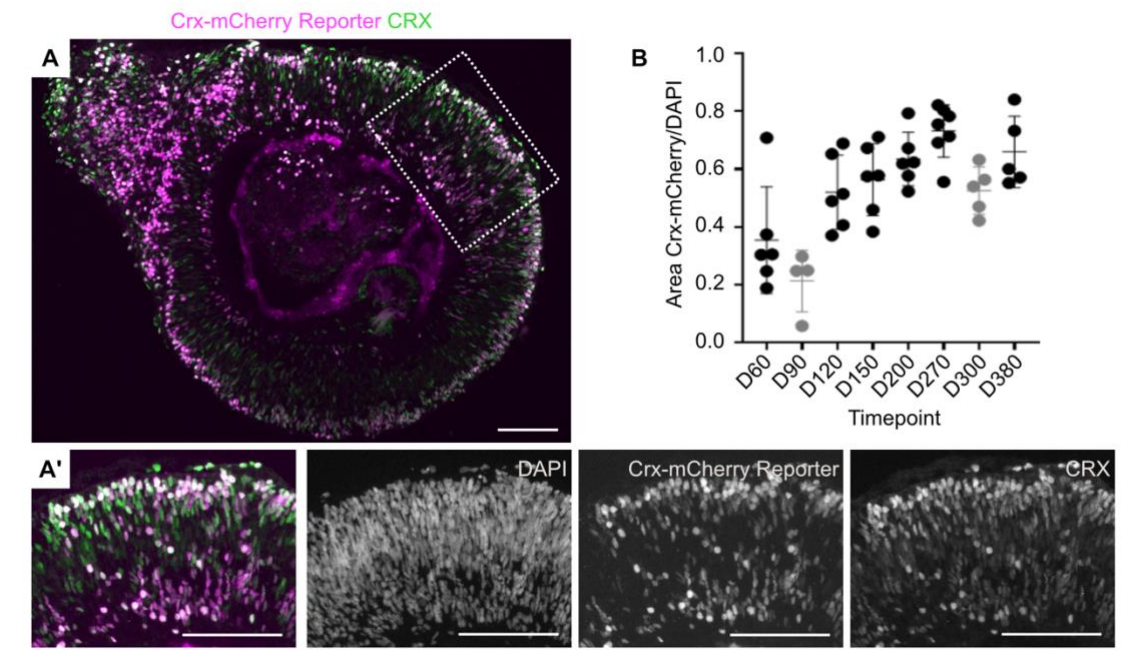


Figure 5. Crx-mCherry co-localization with CRX and Increase over Time.

A. Crx-mCherry reporter signal and CRX antibody signal in section through an entire D120 human retinal organoid (HRO) with a magnification of the neuroretinal rim region (**A'**). **B.** Increase in Crx-mCherry⁺ nuclear area in the neuroretinal rim as fraction of total DAPI area over time. Grey values represent analysis of HRO with poor structure. Adapted from (Shastry, 2020) Scale bars: 100 μ m.

until D270, representing roughly up to 75% of all organoid cells in the neuroretinal region. At later stages, the proportion of Crx-mCherry⁺ nuclei appeared again slightly reduced (ca. 65% at D380, Figure 5B).

2.2.2 Crx-mCherry organoids contain an outer and an inner nuclear layer

While hiPSC are capable of producing HRO containing all retinal cell types, the largest group of cells present in HRO besides photoreceptors are Müller glia (MG). In the retina, MG nuclei normally reside in the inner nuclear layer, extending processes through all layers. Staining for MG markers such as PAX6 and SOX9 showed the correct localization of MG nuclei in the inner nuclear layer below the CRX⁺ outer nuclear layer (Figure 6A, B), while CRALBP⁺/GLAST⁺ MG processes extended throughout the entire neuroepithelium (Figure 6C). Note that the nuclear MG labels and the Crx-mCherry signal were exclusive at the timepoint shown, D150 in culture.

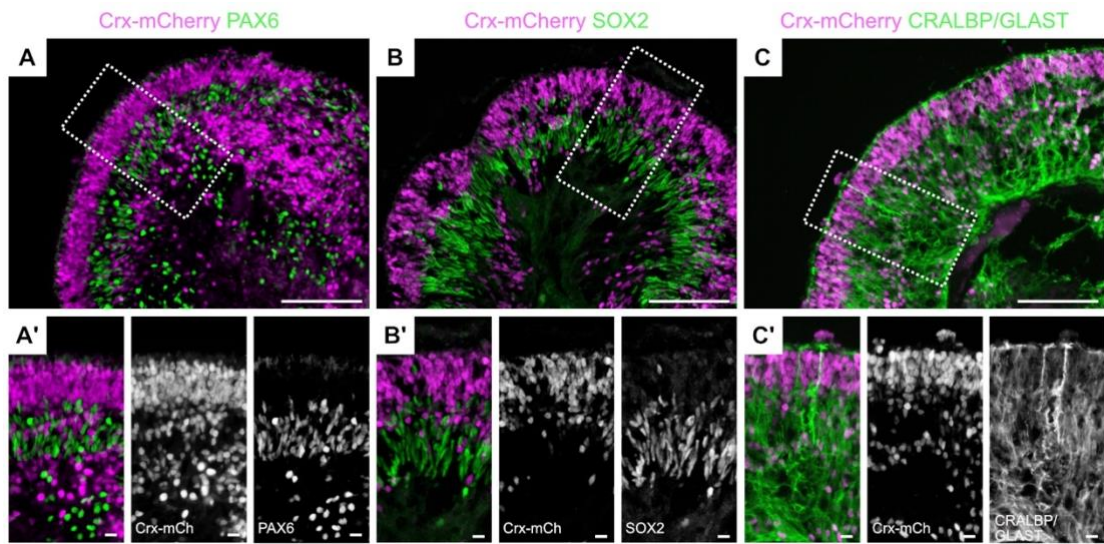


Figure 6. Müller Glia in D150 Crx-mCherry Organoids.

A, B. In Crx-mCherry organoids, Müller glia nuclei marked by PAX6 (**A**) and SOX2 (**B**) correctly localise to the inner nuclear layer below the Crx-mCherry⁺ outer retinal layer. **C.** Müller glia cell bodies extend throughout all organoid layers. Scale bars: A-C 100 μ m; A'-C' 10 μ m.

2.2.3 Crx-mCherry⁺ cells express early and mature rod and cone markers

As an early and continuously active transcription factor inducing photoreceptor fate, CRX expression should be detectable in retinal progenitor cells, rods and cones. In HRO cryosections of D300 HROs, Crx-mCherry in the outer nuclear layer (ONL, Figure 7A) of the neuroepithelium was accordingly found to co-localise with the rod specific transcription factor NRL (Figure 7B) or surrounded by the cytosolic cone marker ARR3 (Figure 7C). As consistent with the in vivo situation, the cones localized to the outer, and the rods localized to the inner portion of the PR layer. Sometimes, Crx-

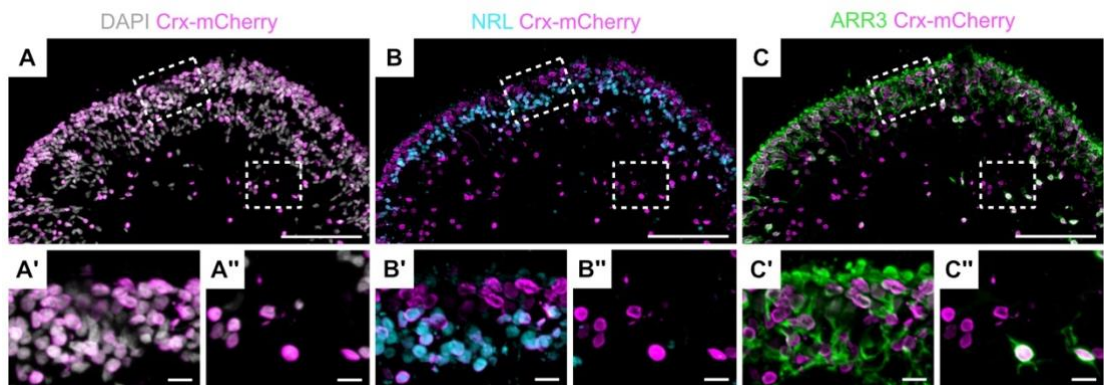


Figure 7. Crx-mCherry⁺ Cells express Early Rod and Cone Markers.

A-C. D300 HRO showing Crx-mCherry expression in the ONL (**A, A'**) colocalizing with NRL expression (**B, B'**) in the inner ONL portion. In the outer ONL portion, the Crx-mCherry signal is surrounded by expression of ARR3, a cytosolic cone marker (**C, C'**). Crx-mCherry⁺ cells in the HRO core occasionally also co-label for photoreceptor markers (**A'', C''**). Scale bars: A-F 100 μ m; A'-C', A''-C'' 10 μ m.

mCherry⁺ cells that were negative for either rod- or cone marker were detected at this late stage. This was however usually only the case for low numbers of Crx-mCherry⁺ in the core structure of the HRO, not the neuroepithelial rim (Figure 7B'', C'').

Mature functional PRs have a highly asymmetric structure, and consist of four distinct compartments, amongst which the inner and outer segments (IS and OS) are particularly important for light detection. Within the OS, PR-specific opsin photopigments are enriched, with rhodopsin (RHO) expressed in rods, and long-, medium- or short-wave opsin expressed in human cones (OPN1LW, OPN1MW, OPN1SW respectively). In HRO cryosections, OPN1L/MW staining can be seen in cell bodies surrounding Crx-mCherry nuclei (Figure 8A) and enriched (bright staining) towards the apical border of the HRO. Looking at an HRO wholemount from the top, the distribution of OPN1L/MW⁺ and OPN1SW⁺ cell bodies can be seen, with OPN1L/MW cells appearing to outnumber OPN1SW cones (Figure 8B).

Similarly, apically enriched RHO staining is also visible in an HRO cryosection (Figure 8C) and an HRO wholemount co-stained with the pan-PR marker RCVRN (Figure 8D). While cytosolic RHO staining is present, its strong enrichment towards a

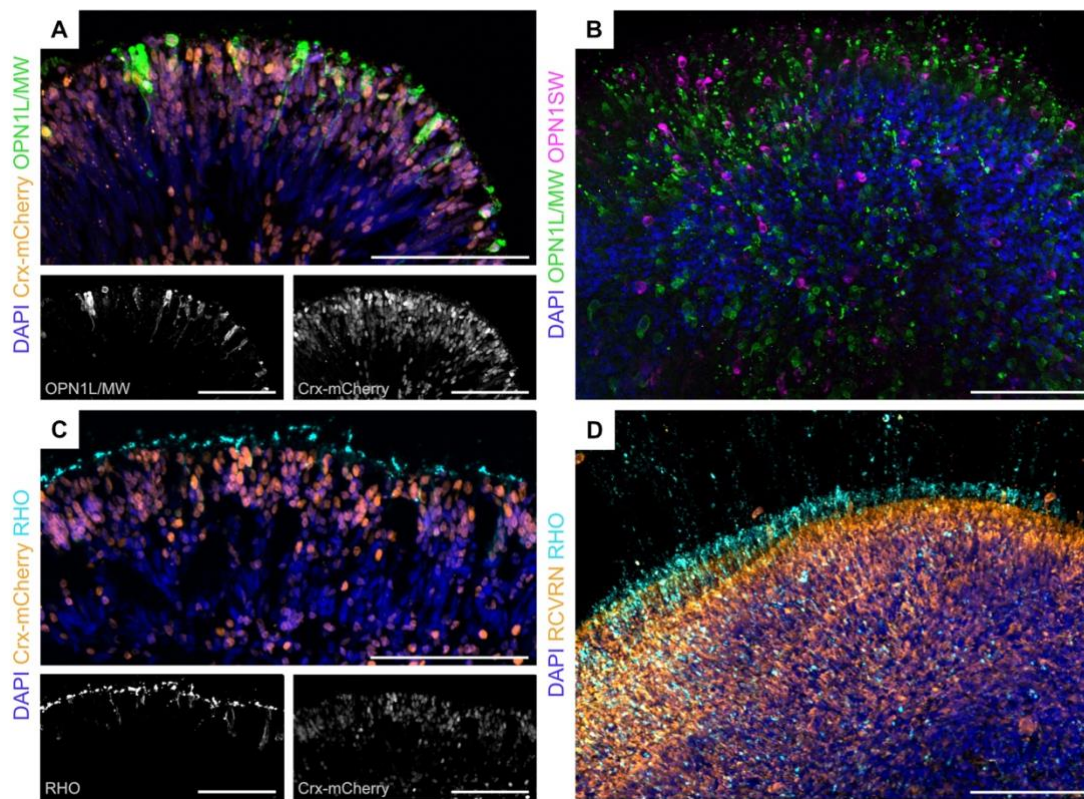


Figure 8. Crx-mCherry⁺ Cells express Mature Photoreceptor Markers.

A, C. D150 HRO cryosections stained for cone (A) and rod (C) opsins. **B, D.** D200 HRO wholemounts looking at the organoid surface (apical PR side) from the top, stained for cone (B) and rod (D) opsins. Scale bars: all 100 μ m.

prospective OS makes the cytosolic label and the association with the Crx-mCherry nuclei difficult to appreciate (Figure 8C, RHO single channel).

2.2.4 Crx-mCherry⁺ cells do not express proliferation markers

Here, the goal for Crx-mCherry HRO generation was the enrichment for Crx-mCherry⁺ photoreceptors and their transplantation into the murine retina. Due to the xenografic nature of the transplantation, survival of the Crx-mCherry⁺ cells in the host animals requires local immune suppression. This can in turn enhance the risk for teratoma formation, should proliferative cells be contained in the transplant cell suspension. Assessment of proliferation in Crx-mCherry organoids showed that in

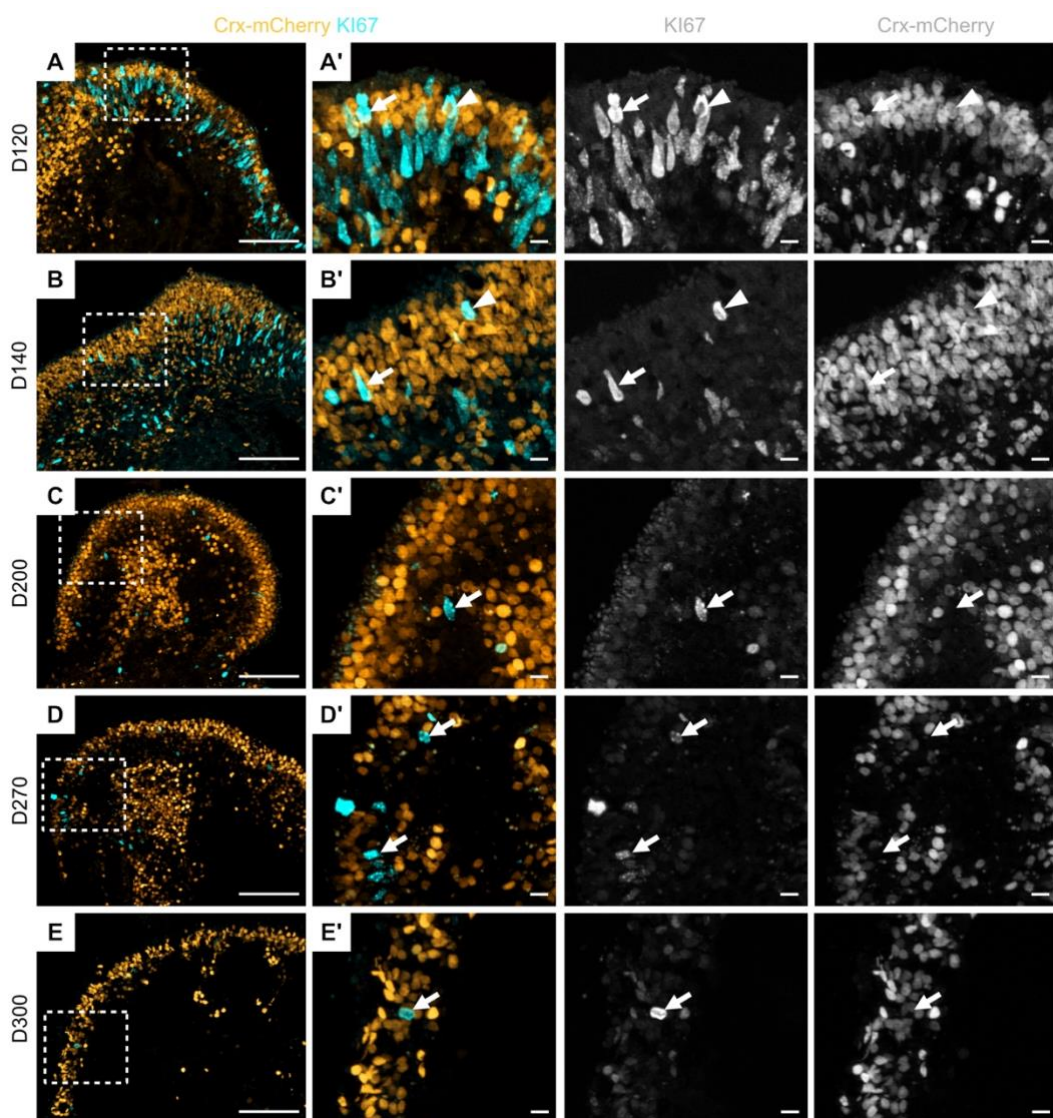


Figure 9. Decrease in KI67⁺ Cell Number during Organoid Maturation.

A-E. Crx-mCherry and KI67 staining of HROs from D120 to D300 with magnifications in **A'-E'**. The vast majority of KI67⁺ proliferative cells is Crx-mCherry⁻ (arrows), while only a few nuclei in **A'** and **B'** show double-labeling (arrowheads). Scale bars: A-E 100 μ m; A'-E' 10 μ m.

HROs younger than D200, occasional co-staining of Crx-mCherry with KI67 could be detected (Figure 9, A', B', arrowheads). The majority of KI67 signal was however exclusive with Crx-mCherry fluorescence (Figure 9, A'-E', arrows) and overall, the proliferative potential of the HRO drastically decreased between D140 and D200 (Figure 9).

2.3 Enrichment and Characterization of Crx-mCherry⁺ Donor Cells

2.3.1 Enrichment of Crx-mCherry⁺ cells by FACS

To enrich for Crx-mCherry⁺ cells, HRO were dissociated and submitted to flow cytometry. Gating out cell debris and duplets by forward and sideward scatter, as well as dead cells by DAPI exclusion yielded a population of live single cells (see methods section 8.3.2.2 for details on gating). This population contained true mCherry⁺ cells, but also auto-fluorescent cells, as defined by their double-positivity in the mCherry channel and in a second channel, which was either GFP- or FarRed-detecting. To reliably select mCherry⁺ cells, mCherry fluorescence was therefore plotted against either fluorescence channel and only mCherry⁺/autofluorescence⁻ cells were selected. The auto-fluorescent intensity increased with HRO age, yet its percentage decreased over time.

Over the course of HRO development the percentage of mCherry⁺ cells in the live singlets increased from ca. 30% at D90 to on average 73% at D200, after which it did not seem to increase further (Figure 10). FACS successfully enriched for mCherry⁺ cells at all ages, gaining a population with 97% to 99% purity (Figure 10).

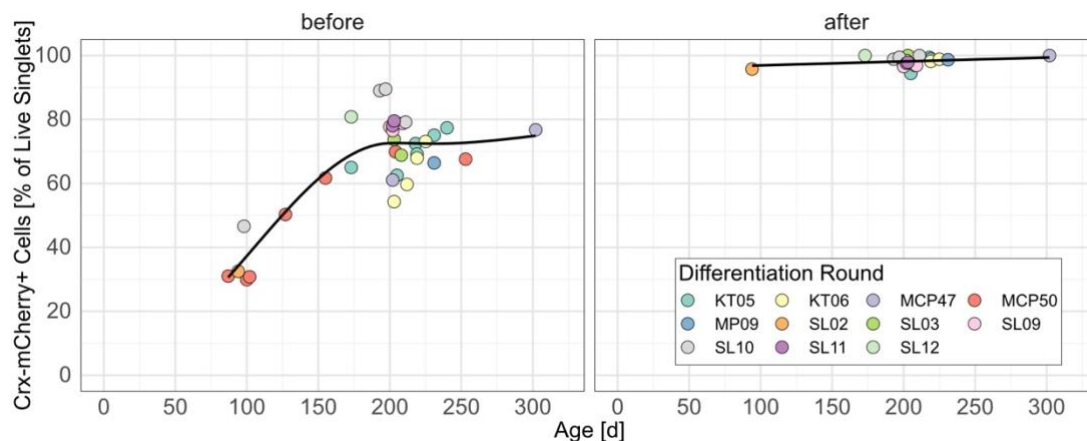


Figure 10. Percentage of Crx-mCherry⁺ cells before and after FACS enrichment.

Percentage of Crx-mCherry⁺ cells as measured by flow cytometry before and after sorting over the course of HRO development. Note that fewer datapoints are present after sorting, as some samples were only analysed, not sorted.

2.3.2 Characterization of Crx-mCherry enriched cells by single cell sequencing

Sorted Crx-mCherry⁺ cells were analyzed for cell identity by single cell sequencing over the course of development at ages D100, D200, D270 and D370. Clustering and manual cell type annotation from known marker genes allowed the identification of cones, rods and Müller glia (MG, Figure 11A-C, E). Two other clusters could not be precisely mapped to a specific cell type as they seemed to contain a mixed population of cells, expressing e.g. bipolar cell (e.g. GSG1, Figure 11D, E) MG genes as well as transcripts present in late neurogenic human retinal progenitor cells and cones (e.g. PLP1, SOX4 and DCT respectively, data not shown). Their identification requires further analysis and the clusters were hence both termed “other”.

Surprisingly, at D100 only 40% of mCherry⁺ cells were found to be clearly identifiable as photoreceptors, with 37% cones and 3% rods (Figure 11F). A small fraction (6%) of Crx-mCherry⁺ cells at D100 was found to be MG, while the majority of cells (54%) at that timepoint were of the “other” type. Importantly, one of the two “other” clusters consisted almost entirely of D100 cells, as can be seen on the UMAP color-coded for cell age (Figure 11G, red cluster on the left). At D200, the MG cluster was reduced to 4%, and completely absent at later stages. The “other” cluster similarly decreased in number over time, representing only 31%, 19% and 11% of cells at D200, D270 and D370. Accordingly, the percentage of photoreceptors increased steadily to

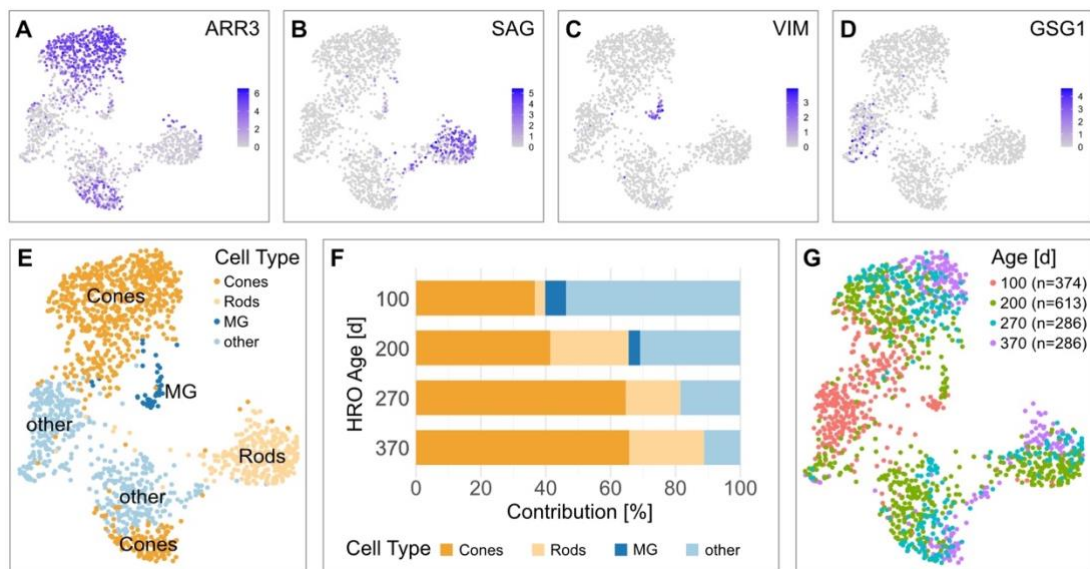


Figure 11. Transcriptome Analysis of HRO Crx-mCherry⁺ Cells by Single Cell Sequencing.

A-D. UMAP plot showing normalised expression levels of representative cell type marker genes allowing the manual identification of clusters containing mainly cones (**A**, ARR3), rods (**B**, SAG) and MG (**C**, VIM) or a mix of cells such as bipolar cells (**D**, GSG1). **E.** UMAP plot color-coded for cell types as manually identified. **F.** Quantification of cell type fractions per HRO age. **G.** UMAP plot color-coded for HRO age.

66%, 81% and 89% until D370, at which point there were 66% cones and 23% rods. The proportion of cones was consistently higher than the proportion of rods across all timepoints.

2.3.3 Characterization of D200 Crx-mCherry-enriched cells by immunocytochemistry

As single cell sequencing measures the presence of transcripts, it is important to validate these findings by detecting the presence of the respective proteins. To assess the donor cell population further, unsorted, positive and negative sorted cells from HRO at D200 were thus assessed by immunocytochemistry (ICC). ICC confirmed the enrichment of Crx-mCherry⁺ cells from on average 68% to 94% in the positive fraction, while the negative fraction only retained 11% of Crx-mCherry⁺ cells (Figure 12). Similar to the results from single cell sequencing, at D200 65% of the positive fraction were photoreceptors, as measured by expression of the pan-photoreceptor marker RCVRN. This represented an increase of 19% from the unsorted fraction. ICC also confirmed that the majority of D200 Crx-mCherry⁺ photoreceptors were cones, as 35% of the unsorted and 46% of the positive fraction were labelled with the antibody against ARR3. The negative fraction was almost entirely depleted of photoreceptors, as only 3% of cells were positive for RCVRN and ARR3. Unfortunately, markers for other cell types could not successfully be stained, leaving the remaining 35% of cells in the positive fraction unidentified.

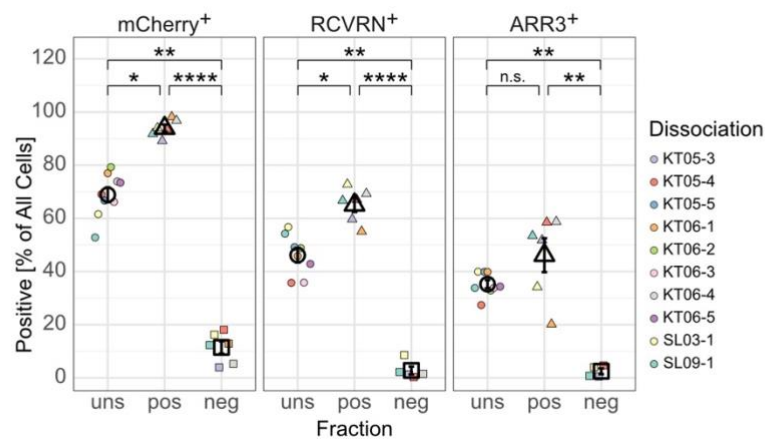


Figure 12. Assessment of D200 Sorting for Crx-mCherry by ICC.

Quantification of mCherry and cell type marker expression in D200 cell suspension fractions before FACS (unsorted, uns), and after sorting for mCherry positive (pos) and mCherry negative (neg). Hollow symbols and bars show mean±SE, n.s. $p > 0.05$, * $p < 0.05$, ** $p < 0.005$, *** $p < 0.0001$, see Table 4 for details on statistical test.

2.4 Summary

Using the optimized in-house human retinal organoid generation protocol, the Crx-mCherry human iPSC line can be used to reliably generate human retinal organoids containing all principle intrinsic cells of the retina mainly organized in the typical layered tissue architecture. Crx-mCherry⁺ cells robustly express endogenous CRX and the majority stain positive for various photoreceptor markers, with only a small sub-population of Crx-mCherry⁺ cells in the organoid core not showing photoreceptor-specific labelling. At D150 in culture, these cells also do not colabel with markers of Müller glia, the third most prevalent cell type in organoids generated with the present protocol.

Upon HRO dissociation and sorting, Crx-mCherry⁺ cells could reliably be enriched. While at D100, roughly 40% of sorted Crx-mCherry⁺ cells were clearly identifiable as photoreceptors with the majority being cones, that value increased to almost 90% over the course of development. The remaining cells could not yet be confidently mapped to a specific cell type, but preliminary data suggests they might represent a heterogenous population of immature photoreceptors, Müller glia or bipolar cells. Immunocytochemistry of D200 single cell suspensions validated the photoreceptor ratios inferred from single cell sequencing results.

Overall, the Crx-mCherry human iPSC line appears as a highly useful source for the generation of large amounts of reporter-labeled human photoreceptors for transplantation experiments.

3 Transplantation of Human Crx-mCherry⁺ Grafts aged D100, D200 and D300 into Cpf1 Mice

3.1 Aims

While several laboratories use human retinal organoid (HRO)-derived photoreceptors for transplantation studies, the optimal donor cell age allowing robust donor photoreceptor survival, maturation and integration into the host retinal circuitry after transplantation has not been determined. In addition, most human photoreceptor transplantation studies so far were aimed at animal models with end-stage retinal degeneration, i.e. with near to complete loss of the photoreceptor layer. Human retinal dystrophies however present with various degrees of photoreceptor degeneration at different stages and not much is known about human photoreceptor transplantation outcome in less degenerated models.

The aim of this chapter was therefore to assess which developmental stage of Crx-mCherry⁺ human iPSC-derived photoreceptors would result in a preferable transplantation outcome upon delivery into the cone-only degeneration Cpf1 mouse. As photoreceptor replacement aims at restoring visual transduction and signal transmission to the host, the optimally desired outcome was defined as mature photoreceptors that are fully integrated in the host retinal circuitry.

3.2 Crx-mCherry⁺ Cells of all Ages can be Transplanted and Survive in the Murine Retina

Human Crx-mCherry⁺ cells from developmental stages D100, D200 and D300 were dissociated, enriched using FACS and transplanted into the subretinal space of adult Cpf1 mice (Figure 13A, B). Directly following transplantation and every 4 weeks thereafter the immunosuppressant triamcinolone acetonide was applied intravitreally to prevent rejection of the xenograft. At 10, 26 or 41 weeks post transplantation (wpt) experimental eyes were collected and analyzed. These timepoints were chosen to account for overall age of the cell, i.e. D100+26 weeks (w) is roughly equivalent in age to D200+10w at around D270 overall. Similarly, D100+41w, D200+26w and D300+10w grafts are approximately D370 (Figure 13B).

At time of analysis, grafts were found in 97% of experimental eyes (88 of 91), which represent a highly successful survival rate using the paradigm described.

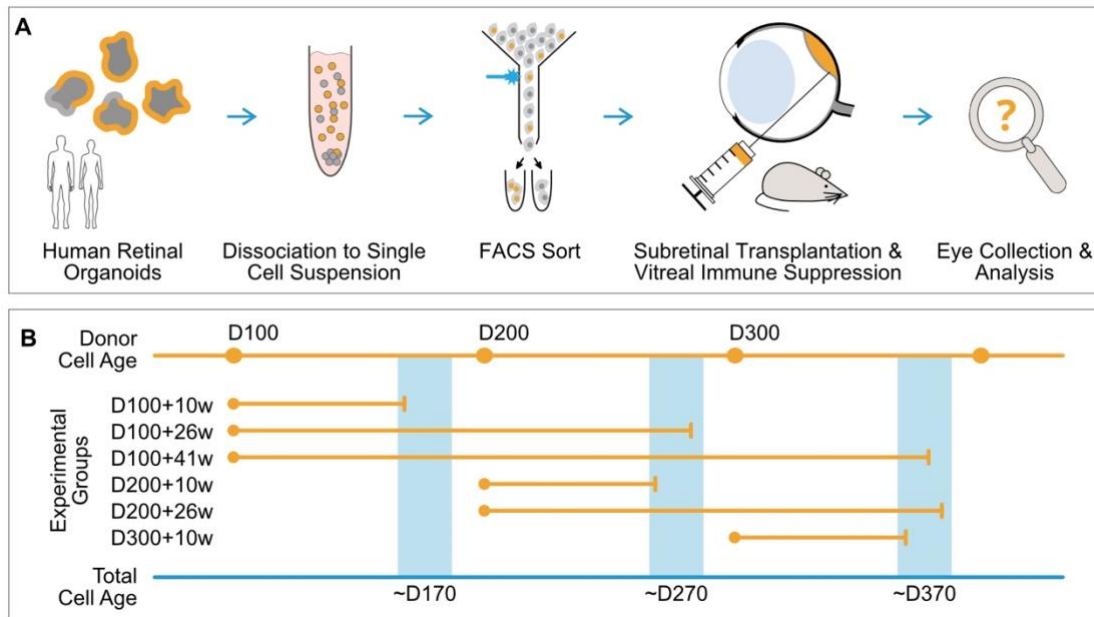


Figure 13. Experimental Setup and Timeline.

A. Human retinal organoid (HRO) cells were dissociated and sorted for Crx-mCherry expression. The mCherry-enriched single cell suspensions were then transplanted subretinally into the Cpf1 mouse host, with local immune suppression through vitreal application of triamcinolone acetonide. **B.** Experimental timeline showing all experimental groups, using donor cells of D100, D200 or D300 old HROs. Following up 10, 26 or 41 weeks also allowed to compare outcomes between grafts of different donor, but similar total age at ~D170, ~D270 and ~D370. FACS: Fluorescence-activated cell sorting, D: day, w: weeks.

3.2.1 Human grafts can be identified by RCVRN staining

While grafted human cells continued to express the Crx-mCherry reporter, the signal intensity was highly variable and thus difficult to use for quantifications. To examine differences in graft size between donor ages, detection of the full graft area via a cytosolic stain was used instead. Staining for RCVRN allowed to detect the cytosol of both rods and cones (Figure 14A-A''). Although the antibody used is not specific for human cells, its signal was much stronger in the transplanted cells than in the endogenous PR (Figure 14A-A'', arrowheads and arrows respectively), making it a viable option for graft size quantification.

3.2.2 D100 Crx-mCherry+ transplants are larger than D200 and D300 grafts

To assess transplant survival, graft size was quantified by measuring the RCVRN⁺ graft area of every fourth serial section per eye. The resulting value was multiplied by four and the section thickness to estimate the full volume. Although each eye received 1 μ l of cell suspension containing 150,000 cells, the graft volume differed strongly between donor ages, with D100 donors resulting in the largest grafts, irrespective of follow-up timeframe (Figure 14B). Due to the large variation in the data

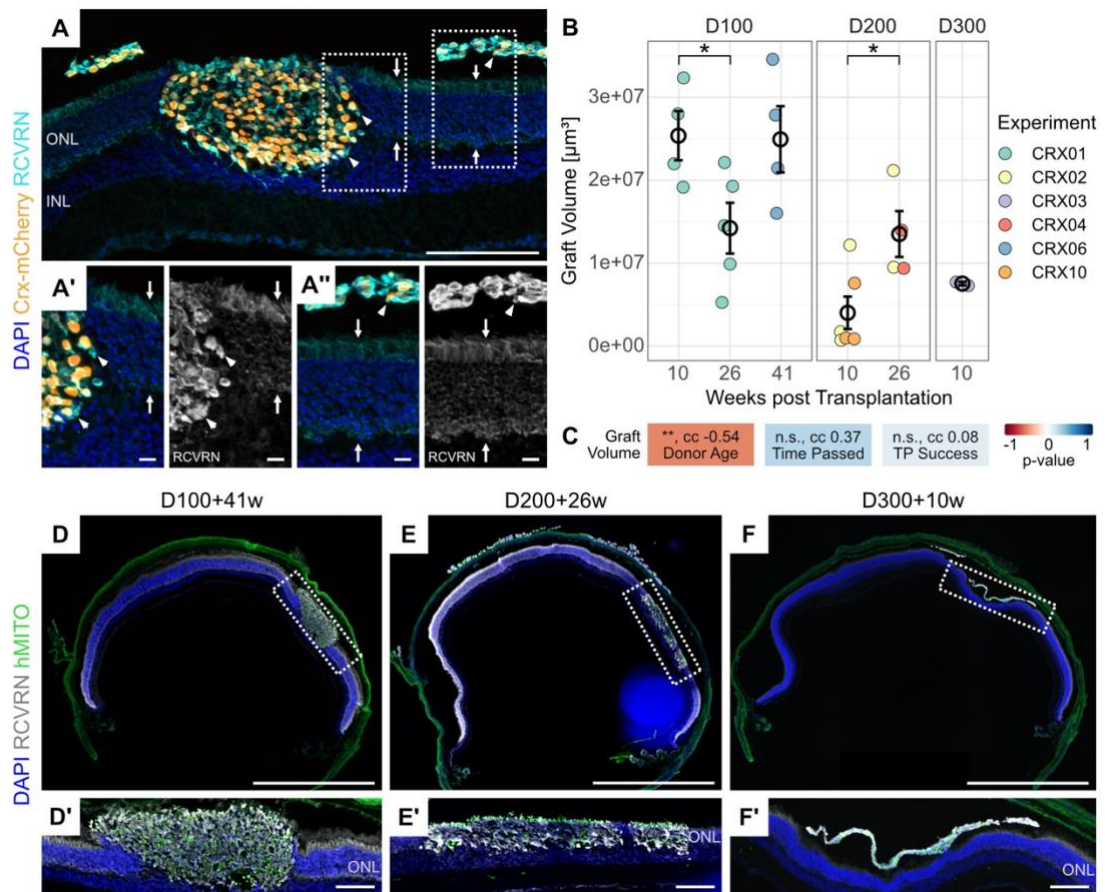


Figure 14. Graft Volumes in D100, D200 and D300 Transplants.

A. Human cells identified by nuclear mCherry signal had a stronger RCVRN fluorescence intensity (**A**, **A'**, **A''** arrowheads) than murine photoreceptors (**A'**, **A''** arrows), allowing identification of their cytosol, D200+26w. **B.** Total graft volume per eye as quantified by IHC analysis of RCVRN⁺ volume. Colors symbolize different experiments, i.e. transplantation rounds. Hollow points and bars show mean \pm SE, * $p < 0.05$, see *Table 4* for details on statistical tests, only significant results from tests irrespective of experimental origin shown. **C.** Correlations between graft volume and donor age, time passed since the first transplantation and estimated transplantation success. **D-E.** Representative images of grafts with a total age of D370 (**D** D100+41w, **E** D200+26w, **F** D300+10w) within full retinal sections. **D'-F'** show magnified views of the transplants. Scale bars: **A**, **D'-F'** 100 μ m; **A'**, **A''** 10 μ m; **D-F** 1 mm. ONL/INL: outer/inner nuclear layer, cc: correlation coefficient, n.s.: not significant.

and samples partially originating from distinct experimental rounds, statistical testing did not show significant differences in mean graft sizes, except when treating samples from different experiments as if they were generated from the same one. Then, the means of D100+10w and D100+26w as well D200+10w and D200+26w samples were found to differ significantly ($p = 0.0369$ and $p = 0.0201$ respectively, see *Table 4* for details on statistical tests). Representative pictures of grafts with a total age of roughly D370 are shown in Figure 14D-F'.

To test which factors may have affected the graft size, a correlation analysis was carried out. Since mostly females animals had been used, no statement can be made about differences between female and males host. Of the other factors tested, graft size

was only negatively correlated with donor age, i.e. younger donor cells yielded larger grafts ($p < 0.01$, Figure 14C). No other factors were found to correlate with graft size, also not the time passed since the first eye in that round was transplanted ($cc = 0.37$, $p > 0.05$) or the transplantation success, i.e. the estimated volume successfully injected into the subretinal space ($cc = 0.08$, $p > 0.05$; note that only eyes where $>50\%$ of the cell suspension was successfully delivered were quantified). This has two important implications: first, it suggests that cells used for transplantation are robust and were equally capable of surviving in the host at the beginning as at the end of one transplantation round (i.e. after several hours on ice and multiple resuspensions). Second, small changes in transplantation volume (mostly an estimated 10-20%) do not strongly affect graft size.

3.2.3 Graft volume increase over time is not due to in vivo proliferation

From Figure 14 it is noticeable that graft volume decreased from D100+10w to D100+26w in the CRX01 experiment, however, graft volume at D100+41w was again larger, albeit not significantly so ($2.5 \times 10^7 \mu\text{m}^3$, $1.4 \times 10^7 \mu\text{m}^3$ and $2.0 \times 10^7 \mu\text{m}^3$ respectively). Here, it is important to note that D100+41w samples originated from a different experiment than D100+10w and D100+26w samples, and the graft size

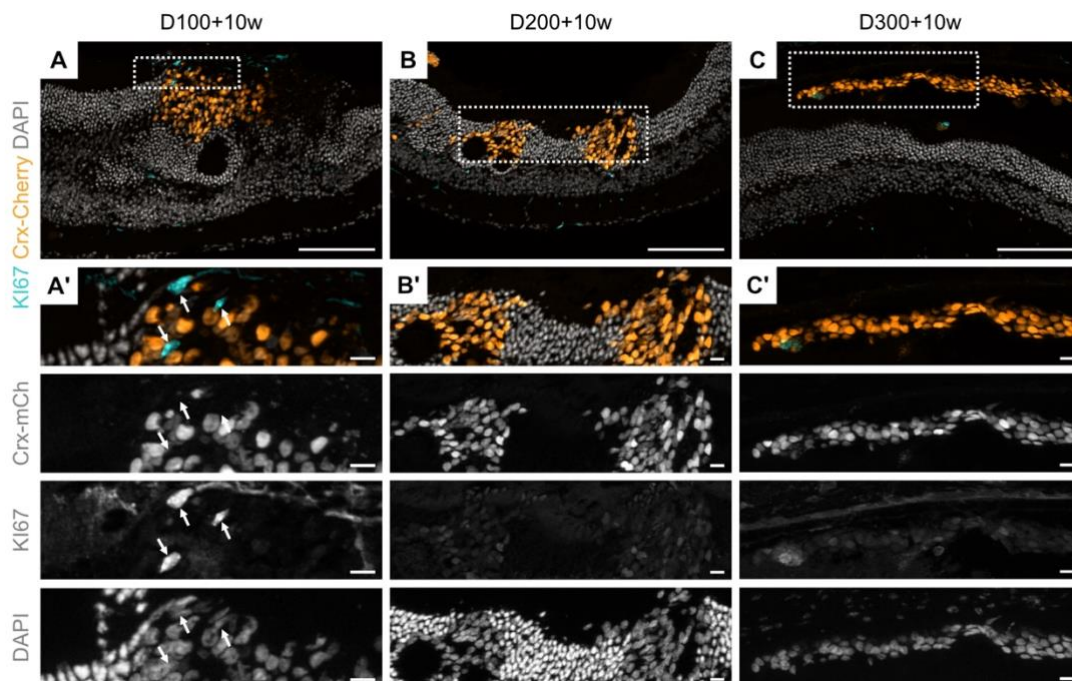


Figure 15. Transplanted Crx-mCherry⁺ Cells are Negative for the Proliferation Marker KI67.

A-C. IHC stainings for the proliferation marker KI67 in D100+10w (**A**), D200+10w (**B**) and D300+10w (**C**) grafts. Only few KI67⁺/Crx-mCherry⁻ nuclei were found in D100+10w samples (**A'**, arrows). No KI67⁺ nuclei were found at other timepoints (**B'**, **C'**). Scale bars: A-C 100 μm ; A'-C' 10 μm .

difference might be due to an experimental batch effect. In D200 experiments, the mean graft size at D200+10w was however significantly smaller than at D200+26w ($0.4 \times 10^7 \mu\text{m}^3$ vs. $1.3 \times 10^7 \mu\text{m}^3$), with samples partially originating from the same experiments. Graft size decrease can be caused by cell death or a decrease in cell size, while graft size increase can be caused by cell proliferation or an increase in cell size. Absence of staining for the proliferation marker KI67 indicates lack of proliferation of Crx-mCherry⁺ cells at the earliest timepoint investigated, 10 wpt (Figure 15). This suggests that graft size may instead reflect changes in cell size, e.g. with maturation or graft reorganization. Interestingly, a similar effect of initial graft size decrease followed by an increase in the long term in the absence of proliferative or inflammatory cells was recently observed in human-to-dog transplantations (Ripolles-Garcia et al., 2022).

3.3 Graft Morphology differs with Donor Ages

3.3.1 Human grafts can adopt an intraretinal position

Human Crx-mCherry⁺ grafts were found to adopt a variety of positions in the host retina. Some grafts were found in the subretinal space, seemingly isolated between the host inner and outer segments (IS/OS) and the retinal pigment epithelium (RPE, Figure 16A and A’’). Other clusters were situated within the IS/OS layer, coming into closer contact with the host ONL, as seen by direct apposition of donor and host nuclei (Figure 16A and A’’). A third group of clusters was placed within the host retina, intraretinally, with their nuclei interspersed between host nuclei (Figure 16A and A’, see also Figure 14D-F’ and *Figure 22. Human Identity of Intraretinal Graft Clusters.*).

It is important to note that the vast majority of Crx-mCherry⁺ cells within the host retina were true human cells and not a result of human-to-mouse material transfer, as shown below in section 3.5.1 *Intraretinal Crx-mCherry+ grafts are largely a result of true morphological incorporation.* While both isolated and apposed phenotypes are already known from mouse-to-mouse and human-to-mouse transplantations, this was the first time that large intraretinal or incorporated clusters of photoreceptors have been described upon the use of human donor cells.

3.3.2 Graft positioning changes over time

For the overall goal of photoreceptor transplantation – functional integration into the host retina – an intraretinal graft position was deemed most beneficial, as it would most closely mimic healthy tissue structure and allow for interaction with secondary neurons. To evaluate which donor ages have the highest chance of yielding such a position, the percentage of intraretinal graft area was measured across all conditions.

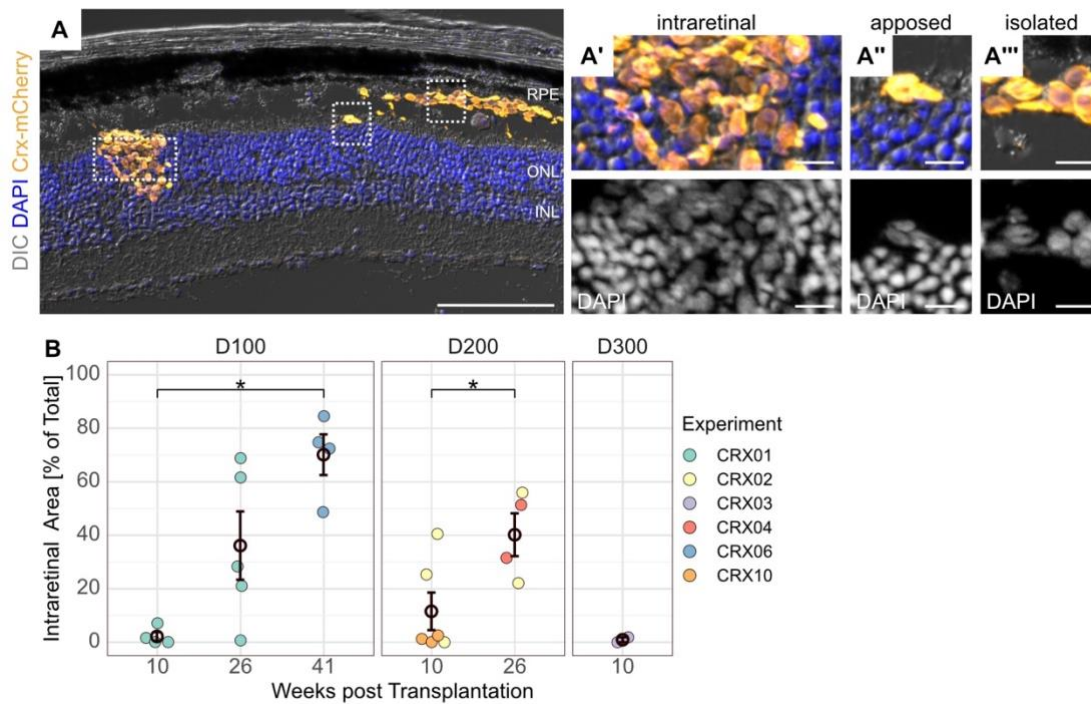


Figure 16. Quantification of Graft Subtypes by Positioning.

A. Example image of grafts present in three different forms: **A'** positioned intraretinally, surrounded by host nuclei (bright DAPI), **A''** apposed, directly bordering host nuclei and **A'''** isolated, without direct contact to host ONL cells and their nuclei. **B.** Quantification of graft area present as incorporated. For details on quantification refer to methods section 8.3.5.2. Hollow circles and bars show mean±SE, * $p < 0.05$, see *Table 4* for details on statistical tests, only significant results from tests irrespective of experimental origin are shown. Scale bars: A 100 μm , A'-A''' 10 μm . RPE: Retinal pigment epithelium, ONL/INL: Outer/inner nuclear layer.

While there was almost no intraretinal graft localization in D100+10w and D300+10w (2% and 1% respectively), D200+10w grafts were already present intraretinally to 10%. This increased to about a third of total graft area for both D100+26w and D200+26w samples, and even further to 70% in D100+41w samples (Figure 16B). Statistical testing did not show those differences to be significant, except when treating samples from different experiments as if they were generated from the same one. In that case, the means of D100 samples were found to differ significantly overall ($p=0.0379$) and when comparing D100+10w with D100+41w ($p=0.0234$). Similarly, when disregarding experimental origin of samples, D200+10w and D200+26w means were significantly different ($p=0.0294$, see *Table 4* for details on statistical tests).

3.3.3 Qualitative differences in graft morphology between donor ages

In addition to the measured difference in graft positioning, there were also obvious differences in graft morphology between the different donor ages from visual inspection (see also Figure 14D-F'). The D100 grafts often appeared as single clusters that were large, round, and contained highly autofluorescent speckles as well as occasionally pigment debris (Figure 17A). Several clusters seemed wrapped by what

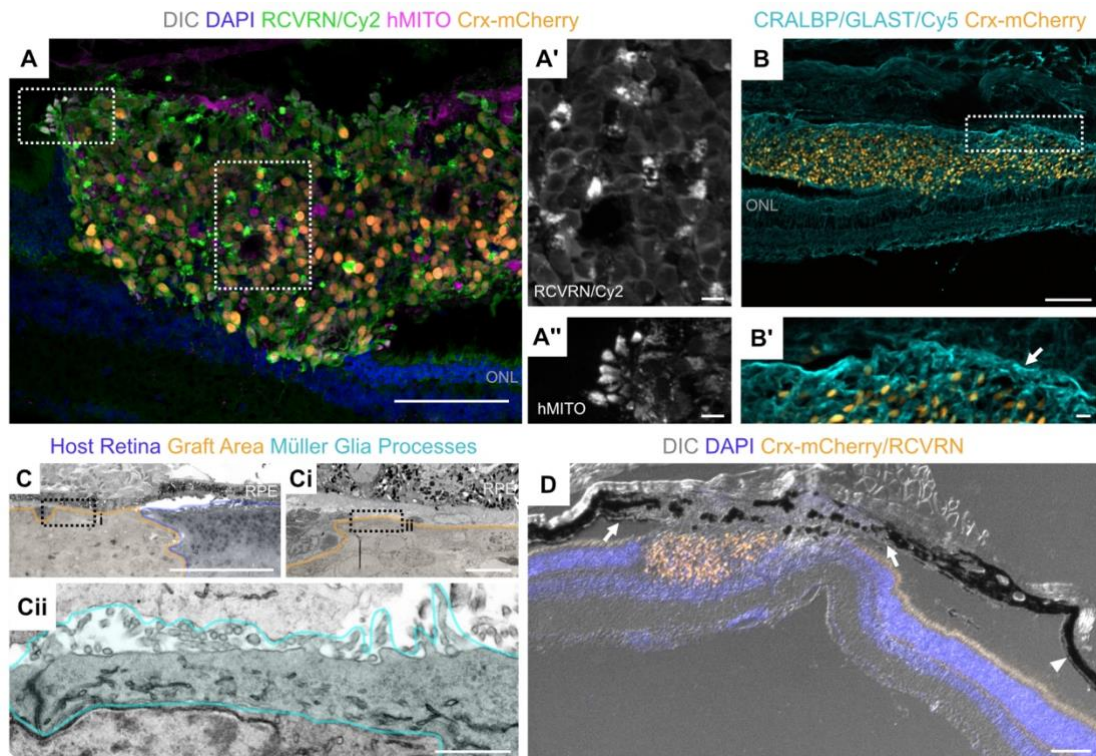


Figure 17. General Morphology of D100 Grafts.

A-D. Typical features of D100 transplants. **A.** D100 grafts often contained material that was autofluorescent in the Cy2 channel (**A'**), D100+41w. **B.** Staining for Müller glia markers CRALBP/GLAST indicated that D100 grafts might be enwrapped by a gliotic seal (arrow), D100+26w. **C.** TEM analysis of a D100+41w sample similarly shows enwrapment by MG processes (**Cii**, cyan overlay) with apical microvilli and tight junctions. **D.** Occasionally, D100 grafts seemed to have a negative impact on the neighbouring RPE and choroid, whose structure and pigmentation were disturbed (region between arrows) in comparison to regions away from the graft site (arrowhead), D100+26w. Scale bars: A, B, C, D 100 μ m; A', A'', B', Ci 10 μ m; Cii 1 μ m.

initially seemed like extracellular matrix material, as it stained unspecifically with secondary antibodies detecting mouse. Additional staining for Müller glia (MG) markers CRALBP/GLAST as well as EM analysis however suggested it could rather be a gliotic seal enwrapping the graft (Figure 17B, B', C-Cii). It was further noted that the presence of D100 derived cells was often accompanied by an aberration in RPE and/or choroidal integrity (Figure 17D) compared to neighbouring regions without an underlying graft.

Due to constraints in donor material, only two eyes containing D300 transplants were assessed by IHC. In both cases the grafts were an elongated, thin layer of cells positioned in the subretinal space (Figure 18), where they extended numerous slim processes towards the RPE, seemingly even stretching between RPE cells (Figure 18A'). D300 transplants were neither "enwrapped" nor contained noticeable autofluorescent speckles. Occasionally, grafts were in direct contact with the host ONL and were able to form mitochondria-rich bulbous outgrowths (Figure 18B, B', arrows).

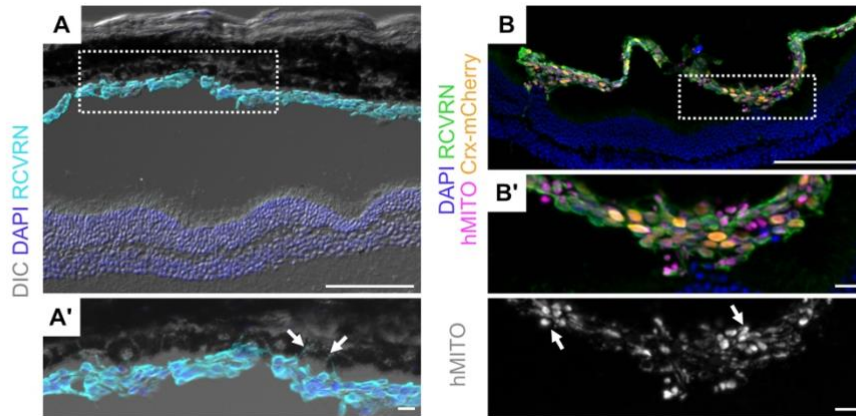


Figure 18. General Morphology of D300 Grafts.

A. D300 grafts were comparatively thin, elongated and mostly positioned in the subretinal space, without Cy2 autofluorescent speckles. Note the extension of RCVRN⁺ processes towards the RPE (**A'**, arrows). **B.** D300 grafts occasionally contacted the host retina and were able to form hMITO-rich outgrowths (**B'**, arrows). Scale bars: A, B 100 μ m; A', B' 10 μ m.

D200 grafts only occasionally contained autofluorescent speckles or pigmented structures, and their surface was rarely observed to be as smooth as seen in D100 samples, but rather uneven with many cellular outgrowths (Figure 19A, B). Upon closer inspection it was found that these outgrowths were highly enriched for mitochondria, which, in photoreceptors, is a feature of inner segments. While this structure was most frequently observed in D200 samples, mitochondria-rich outgrowths could principally be formed by donor cells from all ages (see also Figure 17A'', Figure 18B').

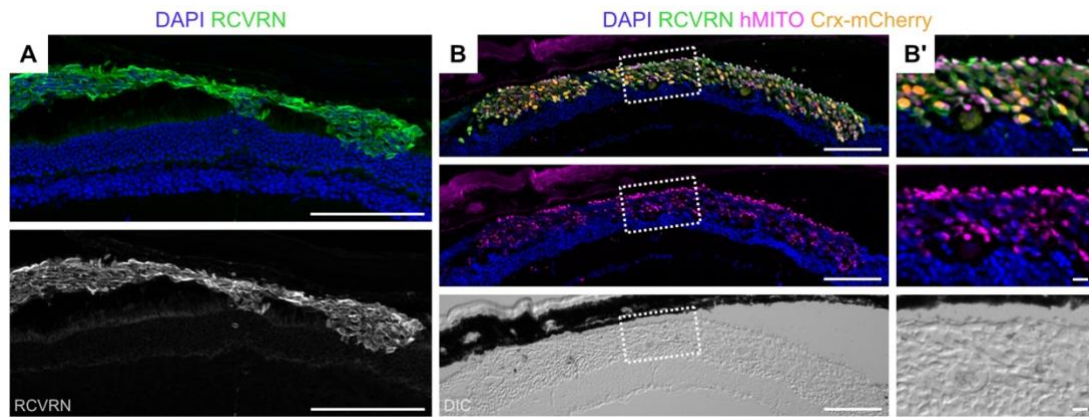


Figure 19. General Morphology of D200 Grafts.

A. D200 Transplants exhibited neither autofluorescent speckles in the Cy2 channel nor the enwrapping seen in D100 grafts, D200+10w. **B.** Instead, their surface was more rugged and contained many hMITO-rich protrusions, D200+26w. Scale bars: A, B 100 μ m, B' 10 μ m.

3.4 Graft Maturation

3.4.1 D200 but not D100 or D300 grafts develop large quantities of inner segments

The accumulation of human mitochondria in bulbous outgrowths directed towards the RPE (Figure 20A) was highly reminiscent of inner segment (IS) formation, an important morphological feature towards obtaining properly polarized and potentially functional photoreceptors. Ultrastructural analysis by EM confirmed the hypothesis that the mitochondria-rich outgrowths were human IS through their ultrastructural

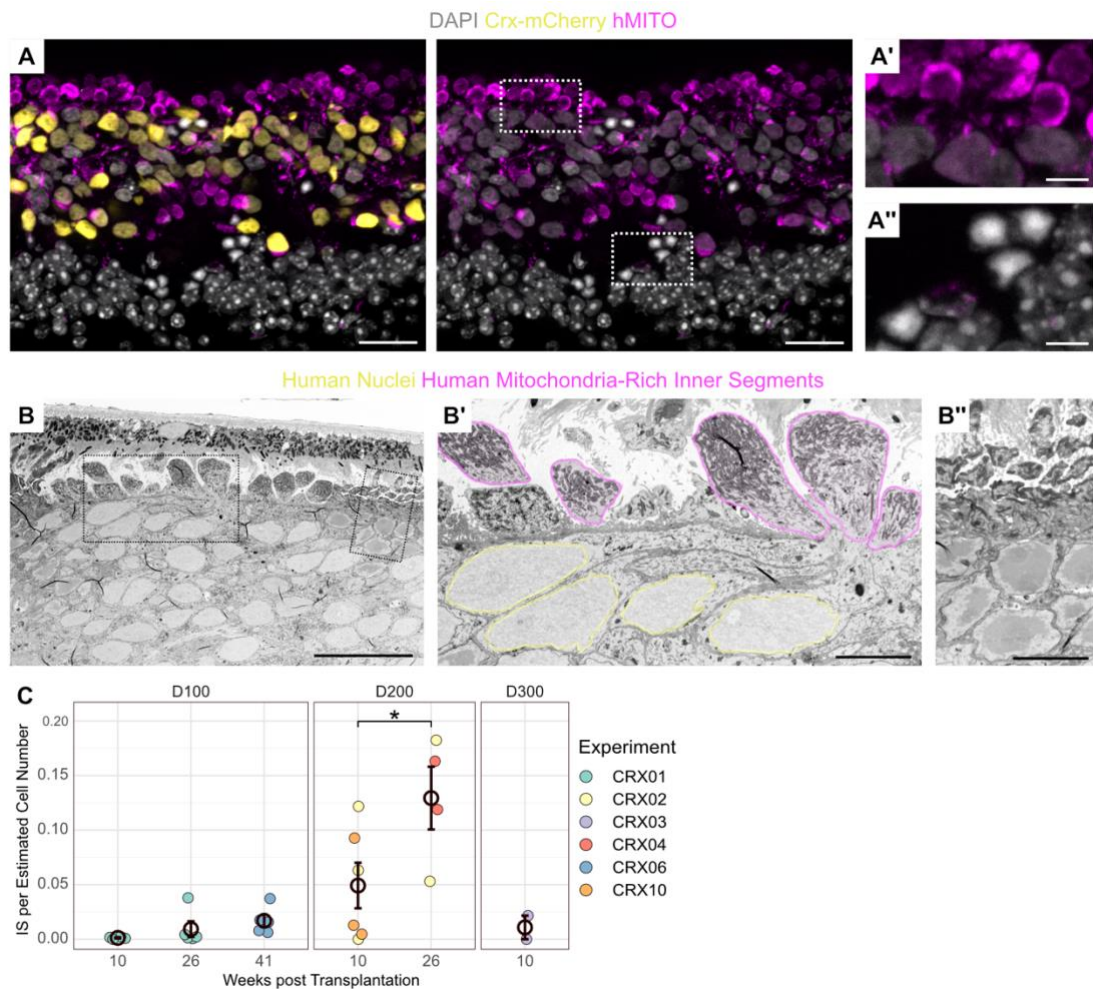


Figure 20. Inner Segments in IHC and EM and Their Quantification in D100, D200 and D300 Grafts.

A. Bulbous human mitochondria-rich outgrowths from Crx-mCherry⁺ cells are enriched towards the RPE, 200+26w. **A'**. Human nuclei are evenly DAPI⁺, while **A''** murine nuclei contain a bright inverted nucleus (rods) or several chromocenters (INL nuclei, most likely bipolar cells), see also section 3.5.1. **B.** A cluster of human cells, identified by nuclear size and organization, positioned intraretinally with mitochondria-packed bulbous outgrowths towards the RPE. **B'**. Human inner segments (IS) were found to extend from the cytosol of human cells. **B''**. Mouse rod nuclei (densely packed heterochromatin) and mouse IS (smaller than human IS, mitochondria distributed along plasma membrane) for comparison. **C.** Quantification of IS formation from IHC in D100, D200 and D300, normalized to estimated cell number. * $p < 0.05$, see *Table 4* for details on statistical tests, only significant results from tests disregarding experimental origin are shown. Hollow circles and bars show mean \pm SE. Scale bars: A, B 20 μ m; A', A'', B', B'' 5 μ m.

morphology, and additionally by their continuity with the cytosol of human cells identified through nuclear size and structure (Figure 20B). Human origin of cells in EM was additionally confirmed by immunogold labeling (Figure 23, see also section 3.5.1).

Quantification showed that D200 grafts indeed generated a much higher number of IS than D100 transplants at all timepoints examined (D100: 0.001; 0.009; 0.017 IS per cell at +10w; +26w; +41w; D200: 0.05; 0.13 IS per estimated cell number at +10w; +26w; Figure 20). This shows that IS formation did not follow the same distribution as intraretinal positioning, as D100 samples had a larger intraretinal graft area. Importantly, this suggests that qualitative differences exist between intraretinal grafts of different donor ages that might affect their maturation capacity. This could be due directly to graft developmental stage, transplant composition or indirectly due to a varying interactions with the host tissue.

3.4.2 Inner segment development is associated with close proximity to the host retina

Although intraretinal graft formation did not reliably correlate with IS generation, IS were mainly observed in graft areas with a direct connection to the host ONL. To quantify the possible dependence of IS formation on a direct connection to the host retina, IS counts were binned into two categories, i.e. proximal and distal. Proximal IS were defined as generated from intraretinal grafts or apposed grafts within 50 μm of the

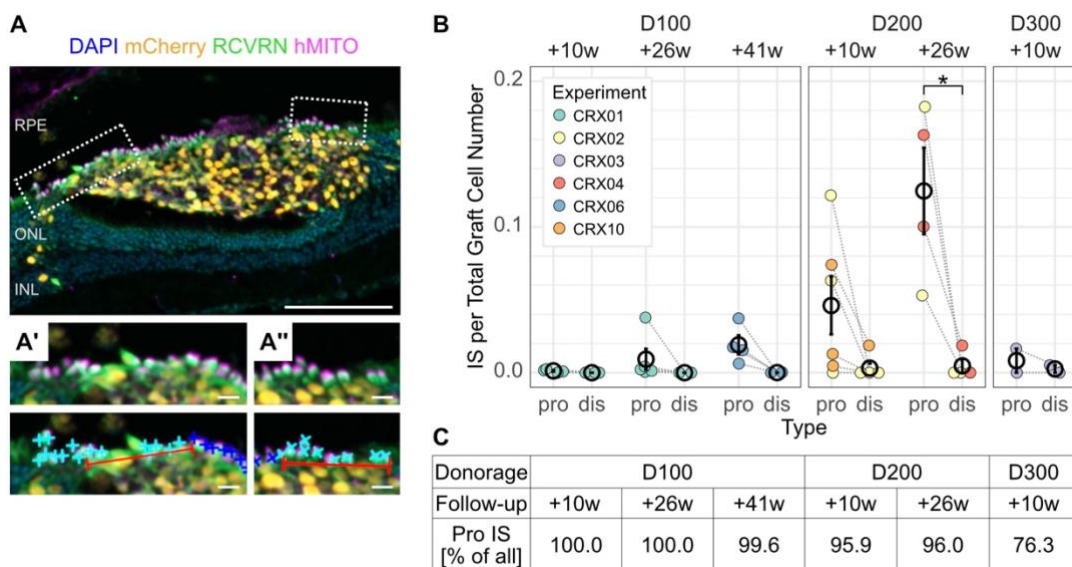


Figure 21. Inner Segment Development in Proximal and Distal Grafts.

A. Example for IS quantification in dependence on ONL contact. IS can be identified through hMITO and RCVRN labelling of outgrowths from the Crx-mCherry⁺ and RCVRN⁺ graft. Inner segment (IS) were considered proximal (light blue x) within 50 μm (red bar) of graft-host contact points, and distal (dark blue x) beyond 50 μm (**A'**, **A''**). **B.** Quantification of proximal (pro) and distal (dis) IS normalised to cell number. Hollow circles and bars show mean \pm SE, grey dotted lines connect data from the same eyes. **C.** Amounts of proximal IS in percent of total IS number. * $p_{\text{adj}} < 0.05$, see *Table 4* for details on statistical tests, only significant results from test disregarding experimental origin are shown. Scale bars: A 100 μm ; A', A'' 10 μm .

contact point. Distal IS referred to IS formed by subretinal clusters and within apposed grafts beyond 50 μm of the contact points (Figure 21A). Quantification confirmed that the vast majority of IS were indeed proximal IS (Figure 21B, C), suggesting that a close interaction with the host retina is required to form high numbers of IS.

3.5 Human Identity of Intraretinal Grafts

3.5.1 Intraretinal Crx-mCherry⁺ grafts are largely a result of true morphological incorporation

It is important to note that vast majority of Crx-mCherry⁺ cells within the host retina were true human cells and not a result of human-to-mouse material transfer. This was inferred from several indicators: Nuclear size, nuclear structure, human-specific antibody labelling in both immunohistochemistry and electron microscopy, and human-specific transcriptome of Crx-mCherry⁺ cells re-isolated from the mouse eye (see *Figure 33. Single Cell Transcriptome Analysis of Ex Vivo and In Vitro Crx-mCherry⁺ Cells*. See also sections 4.3.5 and 4.3.6). While the gold standard to detect material transfer is Y-chromosome probing upon sex-mismatched transplantations, this was not employed here as both the Crx-mCherry hiPSC line and most host animals were female.

Human PR nuclei are reported to have up to twice the diameter of murine PRs with 9-13 μm versus 6-6.5 μm respectively (Collin et al., 2019; Gonzalez-Cordero et al., 2017; Ribeiro et al., 2021). Here, nuclear size difference was generally assessed visually by direct comparison of the nuclei assumed to be human with those of neighbouring murine rods (Figure 22A, B, C). In addition, nuclear diameter was exemplarily sampled from RCVRN-labeled grafts of two eyes by measuring per cell area of the nuclear mCherry signal, which yielded an average nuclear diameter of 8.5 μm . Although a more thorough analysis is required to accurately measure the mean graft nuclear diameter and its distribution in the present data, this measurement confirms human nuclear size of the cells regarded as human transplant.

Beyond size, human PR and murine retina cells differ strongly with regards to their nuclear architecture. As such, murine rods, bipolar and ganglion cells exhibit DAPI-bright heterochromatin speckles (Solovei et al., 2009), a feature not observed in human PRs (Figure 22A, B). In murine rods, the heterochromatin is even more concentrated, as it forms a single heterochromatin center in the nuclear core, yielding an inverted nucleus. This makes murine rods, which are the most prevalent cell type in the mouse retina, particularly easy to discern from human PRs (Solovei et al., 2009). The striking difference in nuclear architecture is a helpful indicator of human graft identity in immunohistochemical stainings (Figure 22C). Additionally, in electron microscopy

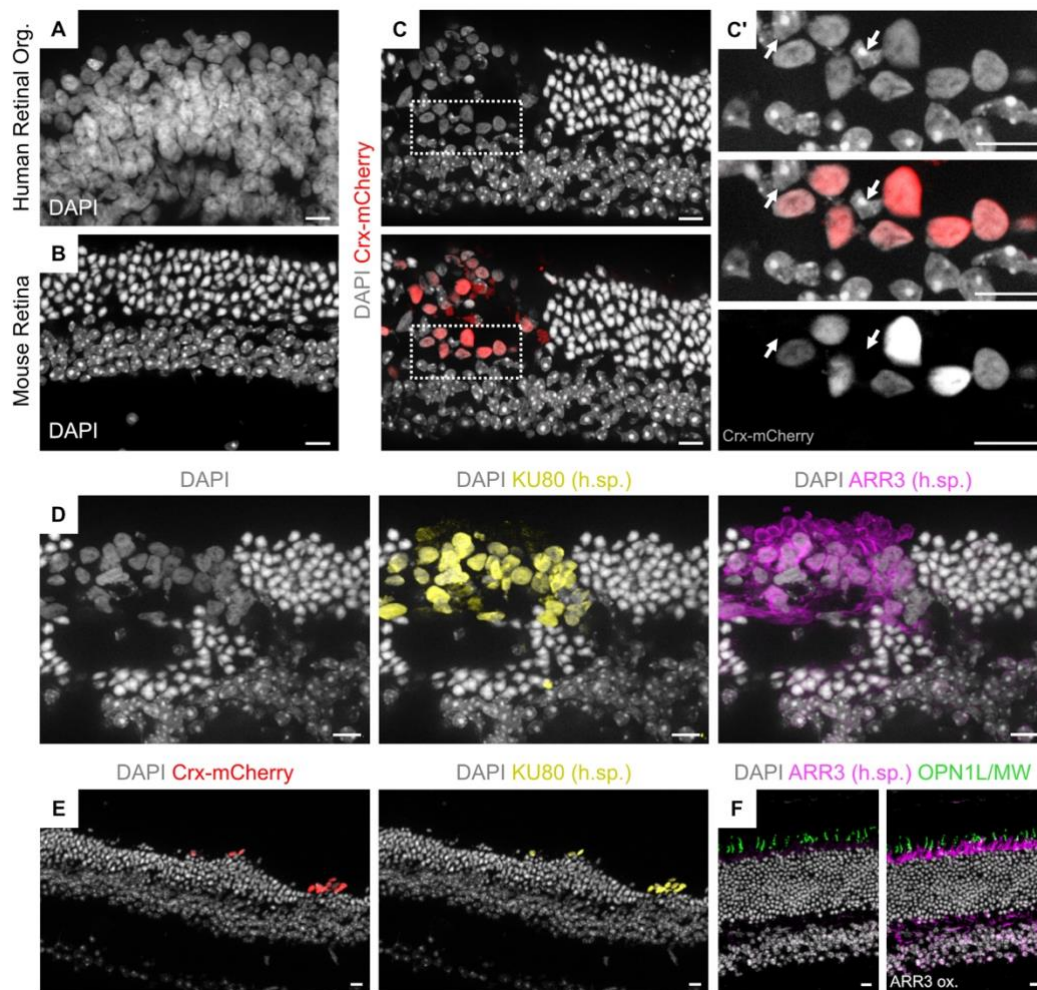


Figure 22. Human Identity of Intraretinal Graft Clusters.

A. Large human retinal organoid photoreceptors show an even distribution of DAPI staining. **B.** The smaller mouse rods show an inverted nuclear architecture with a bright, heterochromatin center. Inner nuclear layer neurons contain several bright heterochromatin centers. **C, C'.** Human grafts identified by Crx-mCherry signal are additionally recognizable by their nuclear size and morphology. Note that nuclei with heterochromatin speckles in the graft do not exhibit Crx-mCherry fluorescence (**C'**, arrows). **D.** Human-specific labelling of an intraretinal transplant again recognizable through nuclear size and morphology by staining with antibodies against KU80 and ARR3. **E.** Human specificity of KU80 antibody which only labels Crx-mCherry⁺ grafted cells. **F.** Human specificity of ARR3 antibody which shows no cone-specific signal in the wildtype mouse retina, despite presence of cones as detected by OPN1L/MW. Overexposure of ARR3 shows diffuse background labeling only. Scale bars: all 10 μ m. Org.: organoid, h.sp.: human specific, ox.: overexpressed.

images, the electron-dense heterochromatin can be seen as well and, together with nuclear size, allows clear distinction of mouse rods from human cells (Figure 20B', B''). In EM, human cell identity was furthermore confirmed by nanogold labeling (Figure 23).

Many antibodies used throughout this study stain both, human and murine protein. Several antibodies used are however human-specific, most importantly the antibodies against ARR3 and hMITO. As such, human specificity of the hMITO antibody can be seen by absence of labeling in the mouse retina (Figure 14D-F', Figure 18B, B', Figure 19B, B', Figure 20A-A''). Human specificity of the ARR3 antibody is additionally shown in Figure 22D, where it labels only cells recognizable as human through nuclear

size and morphology as well as human-specific labeling with anti-KU80. Both KU80 do not exhibit background staining of the murine retina (Figure 22E, F).

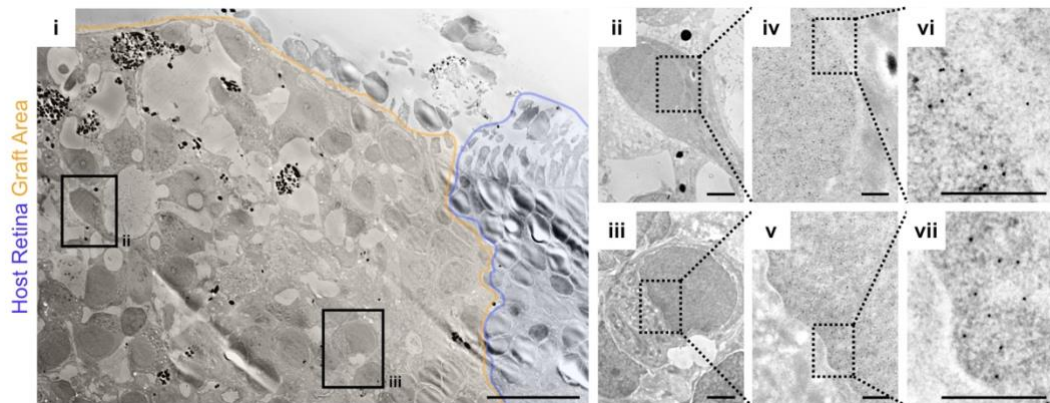


Figure 23. Nanogold Labeling of Human Nuclei in EM.

Murine rods (blue overlay) show dense nuclear packing with long inner and outer segments extending into the subretinal space, while the material on their left does clearly not consist of murine rods. Here, human cells (orange overlay) do not show inner segments (D100+26w), yet are identifiable by nanogold labeling against the nuclear-localized mCherry reporter (black dots in vi, vii). Scale bars: i 20 μm ; ii, iii 2 μm ; iv-vii 200 nm.

3.5.2 Rare indications of potential human-to-mouse material transfer

As described above, cell species identity was inferred from several factors, including Crx-mCherry⁺ signal, human-specific antibody staining and nuclear architecture, allowing to confidently speak of true human identity and morphological incorporation for the vast majority of observations. However, on extremely rare occasions, mismatches between these indicators were observed. As such, strongly positive RCVRN cell bodies of murine morphology were found to surround nuclei of murine architecture (Figure 24A, B, arrows in A'', B'). While the RCVRN antibody used is not human-specific, it labels human PRs much more strongly than mouse PRs (Figure 14A), with its intensity here mirroring that of isolated human cells in the subretinal space (Figure 24A, B). In one example, the putative recipient mouse cell additionally contained material positive for human mitochondria labeling (Figure 24A''', arrowheads). Interestingly, both examples shown mirror the setting observed upon mouse-to-mouse material transfer (Figure 4), where recipient host cells are mostly located closely beneath clusters of donor cells in the subretinal space. Here, human cells can also be identified in close proximity and direct contact to the putative recipient cells (Figure 24A'', Crx-mCherry signal, B).

While these observations are indicative of human-to-mouse material transfer, they are no proof and further examination is required to reliably determine whether human-to-mouse material transfer occurs at all and if so, at what rate.

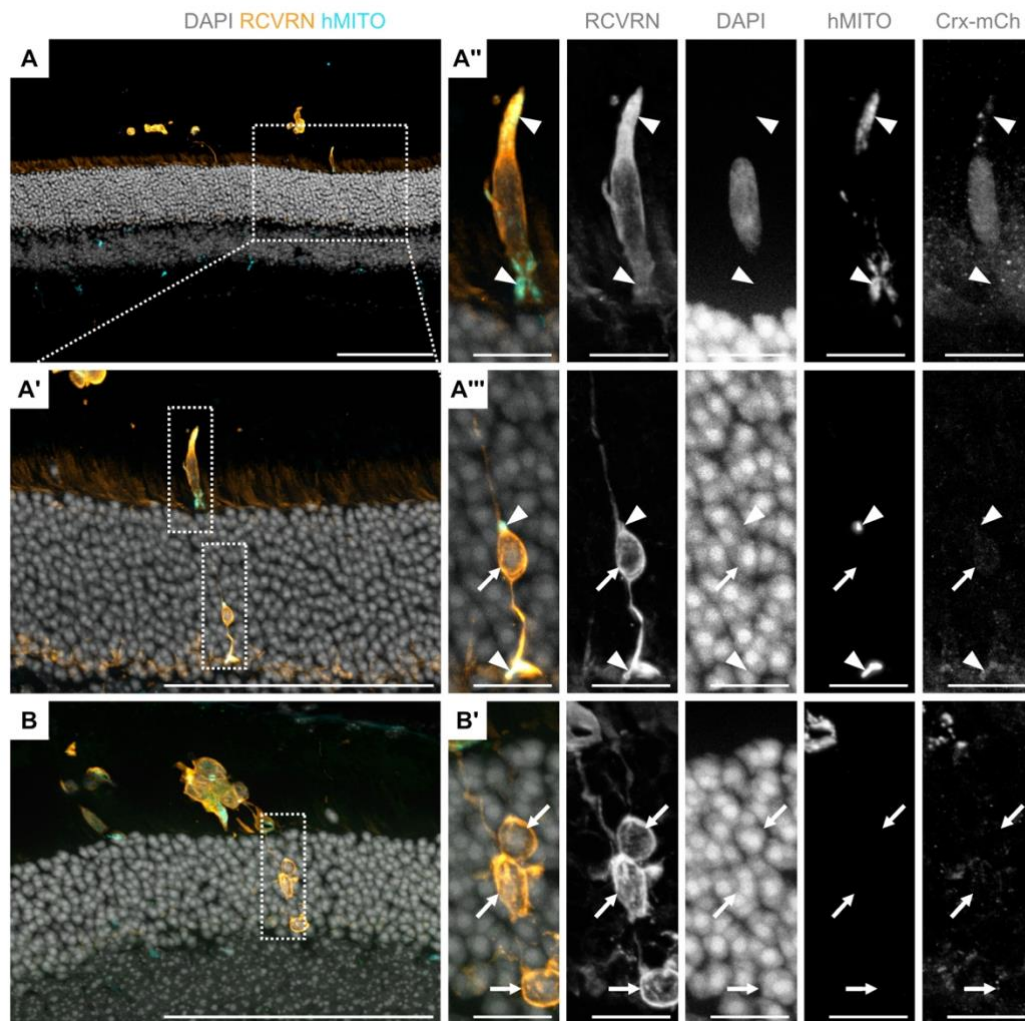


Figure 24. Potential Occurrences of Human-to-Mouse Material Transfer.

A, B. Presence of highly RCVRN⁺ cell bodies in the host retina with murine nuclear morphology (arrows) but lack of Crx-mCherry signal (**A'''**, **B'**) indicates potential human-to-mouse material transfer. While not a human-specific antibody, the RCVRN intensity mirrors that of human subretinal cells, which are positioned in close proximity and with direct contact to the putative recipient cells (**A**, **A''**, **B**, **B'**). Co-localization of RCVRN and human mitochondria (arrowheads in **A''**) supports the notion of human-to-mouse material transfer having occurred. Scale bars: **A**, **A'**, **B** 100 μ m; **A''**, **A'''**, **B'** 10 μ m.

3.6 Summary

Human retinal organoid-derived Crx-mCherry⁺ cells can successfully be enriched by FACS and transplanted into the mouse subretinal space, where they survive, partially incorporate and begin to mature. Depending on donor age, the composition of the Crx-mCherry⁺ cell suspension varies. Consequently, significant differences were found with regards to transplant morphology, size, positioning and capacity to generate inner segments when comparing the different donor ages D100, D200 and D300. Inner segment formation correlated strongly with graft-host proximity, yet despite not having the highest rate of intraretinal positioning, D200+26w cells produced the highest number of inner segments, as normalized to the estimated surviving cell number. This suggests D200 to be the preferential age for transplantation of Crx-mCherry⁺ cells.

While on rare occasions stainings suggested the possibility of human-to-mouse material transfer, it is important to note that this interpretation awaits confirmation. The large-scale intraretinal positioning observed was instead mostly a result of true morphological incorporation of human photoreceptors into the murine host.

4 In Depth Characterization of Transplanted D200 Crx-mCherry⁺ Cells

4.1 Aims

Considering D200 donor cells have the highest propensity for IS formation, they appear to be of the most promising developmental stage for cell transplantation studies. However, it is unknown how grafts become positioned intraretinally, which interaction between graft and host tissue is required for IS formation and whether IS-forming grafts can mature further. The aim of this part of the study was therefore to better understand the emergence of graft incorporation and to examine graft polarization and maturation in more detail.

4.2 Early Post Transplantation Dynamics in Graft Positioning and Graft-Host Interactions

Integration into the host retina is an important prerequisite for human grafted photoreceptors to potentially connect with the host, mature and become functional. As shown in the previous chapter, intraretinal positioning alone does not suffice to generate large quantities of more mature photoreceptor structures such as inner segments, thus, specific interactions between graft and host appear to be necessary. Therefore, it was examined to what extent the intraretinal positioning and graft maturation is also accompanied by graft-host interactions.

4.2.1 Intraretinal and proximal D200 grafts interact with the host retina while isolated and distal clusters show only little interaction

In the mature retina, photoreceptors have several interaction partners that support them structurally and functionally. As such, Müller glia cells (MG) provide a scaffold, nutrients and, in the case of cones, an alternative recycling pathway for visual pigment. Bipolar and Horizontal cells (BC and HC), both second order neurons, receive input from photoreceptors at the synapses in the OPL. Given the close proximity of graft and host cells in the case of intraretinal clusters, it was next analyzed which interactions with host retinal cells occur and how the interactions differ between interactive and isolated graft types.

A high degree of interaction with cytosolic processes from MG (visualized by GFAP and GS) and rod BC (visualized by PKCA) extending from the host retina was evident in many regions where grafted cells were located intraretinally or in close

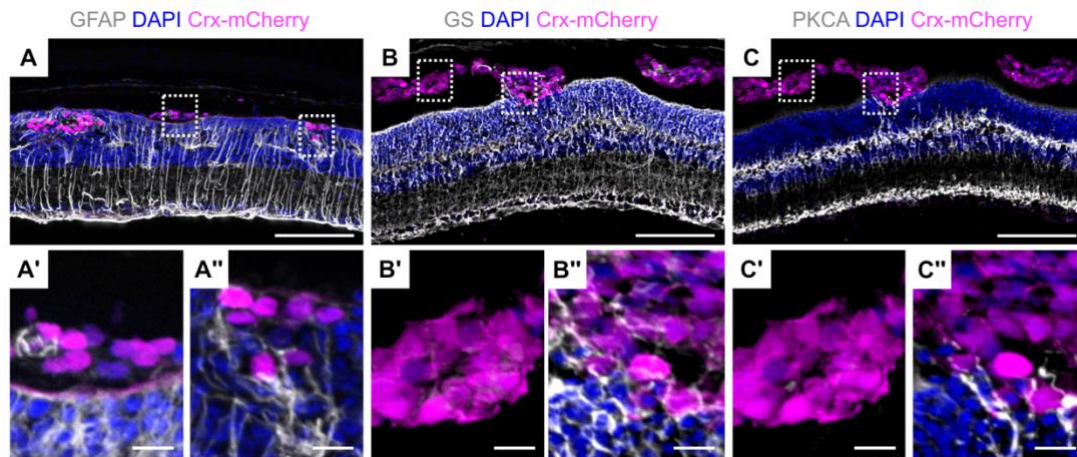


Figure 25. Isolated Grafts interact less with Host Müller Glia and Bipolar Cells.

A-C. Retinal sections containing isolated (**A', B', C'**) and intraretinal (**A'', B'', C''**) transplants show differing levels of interaction with the graft depending on its position. MG processes (**A-A'', B-B''**) and BC processes (**C-C''**) are in direct contact with intraretinal but not isolated grafts. Scale bars: A-C 100 μm , A'-C' 10 μm .

proximity to the host (Figure 25A-C, A'', B'', C''). Moving further away from areas of contact between graft and host neuroretina, these interactions were less frequent (Figure 25B', C') and were mostly absent in completely isolated grafts (Figure 25B', C')

4.2.2 Incorporation of D200 grafts is first evident at 8 weeks post transplantation

As was shown in Figure 16, ca. 10% of graft area is positioned intraretinally at D200+10w. To better understand how morphological incorporation is initiated, earlier stages post transplantation were assessed. Thus, additional experimental eyes were sampled at 2, 4, 6, and 8 weeks post transplantation (wpt) to examine changes in the early timeline. Quantified as before, they are shown together with the previous D200+10w data in Figure 26. D200+2w samples could not be directly compared due to a different staining being used.

The average graft volume as measured by RCVRN⁺ area remained mainly in the same range over all timepoints examined (Figure 26A). It is however important to note that graft size in CRX12 samples was significantly smaller compared to CRX14 samples, (adjusted p-value $p_{\text{adj}}=0.0289$) and that the differences between experimental rounds in total contributed to 32% of the variation in the data, while the follow-up timeframe only contributed to 6% (Two-way ANOVA, see *Table 4. Statistical Analyses* for details).

With smaller graft size, the relative incorporated area was also smaller, representing only 0.7% of the total area in CRX12 D200+8w, but 2.8% of the total area in CRX14 D200+8w samples. Despite the mean incorporated area increasing over time, it can also be noted that there was a large divergence between eyes, with some eyes reaching up to ~30% incorporated area at D200+10w, while others only reached ~2% (Figure 26B). Statistically, incorporation first became significantly evident in D200+8w

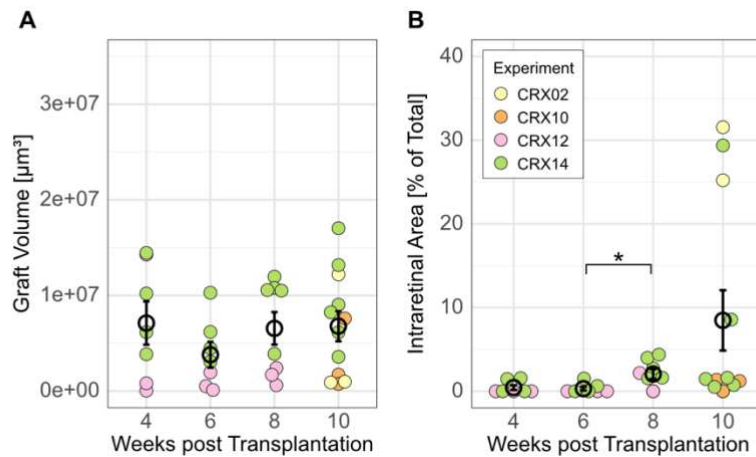


Figure 26. Graft Size and Positioning in D200 Early Timeline Samples.

A. Quantification of graft size in early timeline eyes shows similar overall size distributions at all timepoints. **B.** Intraretinal positioning becomes evident from D200+8w onwards. Hollow circles and bars show mean \pm SE, * $p < 0.05$, see Table 4 for details on statistical tests, only significant results from tests disregarding experimental origin are shown.

samples, reaching on average 2% (6 wpt vs. 8 wpt $p = 0.0210$, 4 wpt vs. 6 wpt and 8 wpt vs. 10 wpt both non significant, Figure 26B). This suggests that the direct incorporation process, while possibly initiated before, reaches a turning point between 6 and 8 wpt.

4.2.3 Host Müller glia extend processes into the graft before host bipolar cells

While the incorporated grafts at later stages interact closely with host retinal cells, it is unclear how and over which timeframe this interaction is established. Staining of early timeline samples indeed showed that Müller glia (MG) can extend processes into subretinally located transplants as early as 2 wpt (Figure 27A, A'). As soon as intraretinal transplants were observed, MG processes were also found in those (Figure 27A, A'). Similarly, rod bipolar cells also extended processes into the grafts, however at D200+2w the neurites were not seen to reach the human cells yet (Figure 27B, B'). By 6 wpt and from then onwards, rod bipolar cell extensions were directly in contact with both intraretinal and proximal human grafts (Figure 27B, B'). To further uncover the timeframe of direct host BC to graft contact, repetition of staining for 4 wpt samples is required.

4.2.4 MG staining in D200 grafts originates from host MG

In the early timeline samples, there was a close proximity between graft and host cells, established e.g. via the extension of MG processes into the human clusters. This interaction continued and could still be detected at D200+10w and D200+26w (Figure 28A, B). Here, for intraretinal clusters, the MG staining also showed a continuous line above the human cells, with MG seemingly incorporating the graft into the retina. In

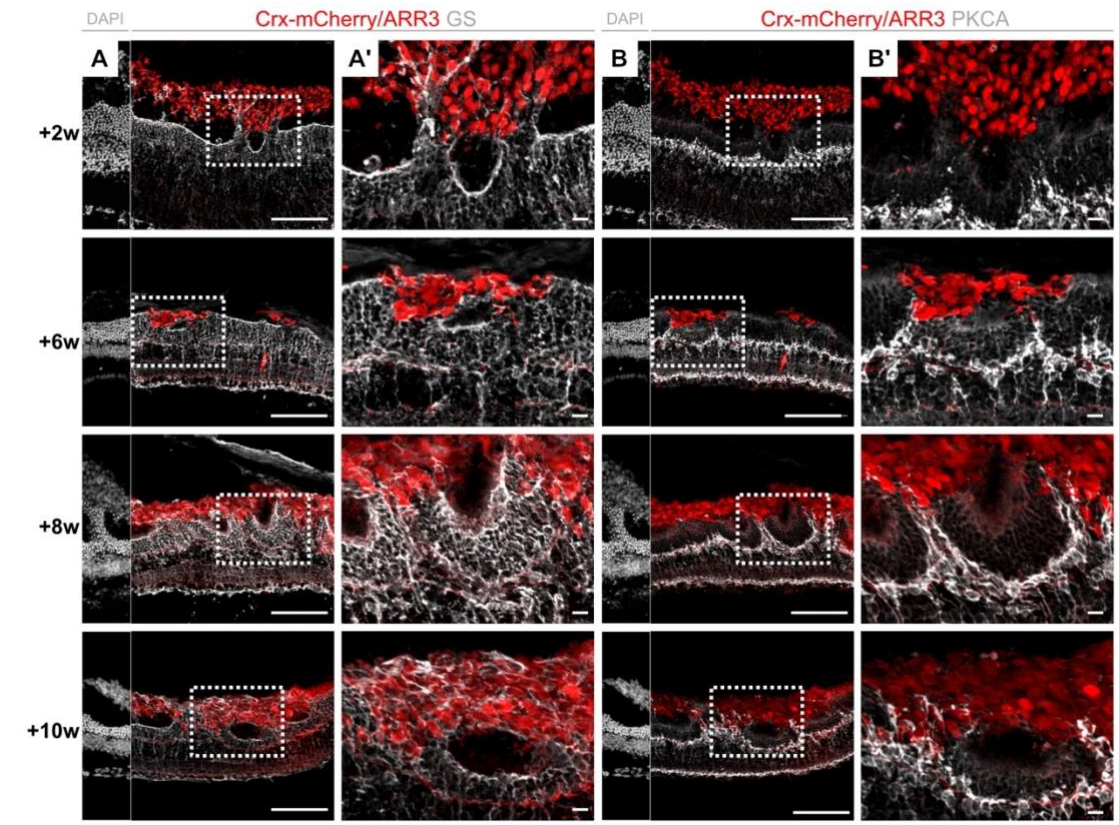


Figure 27. Early Interaction with Host Müller Glia and Bipolar Cells in D200 Grafts.

A, A'. Human graft interaction with GS^+ Müller glia processes. **B, B'.** Human graft interaction with $PKCA^+$ rod bipolar cell processes. Scale bars: A, B 100 μm ; A', B' 10 μm .

addition, $SOX2^+/Crx\text{-}mCherry^-$ MG nuclei were found within the human grafts (Figure 28), with $SOX2^+/Crx\text{-}mCherry^-$ nuclei looking strongly deformed and squeezed (Figure 28A', B'), while $SOX2^+/Crx\text{-}mCherry^+$ nuclei had a round or ellipsoid morphology.

While the absence of Crx-driven mCherry in intragraft MG nuclei suggests they were murine cells that had migrated into the cluster, there was no human-specific marker for MG cytosol available. Also, although FACS enrichment of donor cells yields a highly pure Crx-mCherry population, there was the possibility of a contamination with human Crx-mCherry MG. To obtain an unambiguous readout, D200 Crx-mCherry⁺ cells were therefore additionally transplanted into Hes5-GFP mice, which express GFP in MG cells under control of the Hes5 promoter and resulting sections were stained for SOX2 and a human nuclei specific antibody (HuNu, Figure 28C). Staining showed co-localization of SOX2 with Hes5-GFP cell bodies in both intraretinal (Figure 28C'') and isolated (Figure 28C') grafts. Human nuclear labelling and SOX2 signal on the contrary were exclusive, thus confirming that MG cell bodies and processes within human grafts originated from the recipient mouse retinal tissue.

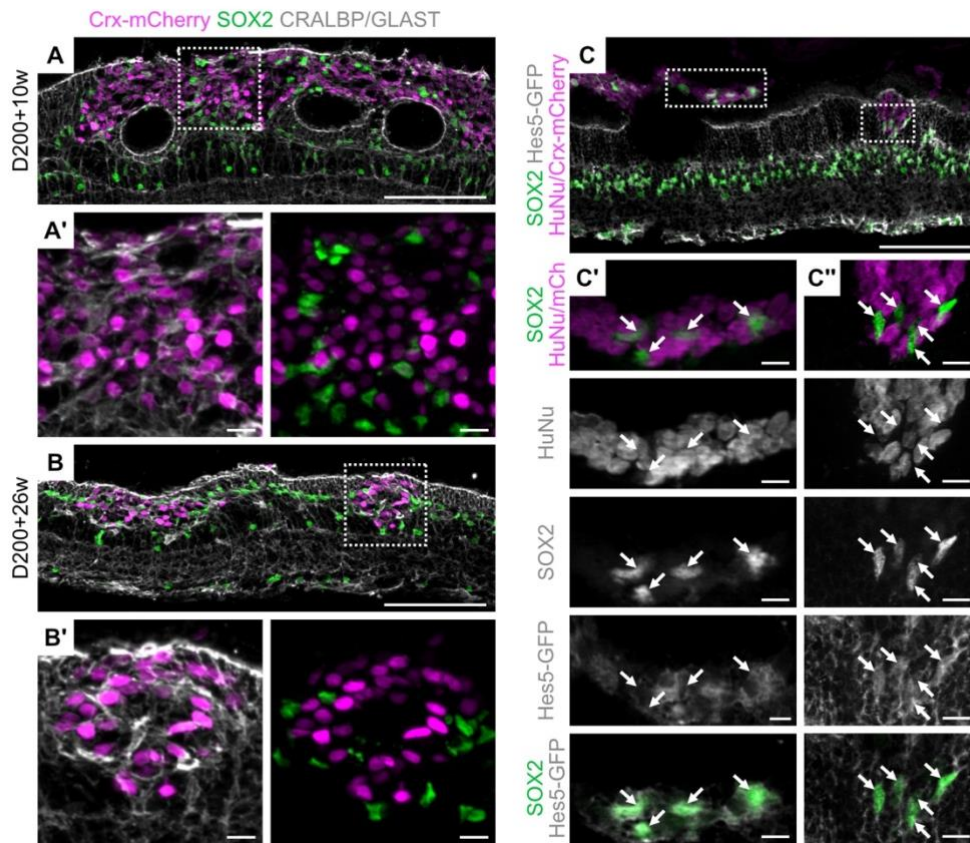


Figure 28. Host MG Nuclei are Present in D200 Grafts.

A-B. Intraretinal D200+10w (**A**) and D200+26w (**B**) grafts are pervaded by CRALBP/GLAST⁺ MG processes and contain SOX2⁺ MG nuclei. **C.** D200+10w grafts in Hes5-GFP mice show that intragraft MG processes and nuclei are of murine origin. For MG nuclei, this is additionally confirmed by SOX2⁺ nuclei being negative for HuNu. Scale bar: A, B, C 100 μ m. A', B', C', C'' 10 μ m. HuNu: Human nuclear antigen; mCh: Crx-mCherry.

4.3 Incorporating D200 Grafts Polarize and form Structures of Mature Photoreceptors

4.3.1 Grafts and host form an outer limiting membrane (OLM)-like structure

While close proximity of grafted cells and host MG is an interesting observation and suggests the existence of glial support for the human cells, MG and photoreceptor interdependencies go much further in the healthy retina. One important interaction is the formation of the outer limiting membrane (OLM), a continuous band of atypical adherens junction formed between MG and photoreceptors as well as MG and MG. This common structure gives the retina mechanical strength but also acts as a semipermeable diffusion barrier between the subretinal and the neuroretinal extracellular space.

In ultrastructural EM images of intraretinal human grafts, electron-dense junctions were indeed visible in the subapical region, i.e. at the base of the photoreceptor IS (Figure 29A). Like in the healthy retina, junctions were formed between

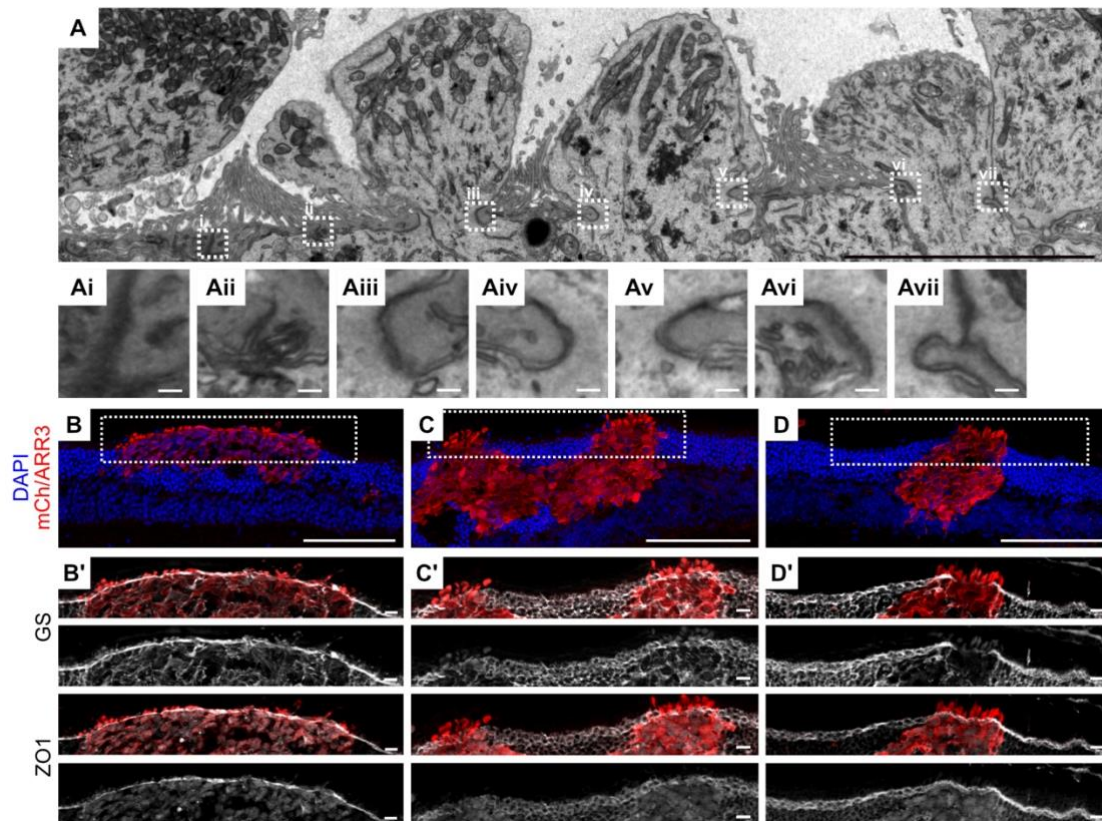


Figure 29. Intraspecies OLM Formation in Intraretinal D200 Grafts.

A. Ultrastructural assessment of intraretinal grafts showed the close association of human photoreceptors and host Müller glia (MG) cells, forming electron-dense junctions reminiscent of an OLM between photoreceptors and MG (Aiii-Avii) and MG and MG (Ai, Aii). **B-D.** Immunohistochemistry confirmed the presence of ZO1, an intracellular component of heterotypic adherens junctions in the OLM in both **(B)** D200+10w and **(C, D)** D200+26w samples mostly costaining with GS⁺ MG processes. Scale bars: A 50 μ m, Ai-Avii 100 nm, B-D 100 μ m, B'-D' 10 μ m. mCh: Crx-mCherry.

MG and MG (Figure 29A, Ai, Aii) as well as between human photoreceptors and endogenous MG (Figure 29A, Aiii-Avii). Costaining of the adherens junction marker ZO1 and the MG marker GS showed that the markers mostly overlapped (Figure 29B), showing the involvement of host MG also in IHC. Occasionally, a continuous ZO1 staining was visible, yet a colocalization with GS was not apparent (Figure 29D). While this could represent photoreceptor to photoreceptor junctions, it is more likely that GS⁺ MG processes here were too thin to yield an observable signal.

4.3.2 Inner segment formation occurs where an OLM is formed

While an OLM was often formed at the border of human grafts towards the subretinal space, its appearance did not guarantee IS formation in the same location. However, the generation of IS appeared to depend on the presence of an OLM, as preliminary staining of human mitochondria and ZO1 showed the presence of an OLM wherever IS were found (Figure 29E, E', arrows). This correlation is further illustrated in

an EM image of a D100+26w subretinal graft, which does not show IS formation (Figure 30B, Bi) except in an inverted fashion by a single cell that has extended a process into the host retina and formed tight and adherens junctions with murine MG (Figure 30Bii, Biii, arrows). Although still awaiting confirmation by proper analysis, this correlation of IS and OLM formation strongly suggests the necessity of endogenous MG interacting with the host cells for proper IS generation.

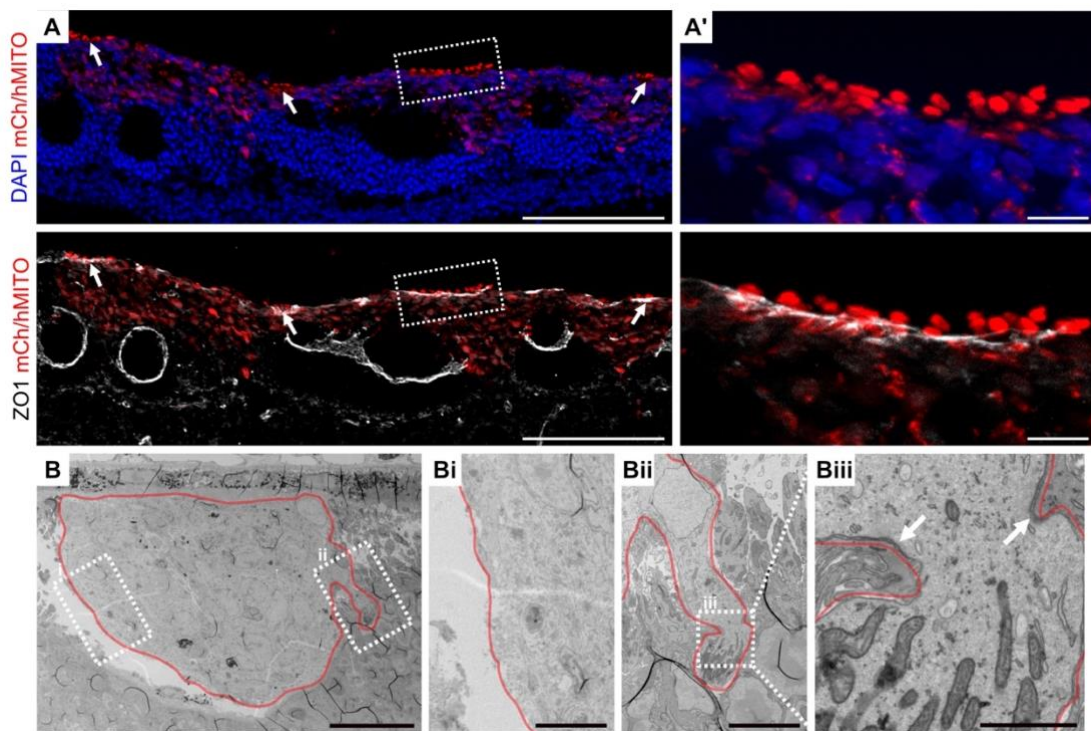


Figure 30. IS Generation correlates with OLM Formation.

A. While an OLM did not warrant the presence of inner segments (IS), IS formation was only found in regions with an OLM (arrows and **A'**). **B.** The depicted isolated D100+26w graft (demarcated by red line) did not generally show IS formation (**Bi**), yet a single cell extending into the murine retina generated an inverted, human mitochondria rich IS (**Bii**, **Biii**), coinciding with the formation of tight and adherens junctions with murine MG processes (**Biii**, arrows). Scale bars: A 100 μm , A' 10 μm , B 20 μm , Bi, Bii 5 μm , Biii 1 μm . mCh: Crx-mCherry.

4.3.3 Incorporating grafts form outer segment-like structures

Mature human photoreceptors perceive light through phototransduction occurring in the outer segment, a highly specialized primary cilium protruding onwards from the inner segment via the connecting cilium. As many IS were found, transplants were further examined for the presence of outer segments.

In cryosections, markers of cone outer segments were found to be expressed and accumulated neighboring IS, as shown through staining for OPN1L/MW, a marker for cone-only OS (Figure 31A, B). It is noteworthy to see that despite similar graft morphology and positioning, the distribution and intensity of OPN1L/MW staining differed between D200+10w and D200+26w samples. In D200+10w, OPN1L/MW was

mainly distributed throughout the cone cytosol, whereas in D200+26w, the signal was strongly enriched within the OS in many cells, suggesting that human cones require a certain timeframe for proper maturation (Figure 31A', B'). Also, in D200+26w samples, there were still several cells with only cytosolic labelling visible, which could be due to their OS being present in a different imaging plane or due to them not (yet) having developed an OS.

Unfortunately, the OPN1L/MW antibody used here was not human-specific. The OS structures were however shown to be human by direct apposition of the OS signal with human IS and, importantly, through colocalization with human-specific ARR3 staining (Figure 31A', B'). Furthermore, in EM images, connecting cilia extending from human IS (Figure 31C-D') were detected, and Figure 31E, E' shows a stacked but disorganized OS in very close proximity to a human IS. While the OS species in Figure

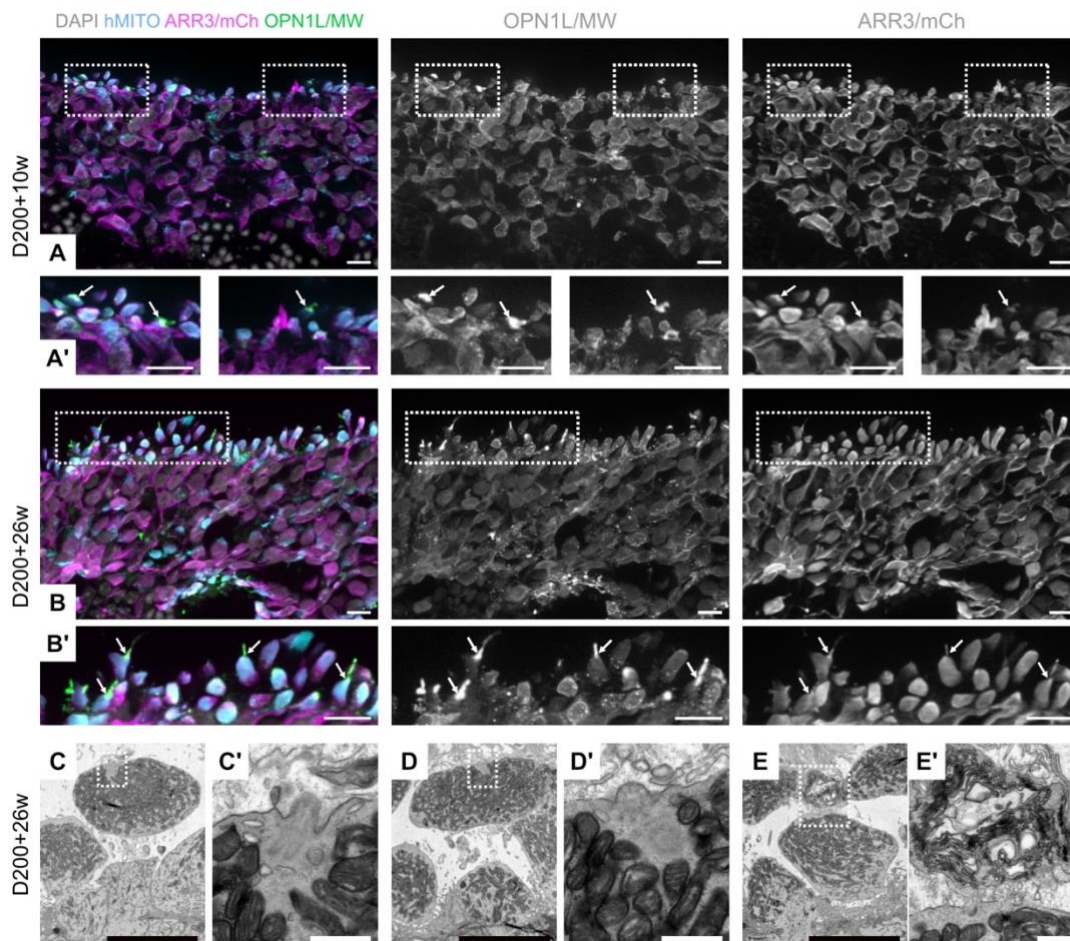


Figure 31. Potential Outer Segment Formation in D200 Grafts.

A, B. Expression of the cone outer segment marker OPN1L/MW in D200+10w (**A**) and D200+26w (**B**) grafts. While not a human-specific antibody, the OPN1L/MW marked OS is considered human due to its close proximity to human inner segments (IS) and colocalization of the signal with human-specific ARR3 (**A'**, **B'**, arrows). **C-E.** Transmission electron microscopy of human IS and associated indicators of outer segment formation. **C, D.** Connecting cilia extending from human IS in the lateral (**C'**) and cross-sectional (**D'**) view. **E, E'.** Close proximity of an IS and a disorganized outer segment of unknown species. Scale bars: A-B' 10 μ m; C-E 5 μ m, C'-E' 500 nm.

31E, E' is not certain, its position suggests it belongs to a photoreceptor from the human transplant. Unfortunately, no combined IS/OS structure were seen and further assessment of EM data is required.

4.3.4 Incorporating grafts form synaptic structures

In the healthy retina, photoreceptors are connected with the following secondary neurons through synapses at the end of their axons. The rod spherules and the cone pedicles are the site of the first cell-to-cell signal transmission required for vision. Similarly, to re-establish vision after cell transplantation, grafted cells need to form synapses with host secondary neurons in order to integrate into the host retinal circuitry. Therefore, the possibility of synapse formation was examined in D200+26w samples.

Staining with antibodies for the presynaptic protein CTBP2, a component of the ribbon synapse, showed presynaptic structures within human grafts in close apposition to MGLUR6, a postsynaptic receptor typically expressed on ON rod bipolar cells (Figure 32A-A''). Orthogonal views of maximum intensity projected image stacks confirmed the colocalization of CTBP2 and MGLUR6 with human-specific ARR3 staining also in the z-plane (Figure 32C, C'). The apparent colocalization of the postsynaptic MGLUR6 with the presynaptic cytosol might be due to the insufficient microscopy resolution, unable to resolve the presynapse itself from the thin bipolar cell processes invaginating the cone photoreceptor pedicle. However, the presence of other synapses seemingly colocalizing in the maximum intensity projected stack with the human cytosol but not in the z-view warrant careful examination of similar stainings (Figure 32C, C'').

In addition to immunohistochemical analysis, presynaptic structures were also found in electron microscopy analysis (Figure 32B-Biii). Here, ribbons and synaptic vesicles were found within human cell clusters as identified by nuclear size and structure (Figure 32B, B', blue overlay). While this again does not undoubtedly prove human identity of the presynapses, the localisation strongly mimics the staining pattern seen in IHC, where synapses were found to accumulate in cytosolic clusters within the human grafts, away from murine photoreceptors (compare Figure 32A-A''). Additionally, the phenotype observed is highly reminiscent of that seen upon transplantation of a cone-specific reporter cell line, where immunogold labeling indeed confirmed the human origin of the presynaptic ribbons (Gasparini et al., 2022).

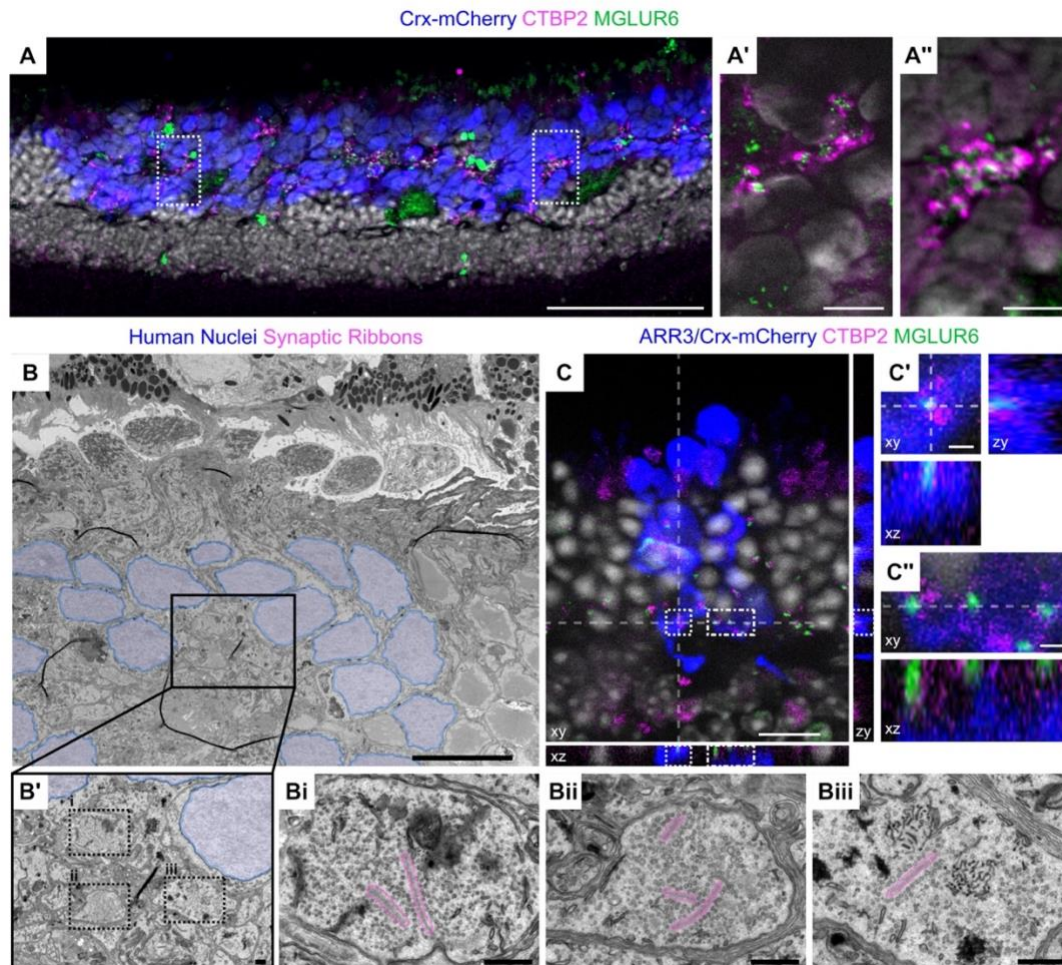


Figure 32. Formation of Synaptic Structures within Human Grafts.

A. Intraretinal human grafts show dispersed labelling for pre- and directly apposed postsynaptic markers CTBP2 and MGLUR6 within the graft. Notice the characteristic horseshoe shape of the presynaptic label also in **A'** and **A''**. **B.** EM images confirm the presence of ribbon synapses (magenta overlay, **Bi-Biii**) in human clusters (blue overlay for human nuclei, **B, B'**) with many vesicles docked or present in the near vicinity. The localisation of the presynaptic structure mirrors the synapse positioning observed in **A**. **C.** Maximum intensity projected image with adjunct side views of the z-stack show that some synapses colocalise with cytosolic human cone staining in z (**C'**) while others do not (**C''**). Scale bars: **A** 100 μm ; **A', A''**, **B** 10 μm ; **B', Bi-Biii** 500 nm; **C** 10 μm ; **C', C''** 1 μm .

4.3.5 Transplanted Crx-mCherry+ cells become enriched for cones

In order to examine human grafts in more detail beyond immunohistochemistry, transplanted cells were retrieved from the murine retina, re-sorted for Crx-mCherry+ expression and submitted to single cell sequencing (scSeq). The transplanted, “ex vivo” cells were then compared with “in vitro” age-matched Crx-mCherry+ cells collected directly from human retinal organoids. The data shown in Figure 33 thus contains the D200, D270 and D370 in vitro data already shown in Figure 11, now combined and clustered anew together with the D200-derived ex vivo samples.

As before, cones and rods were clearly identifiable (Figure 33A, B, E), however now a small subpopulation of bipolar cells was also distinguishable (Figure 33C, E),

while a negligible number of MG cells was found in the D200 donor cell population only (Figure 33D, E, H, I). Furthermore, another cluster was defined by low expression of mitochondrial genes, hence termed “lowMT” (Figure 33E, G). While a portion of lowMT cells also expressed some photoreceptor markers (Figure 33A, E), their expression level was generally below that of cone and rod cells with higher mitochondrial content, suggesting some lowMT cells might represent immature photoreceptors. While detailed analysis of cell types present in the lowMT cluster is still required, interestingly, it was found to consist almost exclusively of in vitro cells of all ages (Figure 33G-I), suggesting that the murine retinal environment might increase photoreceptor-specific gene expression and mitochondrial metabolism. The few ex vivo lowMT cells on the other hand might represent immature photoreceptors, e.g. originating from isolated clusters.

Preliminary analysis looking at in vitro versus ex vivo Crx-mCherry+ cells showed a strong difference in relative cell type ratios. While D200 in vitro samples contained

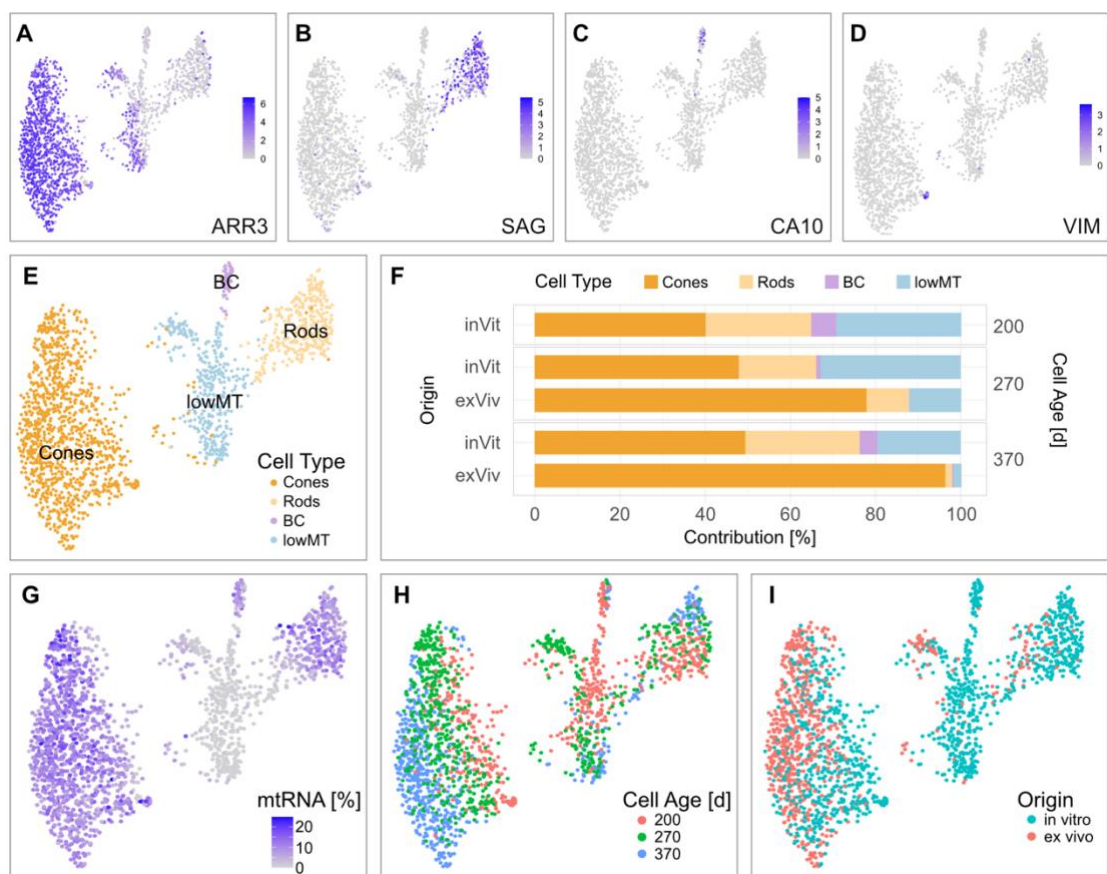


Figure 33. Single Cell Transcriptome Analysis of Ex Vivo and In Vitro Crx-mCherry+ Cells.

A-D. UMAP plots of D200, D270 and D370 in vitro and ex vivo samples coloured for expression levels of exemplary cell-type specific marker genes for cones (ARR3, **A**), rods, (SAG, **B**), bipolar cells (CA10, **C**) and Müller glia (VIM, **D**). Each dot represents a single cell, coloured by normalised and log-transformed expression levels. **E.** UMAP plot color-coded for cell types as manually identified. **F.** Quantification of cell type fractions dependant on total cell age and origin. **G-I.** UMAP plots color-coded for further relevant cell characteristics showing mitochondrial RNA content (**G**), total cell age (**H**) and cell origin (**I**). BC: bipolar cells; lowMT: low mitochondrial content; inVit: in vitro; exViv: ex vivo.

roughly 40% cones and 25% rods, in D270 ex vivo samples (D200+10w) this ratio was shifted towards 78% cones and only 10% rods (Figure 33F). The divergence was further increased at D370 (D200+26w), where 96% of ex vivo cells were identified as cones and only 2% as rods. The single cell sequencing data hence mirrored the previous immunohistochemical stainings, which showed virtually all transplanted human cells labelling positive for the cytosolic cone marker ARR3 (e.g. Figure 25, Figure 27).

The surprising increase in the ratio of cones to rods after transplantation could be due to a better survival of cones within the murine retinal environment or during the transplantation procedure itself. Increased cell age alone however did not explain the change in cone to rod ratio, as in D270 and D370 in vitro samples roughly similar amounts of cones (48% at D270 and 50% at D370) and an even higher amount of rods at the later stage (18% at D270 and 27% at D370) were detected (Figure 33F).

4.3.6 Higher levels of mature photoreceptor markers in ex vivo compared to in vitro cones

To detect changes in cone gene expression in dependence on environmental conditions, differential gene expression analysis comparing D370 in vitro and ex vivo cones was performed. The resulting genes were used to identify statistically overrepresented gene ontology (GO) terms, which indicate common functions of differentially expressed genes. Here, only GO terms of the first hierarchical order are shown to reduce repetitions (Figure 34A).

GO term analysis of genes upregulated in ex vivo cells identified an increase in genes required for mitochondrial respiratory chain formation and function, e.g. “electron transport coupled proton transport (GO:0015990)” or “mitochondrial respiratory chain complex I assembly (GO:0032981)”, suggesting an overall increase in mitochondrial number and activity (Figure 34A). Conversely, in D370 in vitro cells, the biological processes “canonical glycolysis (GO:0061621)” and “positive regulation of ATP biosynthetic process (GO:2001171)” were more prevalent. This, together with increased mitochondria numbers in vivo, could indicate a switch in energy metabolism from glycolysis in vitro to more oxidative phosphorylation after transplantation (Petit et al., 2018).

The second group of overrepresented GO terms in the ex vivo samples was linked to photoreceptor segment formation and function, yielding terms like “phototransduction (GO:0007602)”, “photoreceptor disc membrane (GO:0097381)” and “G protein-coupled photoreceptor activity (GO:0008020)” (Figure 34A). Surprisingly the

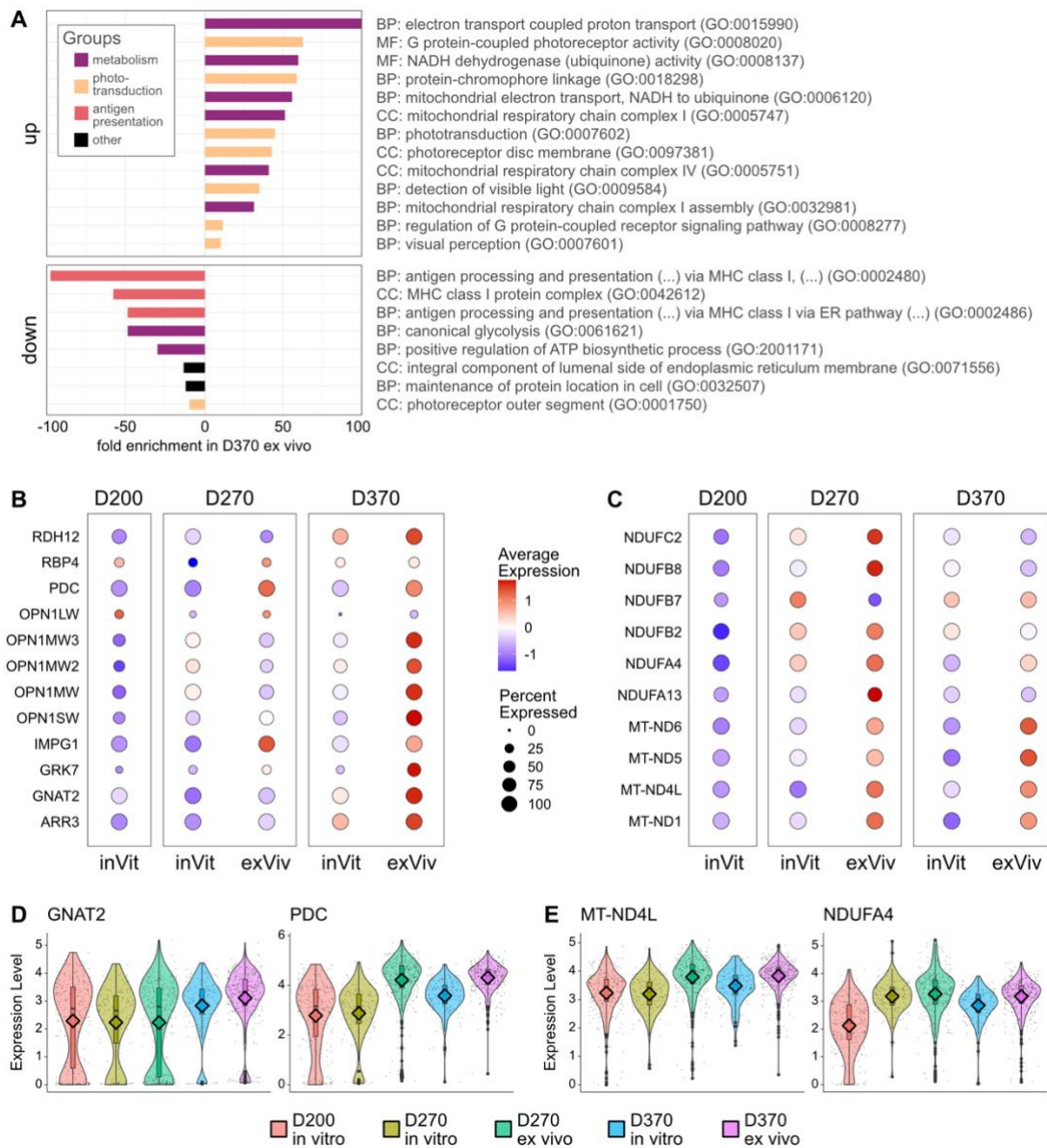


Figure 34. Differences in Functional Gene Expression between In Vitro and Ex Vivo Cones.

A. GO terms over- and underrepresented in D370 ex vivo samples compared to D370 in vitro cell. **B, C.** Dot Plots showing average expression levels of genes involved in GO terms related to **(B)** photoreceptor segment formation and visual perception and **(C)** mitochondrial complex I and IV formation and function. **D, E.** Violin plots showing expression levels of exemplary genes from **A** **(D)** and **B** **(E)**. Each thin black dot represents a single cell, diamonds show means and boxes extend from 25% to 75% quartile, with black bar showing the median and thick black dots showing outliers. BP: biological processes; CC: cellular component; MF: molecular function; inVit: in vitro; exViv: ex vivo.

term “photoreceptor outer segment (GO:0001750)” was enriched in in vitro samples, however this was based on primarily rod-specific genes such as TULP1, CERKL and RP1, which are likely lacking in ex vivo samples due to the overwhelming majority of cones in those samples. Overall, the enrichment of terms related to visual perception in ex vivo cones suggested that transplanted cells were more capable of perceiving light through outer segment related structures than age-matched in vitro samples. This

importantly indicated an improved maturation within the mouse neuroretinal environment compared to retinal organoid culture.

Interestingly, another group of terms upregulated in the in vitro setting was connected to antigen processing and presentation via MHC class I protein complexes (MHC-I, also human leukocyte antigen class I, HLA-I), suggesting that MHC-I mediated antigen presentation is reduced in ex vivo cones. While the immune-suppressive nature of the retinal environment (Mochizuki et al., 2013) may have affected the MHC-I levels, MHC-I expression has also been shown to be downregulated in endothelial cells upon treatment with corticosteroids (Y. Wang et al., 2011), and a similar response may have been induced here by the intravitreal application of triamcinolone acetonide. However, beyond its role in antigen processing and presentation, neuronal MHC-I expression has been implicated in central nervous system development, synaptic refinement, axonal pathfinding as well as axonal regeneration (Cebrián et al., 2014; Higenell & Ruthazer, 2010). Therefore, the reduced MHC-I expression in ex vivo samples might also be an inducer or a consequence of related processes during cone incorporation. Interestingly, this notion is supported by a recent report of photoreceptor sheet transplantation into immune-compromised rats, where HLA-I expression was found to differ between graft regions proximal or distal to the endogenous retina, with the proximal grafted cells expressing no or only low amounts of HLA-I (Yamasaki et al., 2021).

To better visualize the significance and underlying data of the GO term analysis, several genes of interest involved in the abovementioned GO terms were selected and compared across experimental conditions, showing their average expression (B, C) and, for a few representative genes, their expression levels per cell (Figure 34D, E). Here, it was again noticeable that D370 ex vivo cells, i.e. D200+26w, had the highest expression level of genes involved in visual perception and outer segment formation (Figure 34B, D). Similarly, in genes relevant for mitochondrial complex I and IV formation, the average expression level was higher in D370 ex vivo than D370 in vitro samples (Figure 34C, E).

Interestingly, although not the focus of this comparison, the differential expression of genes involved in visual perception and mitochondrial function was already observable at D270 (Figure 33D, E). Here, many of the respective genes were also expressed more highly in the D270 ex vivo cells than the D270 in vitro samples, yet at D370, this trend was much more pronounced. Together, this was a strong indicator of ex vivo cones maturing to a greater extent than age-matched cells kept in the in vitro setting – importantly despite the xenograft environment.

4.4 Incorporation and Maturation Capacity depend on the Host Environment

4.4.1 Graft morphology and maturation in C57BL/6JRj recipients resembles that in Cpf1 hosts

Degeneration of mouse photoreceptors can affect the retinal microenvironment differently depending on the degenerative cause and dynamics, influencing transplantation outcome. To assess whether the graft phenotype observed in Cpf1 hosts is restricted to this mouse strain, which for example exhibits a moderate gliotic activation of MG, D200 Crx-mCherry⁺ cells were additionally transplanted into age-matched wildtype hosts. While detailed assessment of graft incorporation, maturation and interaction are still pending, the general graft morphology strongly resembled that seen in Cpf1 animals (Figure 35). As such, the human transplants were able to contact the host retina, begin inner segment formation in vicinity to the contact points (Figure 35A') and extend their interaction and inner segment formation over time (Figure 35B, B').

4.4.2 Graft morphology and maturation in highly degenerated rd1 and tgCR host lines differs strongly from the outcome in models with an ONL

To investigate the outcome of Crx-mCherry transplantation in highly degenerated mouse models, D200 cells were further grafted into retinal degeneration 1

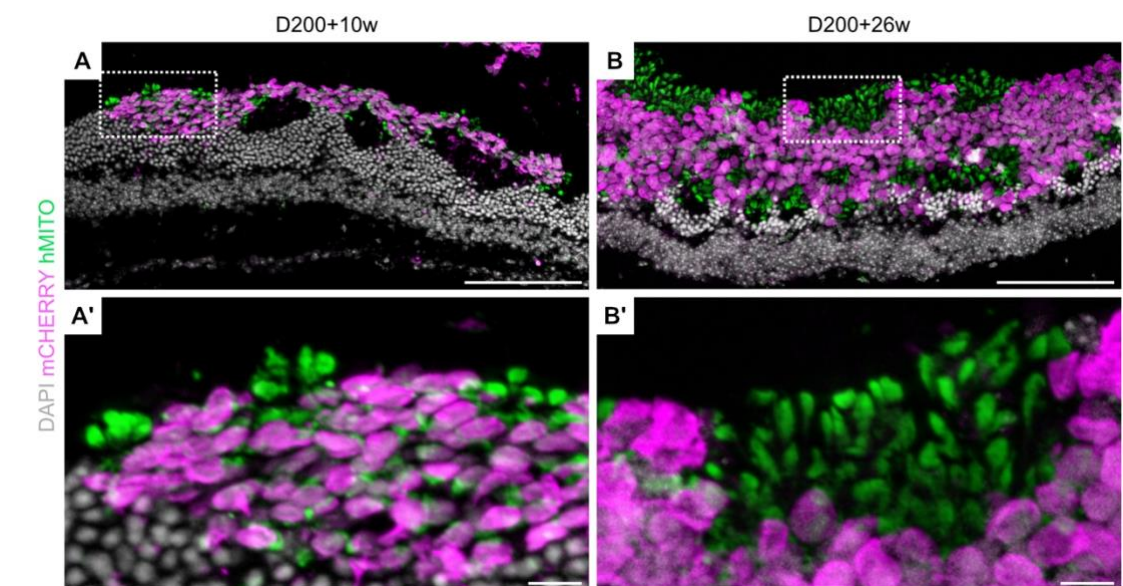


Figure 35. D200 Grafts in C57BL/6JRj Hosts.

A, B. D200 Crx-mCherry⁺ cells grafted into C57BL/6JRj retina show a similar morphology to transplants in Cpf1 animals at both D200+10w (**A**) and D200+26w (**B**), with inner segment formation (**A'**, **B'**). Scale bars: A, B 100 μ m; A', B' 10 μ m.

(rd1) and tg(Cpfl1; Rho^{-/-}) (tgCR) mice. Rd1 animals exhibit a severe, early onset degeneration of rod photoreceptors due to aberrations in the Pde6b gene. tgCR animals are a cross of Cpfl1 and Rho^{-/-} mice, with Rho^{-/-} animals having a deletion in exon II of the rhodopsin gene, which causes a lack of proper rod outer segment formation and a complete degeneration of rods until 3 months of age, with a secondary cone degeneration. Correspondingly, in adult retinal cross-sections, no outer nuclear layer can be discerned in either mouse line (Figure 36B, C, compare Figure 36A for adult Cpfl1 retinal cross-section).

Graft morphology in both rd1 and tgCR animals differed strongly from the outcome in the Cpfl1 mouse: In Cpfl1 mice, human cells were mostly present in clusters containing many layers of cells, with mitochondria-rich inner segments (IS) mainly oriented towards the RPE (Figure 36A, A'). In both rd1 and tgCR mice on the other hand, the cells were distributed over a larger area in the subretinal space, and only formed small cell clusters, if any (Figure 36B-C'). They were usually present in a thin layer as a row of single or only very few cells. Occasionally, grafts accumulated human mitochondria in what looked like nascent IS (Figure 36E, E'), however this was observed much more rarely than in age-matched Cpfl1 hosts (Figure 36D, D') and IS appeared less oriented.

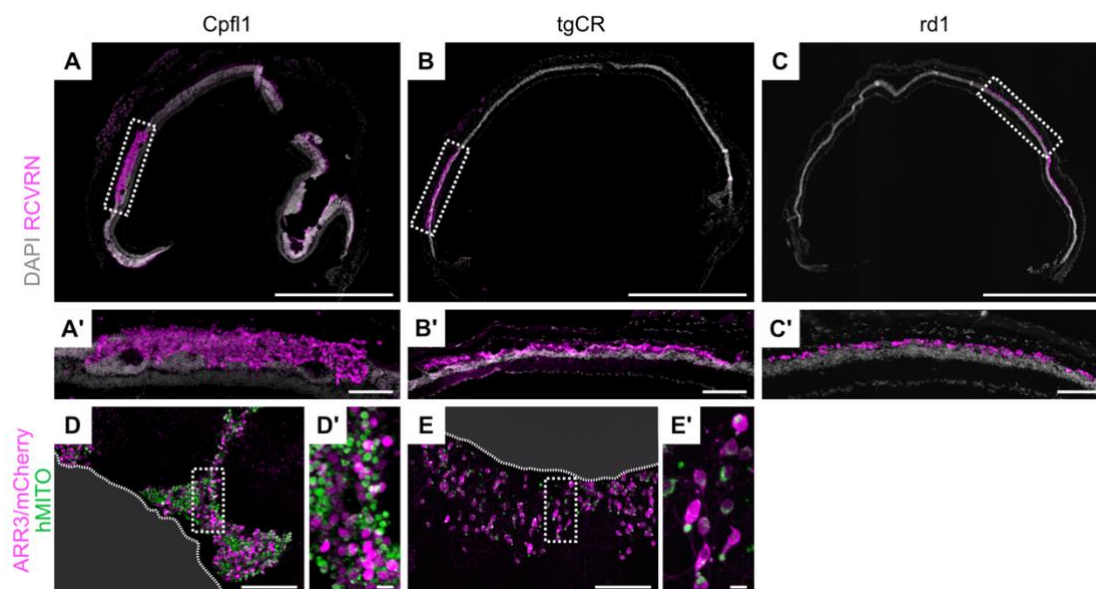


Figure 36. Qualitative Comparison of Graft Morphology in Cpfl1, tgCR and rd1 Mice.

A-C. Retinal cross-sections of cpfl1, tgCR and rd1 mice containing RCVRN⁺ D200 grafts show a thick human cell cluster in the Cpfl1 eye (**A, A'**, D200+10w), while cells in the tgCR and rd1 eyes are present in a thin layer (**B, B'**, **C, C'**, D200+26w). **D,E.** Retinal flatmounts facing the subretinal side confirm the appearance of human cells in clusters in the Cpfl1 eye (**D, D'**) and show a large number of inner segments formed while the graft appears as mostly separated cells in the tgCR eye, with inner only small, occasional inner segments being formed (**E, E'**), both D200+10w. Scale bars: A, B, C 1 mm; A'-C', D, E 100 μ m; D', E' 10 μ m.

The grafts in animals with strong retinal degeneration were further examined for their maturation and their interaction with the host. In tgCR mice, the human cells were found in close proximity to host GFAP⁺ MG processes (Figure 37A, A'), however they were usually positioned above said processes. Unlike in Cpf1 hosts, there were no MG processes extending beyond the human cell bodies, and, correspondingly, there was no indication of a continuous OLM-like structure being formed. Maturation of human inner segments was only rarely observed (Figure 36), and similarly, even at D200+26w, no oriented deposition of cone IPM was evident (Figure 37B, B'). Interestingly, grafted cells were however found capable of forming presynaptic structures in the tgCR host, as shown by CTBP2 signal colocalizing with human-specific ARR3 staining (Figure 37C, C').

In rd1 mice, the interaction with Müller glia appeared different, as GS⁺ processes were found to extend beyond the human cell bodies and “include” them in the host retina (Figure 38A, A'). Furthermore, ZO1⁺ staining colocalizing with the MG cytosol above the human cells was found (Figure 38B, B'). Further analysis is required to understand whether this signal is representative of a potential OLM-like structure aiding IS

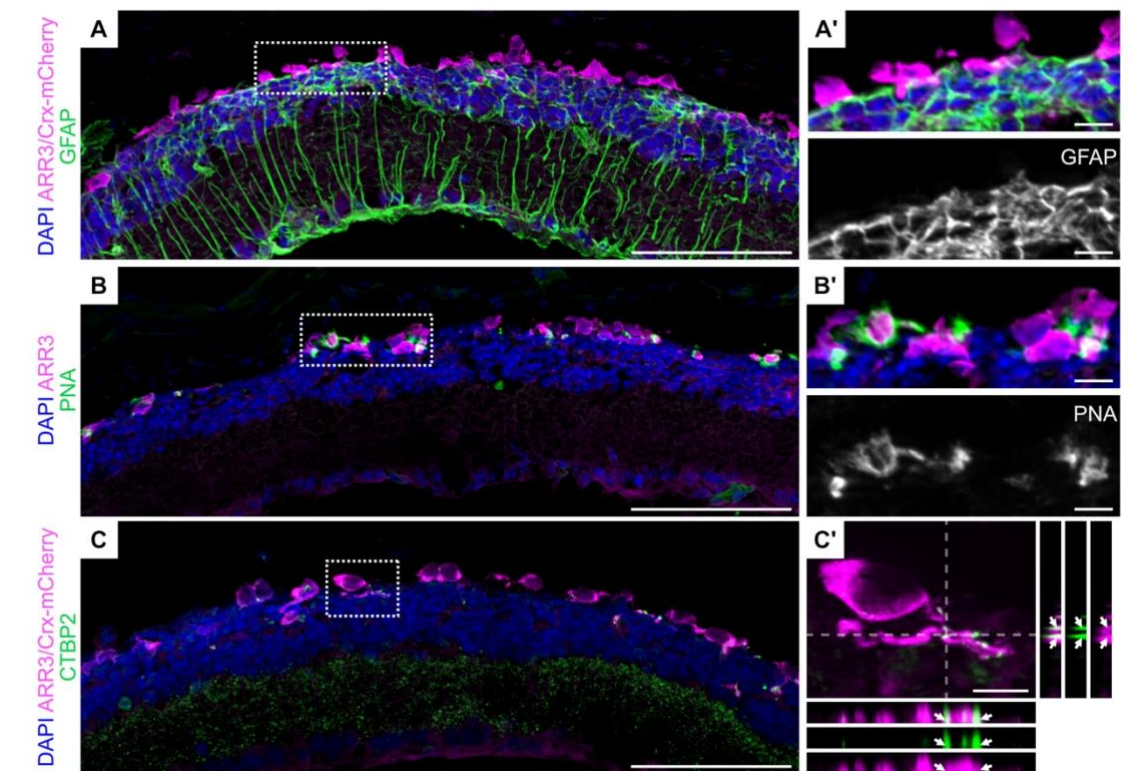


Figure 37. Graft Interaction and Maturation in tgCR Hosts at D200+26w.

A, A'. Grafted cells are in vicinity to GFAP⁺ host MG processes, yet there is no indication of enwrapment of human cells by MG processes or an OLM formation. **B, B'.** Some grafted cells accumulate PNA⁺ IPM, yet there is no clear directionality towards the RPE. **C.** Grafted cells occasionally express the presynaptic marker CTBP2 as shown by CTBP2 staining overlapping with the human-specific marker ARR3 in the maximum intensity projection of a z-stack in xy as well as in the xz and zy plane (C', arrows). Scale bars: A-C 100 μ m; A'-C' 10 μ m.

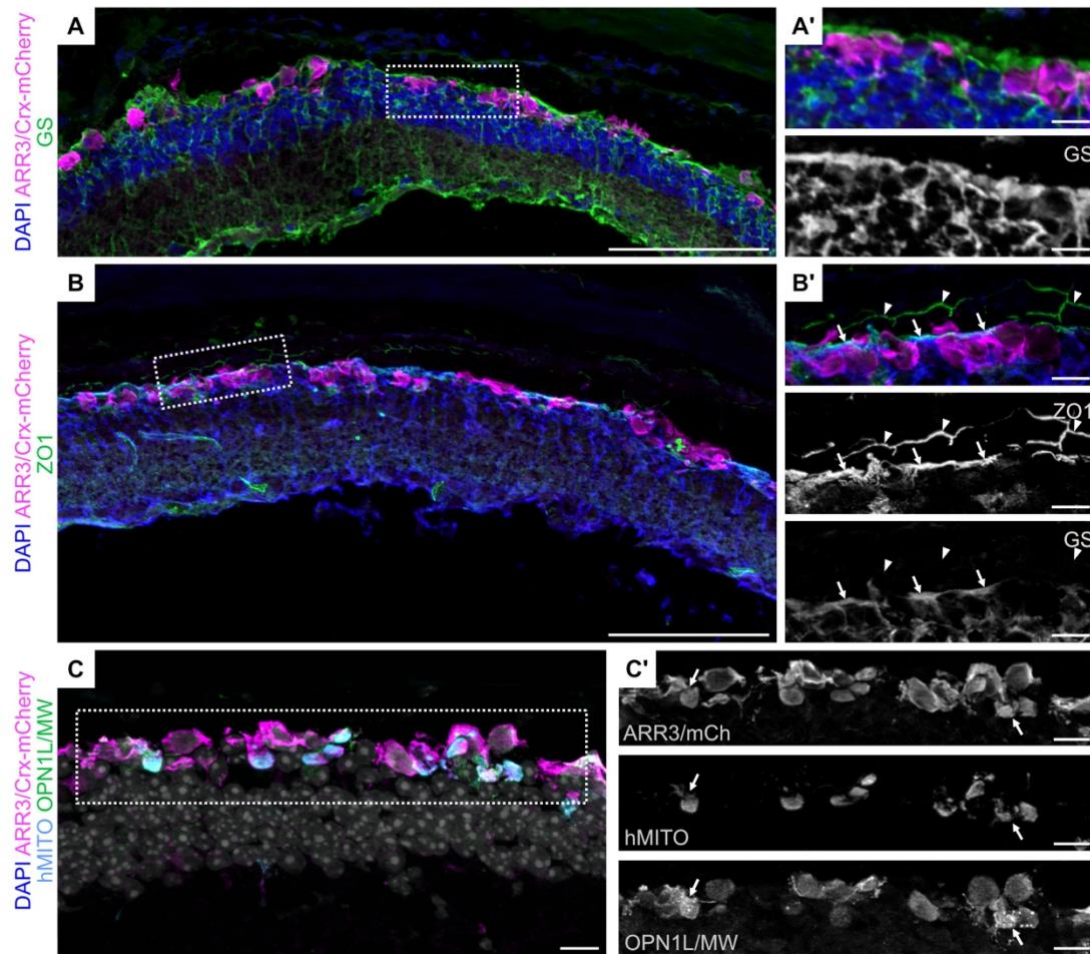


Figure 38. Graft Interaction and Maturation in rd1 Hosts at D200+26w.

A. Host Müller glia extend processes beyond the human cells and seem to enwrap them (**A'**). **B.** ZO1 staining shows the presence of junctions in MG cells (**B'**, arrows) mostly above the human cells. ZO1 staining in the upper portion of the magnified image shows junctions between RPE cells (**B'**, arrowheads). **C.** Many human cones show inner segment-like structure and express low levels of OPN1L/MW, some in a punctate fashion in the cytosol (**C'**, arrows), however without clearly forming outer segments (compare Figure 31B, B'). Scale bars: A, B 100 μm ; A', B', C, C' 10 μm . mCh: Crx-mCherry.

formation. While inner segments were indeed formed (Figure 38C, Figure 36C), no outer segments were detected so far (Figure 38C'). The human cells did however express OPN1L/MW, albeit at low levels, in a mostly even distribution in the cytosol. Sometimes, an accumulation of OPN1L/MW⁺ speckles was detected (Figure 38C, C' arrows), similar to that in Cpf1 animals (compare Figure 31B'), which might represent an enrichment of OPN1L/MW-derived proteins towards OS formation.

4.5 Summary

Although not showing the highest rate of intraretinal positioning, D200 Crx-mCherry⁺ grafts generate the most inner segments, both absolute and relative to graft size, and interact extensively with host Müller glia and bipolar cell processes. In Cpf1 mice, instead of sealing human grafts out, host Müller glia can enter the transplants and form an OLM in conjunction with the human cells. Inner segment formation relies on the proximity of human cells to the host retina and possibly also on the generation of said OLM, underscoring the importance of graft-host interactions for transplanted photoreceptor maturation.

Human D200 Crx-mCherry⁺ photoreceptors are further capable of polarizing and developing additional mature structures that are indispensable for proper photoreceptor function. The presence of outer segments and axonal terminals, that most likely represent a structural connection to host secondary neurons, shows the capacity of human photoreceptors to mature and potentially connect with the host. Importantly, as detected by single cell sequencing, transplanted cones are able to supersede the maturation level of cones kept in *in vitro*.

Lastly, comparison of transplantation outcome in the Cpf1 host versus graft morphology and maturation in other mouse models again highlights the influence of host retinal architecture on graft maturation. While grafts in wildtype mice are able to incorporate and form large quantities of inner segments, transplants in mouse models with strong retinal degeneration mostly lack proper polarization and maturation, which has important implications for the potential use of photoreceptor replacement therapy in end-stage retinal disease.

5 Functional Assessment of Transplanted Crx-mCherry+ Cells

5.1 Aims

The photoreceptor polarization and maturation observed in D200 Crx-mCherry⁺ grafts arguably represents the foundation to potentially re-establish vision through cell replacement therapy. While important structures for photoreceptor function such as inner segments, outer segments and putative synapses were found in the human grafts, the presence of said structures alone however does not confirm their functionality. The aim of this chapter was therefore to assess potential graft-mediated function by behavioral and electrophysiological readouts.

5.2 High-Level Function

5.2.1 Light-Dark Box

As nocturnal animals, mice are mostly active in the dark and have an innate aversion against brightly lit spaces, causing them to preferentially remain in the dark if they can perceive light. The light-dark box (LDB) assay uses this light-aversion guided behavior as a readout for visual function. In the present setup (Figure 39A), the animals were placed in the illuminated compartment of the LDB and were free to explore the space. After 30 s, a doorway opened towards a dark compartment of the same size and the animals could move unrestrained between the two parts for an additional 10 min, the assay time. The fraction of time spent in the dark was then used as a measure of light aversion.

Here, a light intensity of 620 lux at the bottom of the lit compartment was used, which was shown to be sufficient to induce light-aversion guided behavior (Costall 1989). Under those conditions, C57BL/6JRj wildtype mice were found to spend on average 62% of the assay time in the dark (Figure 39B). This value is never 100% as the light-aversion behavior is balanced by the animal's propensity to explore the illuminated compartment, e.g. with respect to food or escape sites. Similarly, untreated Cpf1 mice as well as Cpf1 mice transplanted with Crx-mCherry⁺ cells spent on average 58-66% of the assay time in the dark compartment (Figure 39C). This reflected the fact that the cone only degeneration Cpf1 mice possess normal, functioning rods, which can mediate the light-aversion behavior. Accordingly, no significant difference between any of the groups compared to the control conditions or between +10w and +26w animals of the same donor age could be detected (see *Table 4. Statistical Analyses* for details on the statistical tests used).

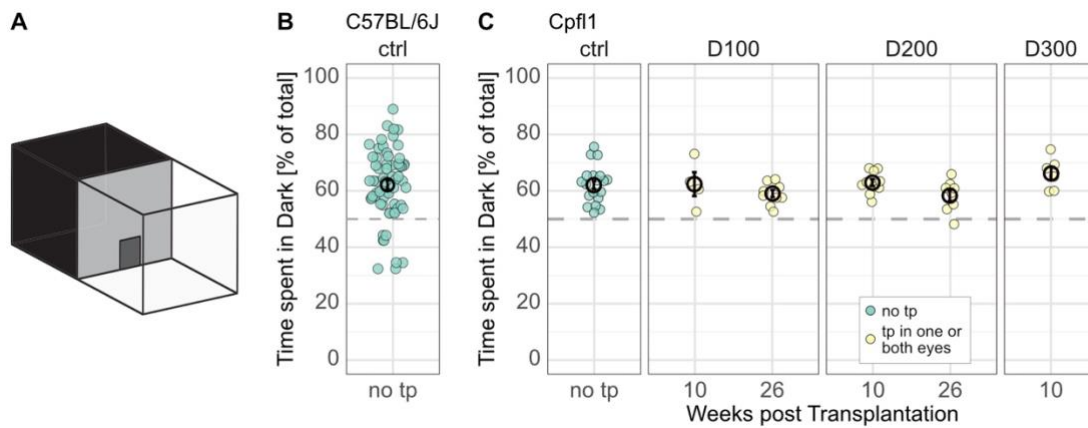


Figure 39. Light-Dark Box Results of C57BL/6Jrj and Cpf1 Animals

A. Schematic depiction of light-dark box (LDB) with a bright and a dark compartement connected by a doorway, from (Gasparini et al., 2018). **B, C.** Light aversion of experimental animals as measured by percent of assay time spent in the dark compartiment in untreated C57BL/6Jrj wildtype (**B**) and untreated or transplanted Cpf1 (**C**) mice, separated by donor cell age. Statistical analysis showed no significant difference between any group compared to the Cpf1 control data or between different weeks post transplantation within the same donor age. No significant differences found, see *Table 4* for details on statistical tests. Hollow symbols and bars show mean±SE. ctrl: control, tp: transplantation, D: day.

In contrast to Cpf1 animals, rd1 and tgCR mice beyond 4 weeks and 3 months of age respectively lack endogenous rods, which should greatly reduce their light-aversion guided behavior. In the LDB, tgCR control animals consequently spent only 54% of the assay time in the dark compartiment. Transplantation of Crx-mCherry⁺ cells however did not increase that value, as the time spent in the dark remained at 48-50% (Figure 40A). This did however mirror the little evidence for inner and outer segment

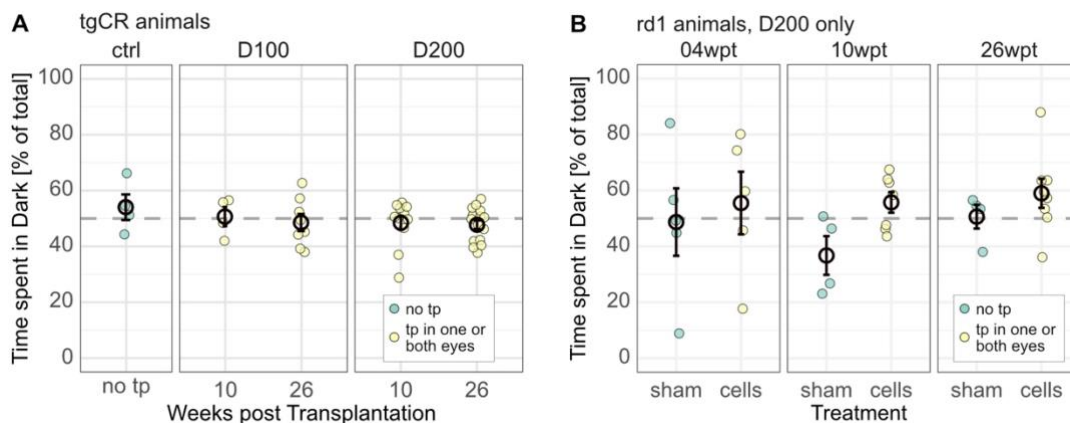


Figure 40. Light-Dark Box Results of Strongly Degenerated Animals.

A, B. Light aversion of experimental animals as measured by percent of assay time spent in the dark compartiment in untreated or transplanted tgCR mice separated by donor cell age (**A**) and treated rd1 mice separated by weeks post transplantation of D200 donor cells or sham transplantation (**B**). Statistical analysis showed no significant difference between any group compared to the tgCR control data (**A**) or between rd1 treatment groups of the same follow-up timeframe (**B**). No significant differences found, see *Table 4* for details on statistical tests. Hollow symbols and bars show mean±SE. ctrl: control, tp: transplantation, D: day.

formation of the grafted cells in these mice, which was likely insufficient to re-establish vision-guided behavior.

Rd1 animals on the other hand reacted differently to the LDB paradigm depending on whether they had received subretinal injections of Crx-mCherry⁺ cells or buffer only. At the timepoints examined, animals treated with cells in one or both eyes on average spent more time in the dark (56%, 56%, 59% at 4, 10 and 26 wpt respectively compared to 49%, 37% and 51% for sham injected animals, Figure 40B). While this trend was observable at all timepoints measured, the difference was not significant except at 10 wpt (Figure 40B). This suggests rd1 animals might regain some visual function through D200 Crx-mCherry⁺ cell transplantation. It is however important to note that behavioral assays are inherently variable, which can be seen in the standard error of each experimental group, but also in the fluctuation of values for the sham-transplanted animals over time. The values from the 10 wpt sham group for example lie below the 4 wpt and 26 wpt sham groups. While this could reflect true biology, it could also be an effect of sample size and requires further repetitions. Regardless, transplanted rd1 animals did show a trend towards increased light susceptibility compared to sham-injected controls.

5.3 Tissue-Level Function

5.3.1 Multi-electrode array assessment of D200+26w grafts in Cpf1 mice

Behavioral assessment of visual function is difficult as it is affected by many factors. The animal's behavior in the LDB assay is for example influenced by its anxiety and curiosity in addition to its visual function, making the response of the cohort overall highly variable and requiring large animal numbers to obtain solid data. These confounding factors can however be bypassed by reading out visual function on a tissue level, e.g. by directly measuring the response of downstream neurons to optical stimuli through electrophysiological approaches. Here, multi-electrode arrays (MEA) were used to record the graft-mediated response of retinal ganglion cells (RGC) to light stimulation. All MEA assessment and analysis was performed by Miriam Reh in the laboratory of Dr. Günther Zeck at the Naturwissenschaftliches und Medizinisches Institut Tübingen.

5.3.2 Isolation of cone-mediated RGC response through photopic light stimulation and L-AP4 addition

To analyze the response of RGCs to light in transplanted versus untransplanted retinal regions, Cpf1 retinas were explanted, placed onto the MEA and stimulated with different intensities and patterns of green light. As Cpf1 mice do not exhibit cone

function but have morphologically normal and functional rods, potential re-establishment of vision by the transplant was only assessable for cones. To isolate the cone response, a photopic stimulation regime was used. However, cells were still found to exhibit a photopic light response in transplant-free control samples when fluorescent light was applied beforehand (Figure 41), a measure required to locate the graft in transplanted samples. As this was most likely caused by an aberrant rod activation (Tikidji-Hamburyan 2017), L-AP4 was applied, blocking mGluR6 metabotropic ion channels. MGLuR6 channels are mediators of the ON-pathway, which is the main pathway responding to rod activation, while cones signal through both, the ON- and the OFF-pathway. L-AP4 application indeed abolished the photopic light response after fluorescence (Figure 41) and hence allowed to isolate the OFF-pathway responses.

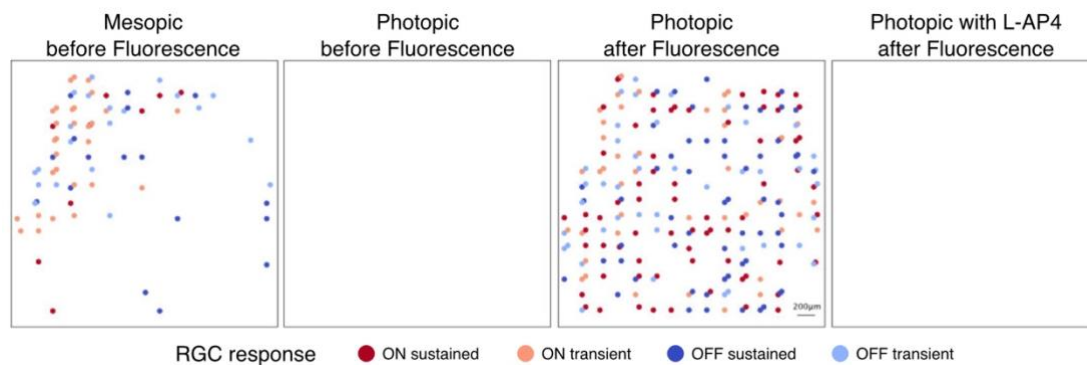


Figure 41. Rod Response after Fluorescent Light Exposure in Untransplanted Cpf1 Retina.

MEA electrodes detecting RGC activity upon stimulation of a transplant-free Cpf1 retina with mesopic and photopic light. While there is no photopic response initially, exposure to fluorescent light, as used for localisation of the cell mass in transplanted retinas, induces a photopic response, which is suppressed upon application of L-AP4.

5.3.3 Graft-containing retinal portions exhibit cone-mediated light responses

For each experimental retina, a transplant region containing the human graft, and a non-transplant control region, isolated from the retinal side opposing the graft, were analysed by MEA. Different types of RGC responses were identified (ON and OFF, sustained and transient, Figure 42) and the percentage of RGCs of either type was expressed as percentage of all responsive RGC (Figure 42E, F).

Under mesopic and photopic conditions without L-AP4, ON and OFF RGCs were detected in both transplant and control regions (Figure 42A,C). Interestingly, the number of ON and OFF RGC was consistently higher in transplant regions (Figure 42E,F). When samples were stimulated using photopic conditions with L-AP4 application, the ON RGC response was completely abolished as expected (Figure 42B, D, E), irrespective of the presence or absence of human grafts. OFF RGC responses on the other hand could be detected in 31% (5 of 16) of transplanted samples, with on average 6% of all previously

detectable RGCs showing OFF RGC activity (Figure 42D, F, only regions from OFF RGC responsive retinas shown). On average, this represented 25 responding cells. While rods can in principle also signal through the OFF RGC pathway, no OFF RGC responses were detected in control regions without a transplant upon photopic stimulation with L-AP4 (Figure 42B, F, only control samples of responsive retina shown), suggesting that there was no rod interference in the present setup and that the OFF RGC responses in transplant regions were indeed brought about by cones.

The presence of cone mediated OFF RGC spiking in transplanted regions of the otherwise cone-dysfunctional Cpf1 retina strongly suggests that the human grafts were indeed able to drive light-induced responses. Also, the increase in light-responsive RGCs upon mesopic and photopic stimulation implies additional human graft-mediated reactions that require further assessment.

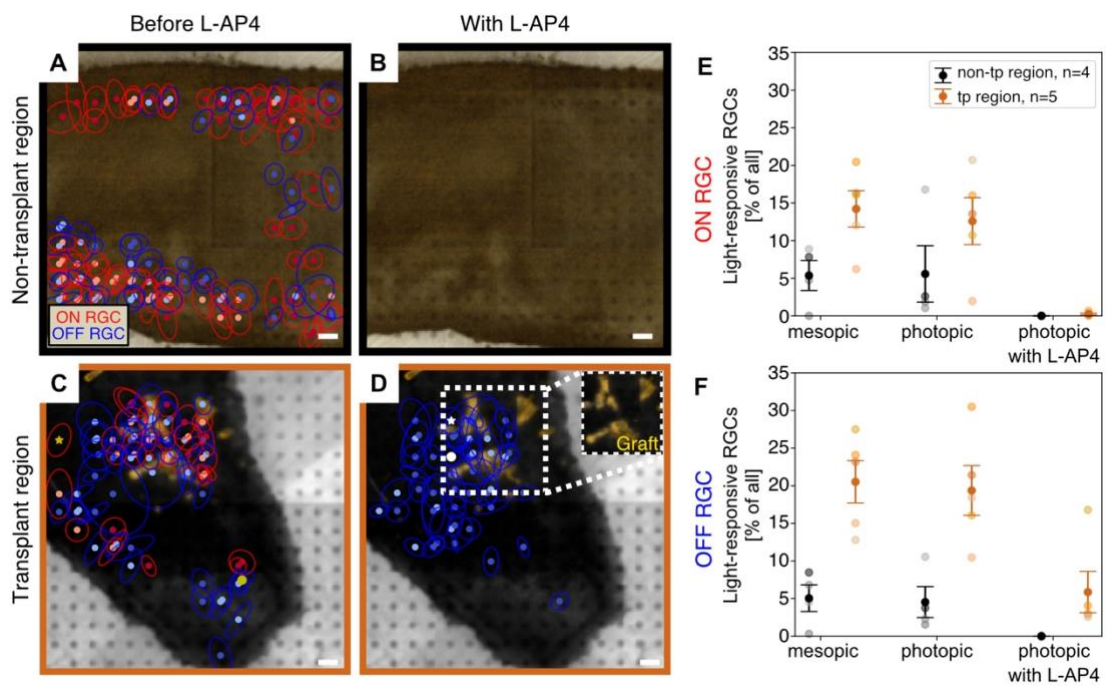


Figure 42. Increased OFF RGC Activity in Transplanted Cpf1 Retinas.

A-D. Receptive fields of ON and OFF RGCs upon photopic stimulation before (**A, C**) or during (**B, D**) application of L-AP4. Receptive fields are superimposed on the explanted mouse retinas on the MEA chips they were recorded from. While ON RGC responses are absent in both, non-transplant and transplant regions (**B, D**), OFF RGC responses remain in the latter (**D**), and partially overlap with the graft. **E, F.** Quantification of the proportion of light-responsive RGC in transplant and non-transplant regions upon stimulation with mesopic and photopic conditions, as well as upon photopic stimulation with L-AP4 addition. Responses are separated into ON RGC (**E**) and OFF RGC (**F**).

5.4 Summary

As human retinal organoid D200 Crx-mCherry⁺ grafts show strong evidence for polarization, maturation and incorporation upon transplantation into Cpf1 host mice, vision could potentially be improved. Vision-based behavioral assays such as the Light-Dark Box (LDB) test represent a potential read-out of graft-mediated function, however the LDB paradigm does not show differences between transplanted and control Cpf1 animals. With the LDB test relying on light-aversion behavior that is in a large part mediated by rods, this is most likely due to normal rod morphology and function in Cpf1 mice, and thus the LDB test requires adaption in order to be used as a read-out of cone function only.

To circumvent interference by endogenous rods, the LDB test can be performed on rod-cone degeneration mouse lines containing human grafts. Although only moderate levels of polarization and maturation are observed in tgCR and rd1 mice, transplanted rd1 mice show a trend towards improved vision-guided light-aversion behavior compared to sham-injected controls, implying some functional vision restoration through the human cells.

In multi-electrode array (MEA) analysis of transplanted retinas, it is possible to separate rod- and cone-mediated light responses by the exposure to specific light intensities, the inhibition of rod-mediated visual pathways, and thorough analysis of the detected spike characteristics. In MEA, graft-mediated retinal ganglion cell responses can clearly be identified in Cpf1 recipients, showing that human Crx-mCherry⁺ D200+26w grafts are not only able to morphologically incorporate and mature in the murine environment, but that they also functionally connect with the host retina to mediate light-induced responses on the tissue level.

6 Discussion and Future Perspectives

Retinal degenerative diseases impeding vision represent an increasing health burden to worldwide society. Conditions under the umbrella term of inherited retinal degenerations (IRDs) alone were estimated to affect 5.5 million individuals in 2020, yet no cure exists for most of them. Despite a diverse array of causative mutations, IRDs ultimately encompass the dysfunction and death of photoreceptors and hence the irreversible loss of the main light-sensing cell in the human eye, leading to blindness. Photoreceptor (PR) replacement therapy has thus emerged as a potential future treatment strategy as its capacity to restore vision in pre-clinical animal models was researched. Due to scarcity of human PR donor material, a substantial amount of the work so far depended on the use of rodent cells. Yet thanks to improvements in cell culturing methods, it is now possible to reliably generate and isolate large numbers of high-quality human PRs from human retinal organoids (HROs).

Using these cells in a meaningful way will require in depth knowledge about the optimal conditions to obtain the highest possible amount of mature, functional and properly integrated PR after transplantation. The overarching aim of this work was therefore to provide a better understanding of human PR transplantations and how their outcome is affected by factors such as donor cell developmental stage and the host retinal environment.

6.1 Human grafts can morphologically incorporate into the moderately degenerated mouse retina

In the past, most research has been performed assessing mouse-to-mouse photoreceptor (PR) transplantation. Human-to-mouse transplantation on the other hand is a younger discipline, as true in vitro generated PRs have only recently become available at large scale thanks to human retinal organoid (HRO) culturing. Generally, HRO PR single cell transplantations have focused mainly on targeting highly degenerated animals. While this focus on end-stage degeneration is understandable given that photoreceptor replacement therapy is generally considered a last resort after cell rescue or protecting interventions like gene therapy, human retinal degenerative phenotypes present in various gradations of photoreceptor loss (Wert et al., 2014). It is thus important to understand better how grafted cells behave under different circumstances and one main aim of this thesis was therefore to extend the knowledge in the field by examining human PR transplantations into a less degenerated mouse model in more detail.

Detailed reports about transplantations into less degenerated hosts are rare. As such Barnea-Cramer et al. transplanted into C57BL/6Jrj wildtype hosts, yet only to establish the setup and without showing the data (Barnea-Cramer et al., 2016). A few pictures of cell-surface marker enriched D100 PR grafted into C57BL/6Jrj were shown by Lakowski et al., but the grafts were only assessed for human cell identity and cell type specificity, not with respect to maturation or function (Lakowski et al., 2018). In another publication where immune-deficient host animals without retinal degeneration were used, the authors reported human graft integration as identified by virally labeled reporter fluorescence. While single cells may have been incorporated, the interpretation overall was likely inaccurate, as the figures rather suggest aberrant fluorescent labelling of endogenous host photoreceptors, given their murine size, morphology and positioning (J. Zhu et al., 2017). Similarly, in the retina of P4 Rag1^{-/-}xCrb^{-/-} mice integration of patient-derived rod precursors was described, yet the outcome was not controlled for material transfer (Tucker et al., 2013).

In this work, for the first time, an extensive bulk morphological incorporation of grafted human cells into the host retina was shown, accompanied by maturation of high numbers of inner segments. Both incorporation and maturation were increased beyond 10 weeks after transplantation and upon use of D200 donor PR in cone only degeneration hosts. In previous reports grafting into highly degenerated retinas, human cells were found in contact with the residual INL, yet never intercalated to the same extent with murine cells as shown here. This observed difference is most likely due to the fully degenerated state of the host retina in the other studies. It could additionally be due to different donor cell ages and shorter follow-up times, as grafts were mostly assessed at 3-10 weeks, rarely 16 weeks, a timeframe in which incorporation and maturation here were still proceeding (Collin et al., 2019; Gagliardi et al., 2018; Gonzalez-Cordero et al., 2017; Ribeiro et al., 2021; Zerti et al., 2021).

6.2 Intraretinal grafts mostly represent true incorporation events, not material transfer

It is important to note that the large scale incorporation shown in the present work was not an effect of material transfer through nanotubes as observed in mouse to mouse transplantations (Kalargyrou et al., 2021; Ortin-Martinez et al., 2021; Santos-Ferreira, Llonch, et al., 2016; M. S. Singh et al., 2016; Waldron et al., 2018). The vast majority of intraretinal Crx-mCherry⁺ cells, especially in multi-cell clusters, were of human origin. Here, true human identity of Crx-mCherry⁺ cells was confirmed by qualitative assessment of nuclear size, inner segment size and morphology when

applicable, as well as single cell sequencing of Crx-mCherry⁺ cells retrieved from experimental eyes.

Occasionally, immunohistochemical stainings indicated that material transfer from human to mouse may have occurred, as single cells within the murine retina showed human-specific ARR3 labelling or strong RCVRN positivity and Crx-mCherry⁺ expression despite having a morphologically murine nucleus. However, this was only observed rarely and within the first 10 weeks after transplantation. Further analysis is needed to examine whether these cells were indeed a result of inter-species material transfer, for example by detecting mouse-specific chromosomal regions or Y-chromosome probing after sex-mismatched transplantations. While human-to-mouse cytoplasmic transfer might be possible, only one report assessed this option and came to the conclusion that material transfer did not occur (Gonzalez-Cordero et al., 2017). Similarly, there was no evidence of material transfer in human-to-dog transplantations (Ripolles-Garcia et al., 2022). It is conceivable that the capacity for material transfer is reduced in inter-species conditions, but it is also possible that human PR are in general less prone to exchange material. Species-specific material transfer characteristics could be assessed, e.g. through in vitro transplantations of human photoreceptors into human retinal organoids or transplantations into animal models closer to the human eye such as pigs or non-human primates. Understanding the potential for human-to-human cytoplasmic transfer could provide relevant insights impacting cell support strategies that use transplanted cells as neurotrophic depots rather than for cell replacement.

6.3 Graft Maturation depends on graft-host interaction

A second novel observation of the present work was the extensive and correctly oriented formation of a large numbers of inner segments (IS). A similar degree of IS and outer segment (OS) formation was, until now, only described in transplantations of human retinal organoid sheets, not single cells. Interestingly, in those cases the segments were formed almost exclusively within neural rosettes of the grafted structure rather than oriented towards the RPE (Iraha et al., 2018; McLelland et al., 2018; Shirai et al., 2016; Watari et al., 2022). While IS and OS have been reported as a result of human single cell suspension PR transplantations into end-stage degeneration models, they were commonly positioned within graft clusters, without a clear orientation detectable and relatively infrequent (Ribeiro et al., 2021). Arguably, the proper orientation of inner and prospective outer segments and their proximity to the RPE is however required for continued support of photoreceptor function, making the phenotype observed in the present work much more intriguing.

Importantly, particularly high numbers of IS were found upon close contact with the host retina, either in cases of intraretinal positioning or close proximity of graft and host ONL. In the case of intraretinal grafts, IS formation was further associated with the presence of an outer limiting membrane- (OLM) like structure, suggesting that the interaction with host MG might be beneficial or potentially even necessary for IS growth. In flies, a continuous OLM is required for proper stalk membrane formation and photoreceptor morphogenesis (Izaddoost et al., 2002; Pellikka et al., 2002). If the OLM is disrupted in mice, e.g. through mutations in the *Crb1* gene, a component of OLM adherens junctions, both IS and OS development is disturbed and photoreceptors are lost over time (Mehalow et al., 2003). Further assessment is required to unequivocally delineate the order of events in the relationship between OLM and PR segment formation in the present transplantations. Irrespectively, the apparent necessity of an OLM-like structure for segment homeostasis also after grafting of human cells has important implications for the selection of the proper patient retinal environment to allow promising post-transplantation segment maturation.

6.4 Establishment of graft-host interaction and graft incorporation

While many grafts were found interacting with the host retina or even incorporating into host neuroretinal layers, this was not always the case. Curiously, even within the same eye a portion of the graft may have been found intraretinally, while directly next to it, a second cluster may have remained in the subretinal space. At this point, it is unclear how this differential graft behavior arose and how the incorporation process itself took place, yet a better understanding of the process and hence the potential to encourage it could be key to improving PR replacement approaches.

In an effort to better characterize the incorporation process, D200 cells were grafted and experimental eyes were analyzed at early stages thereafter. A time window between 6 and 8 weeks post transplantation was identified in which the incorporation process seemed to advance from a contacting to an intraretinal stage. Also, it was found that already as early as 2 weeks after transplantation, human and mouse retinal somata could be in close apposition, allowing murine MG processes to extend into the graft. While mouse bipolar cell neurites were also extending towards the human cells, they were only found reaching them as early as 6 weeks after transplantation. More detailed assessment of earlier samples is required to further narrow down the timing of bipolar cell contact to the grafts.

It is tempting to speculate about the mechanics of incorporation, especially since the early reaction of MG to the grafting suggests a key involvement of these retinal macroglia in the process. MG have a plethora of roles in maintaining retinal health and

are known to sense and react to a variety of stimuli (Reichenbach & Bringmann, 2020), including retinal detachment. As such, massive gliosis, entailing extensive MG proliferation and the formation of a glial scar on the periretinal surfaces, is a detrimental response to retinal insult that ultimately damages the photoreceptors and results in a barrier, inhibiting neurite outgrowth. Conservative gliosis on the other hand is deemed neuroprotective, characterized by the upregulation of intermediate filaments and cellular hypertrophy, yet only no to moderate proliferation. Such an environment can conversely support neurite outgrowth, as in human samples of retinal detachment, rods were found to sprout neurites preferentially along hypertrophied MG trunks, seemingly using the MG as a scaffold (Sethi et al., 2005). Although it remains to be elucidated whether the graft intraretinal positioning is at all the results of an active photoreceptor migration into the host retina, it is conceivable that the grafted human photoreceptors here use similar tracks to move into the host retina along MG appendices.

Interestingly, MG response to injury is not homogenous, and neighboring MG were found to react differently to the same stimuli, e.g. in NMDA-damaged chick retina (Fischer & Reh, 2003). Similar differences in response to human grafts might therefore also account for the presence of intraretinal and isolated grafts in close vicinity to each other.

Beyond the direct MG reaction to the human graft and the retinal detachment, various other factors might play into the human graft incorporation. The physical barrier introduced by the presence of the human graft between endogenous PR and RPE is likely to negatively affect the PR in particular. Graft presence in the subretinal space further disturbs the natural geometry of the tissue and thus the pressure exerted on neighboring cells and cell-cell connections. Signaling from the grafted cells could induce retinal remodeling in both the short and the long term, with potentially damaging signals arising from a wave of initial graft cell death, as well as continued signaling by the surviving cells. All these factors might play into the host response to the grafting and at this point, it is impossible to disentangle. Therefore, pilot experiments were initiated to characterize the transcriptomic reaction of host cells to the graft, comparing cells in the grafted area with distant control regions of the same eye. Hopefully, this approach will yield a clearer picture of the host reaction to the grafted cells and their interaction with each other.

6.5 D200 Crx-mCherry⁺ cells are the preferable donor population compared to D100 and D300

A main aspect of this study was to determine the preferable donor cell age for human-to-mouse PR transplantations. By comparing the transplantation outcome using donor cells aged D100, D200 and D300, D200 cells were identified as those yielding the most inner segments and thus potentially also the best chances for outer segment formation.

Despite a higher proportion of PR in D300 HRO cell suspensions, D300+10w samples did not show any intraretinal position and only very limited areas of interaction with the host. This was corroborated by previous findings from our group using PR generated from a human cone-reporter iPSC cell line, in which incorporation and maturation of D250 grafts was also strongly reduced (Gasparini et al., 2022). Additionally, D300 cells showed a decreased viability before sorting, possibly due to increased vulnerability of older and more mature photoreceptors to the (shear) stresses employed during dissociation. Overall, D300 Crx-mCherry⁺ cells were thus deemed less suitable for PR replacement than D200 donors.

D100 grafts on the other hand showed the highest propensity for intraretinal positioning, yet these cells generated far fewer inner segments relative to graft size than D200 grafts, even when comparing samples of the same total cell age. This was especially surprising given the vicinity of graft and host being an important factor in inner segment development.

One possible reason for the difference in apical maturation is the younger developmental stage of D100 Crx-mCherry⁺ cells at the time of transplantation. Upon preliminary single cell sequencing analysis, 60% of D100 cells could not be clearly mapped to a specific cell type as they expressed markers from various cell types. Some of those markers are however expressed in cone precursor cells and late neurogenic retinal precursor cells which give rise to photoreceptors (Lu et al., 2020). It is therefore possible that these “other” cells were indeed neurogenic retinal progenitor cells that had not yet adopted their mature photoreceptor fate. Perhaps these cells therefore show different maturation trajectories within the murine environment than more developed photoreceptors, reducing their propensity for inner segment formation in a direct (lack of required gene expression profiles) or indirect fashion (differential interaction with the host environment ultimately inhibiting inner segment formation). This is corroborated by the observation that despite the same total age of roughly 370 days, phenotypes differed between D100+41w and D200+26w samples, indicating the high relevance of the time of transplantation. It would be interesting to examine whether enrichment of more

mature Crx-mCherry⁺ photoreceptors from D100 organoids, e.g. through additional expression of a reporter driven by a promoter expressed in mature cones, would resolve the difference between D100 and D200 transplantation outcome.

Another possible reason for a lack of inner segment formation in D100 grafts due to differential interaction with the host environment is the presence of a border seemingly encasing the vast majority of D100-derived grafts. Inner segments, when present, were found primarily in regions where this enwrapment was absent, such as at some contact points of graft, murine ONL and the subretinal space. Understanding the exact nature of this border could therefore help to increase PR maturation from younger grafts. While it on one hand stained unspecifically for secondary antibodies targeted against murine IgG, it also stained positive for markers of MG cytosol, and was thus reminiscent of a gliotic MG seal. Although continuity with endogenous MG processes suggests the presence of murine MG cell bodies in human transplants, in D100 grafts, ca. 6% of all donor cells were identified as MG. This leaves the possibility of MG cytosol in D100-derived grafts originating from human cells and co-staining with human-specific MG markers is required to be certain. A similar phenotype was observed of full dissociated HROs in human-to-dog (Ripolles-Garcia et al., 2022) as well as human-to-macaques transplantations (Aboualizadeh et al., 2020) where, in both cases, the graft itself developed a gliotic seal, isolating it in the subretinal space and impeding direct graft-host interactions. Interestingly, both studies used similarly young (dog: D133, macaque: D74 or D96) yet unsorted donor cells and the phenotype was only observed in the wildtype, not the retinal degenerative host.

If the enwrapment indeed originates from human cells, removing MG from the donor cell suspension could improve the transplantation outcome. Should such a removal lead to a phenotype similar to that of D200 donor cells, it would allow to greatly reduce cell culture time before transplantation, simplifying the logistics of potential PR replacement interventions. If the enwrapment however originates from murine cells, it could be beneficial to examine in more detail how the D100 cells differ from the D200 cells with respect to e.g. secretion of factors modulating MG responses. Similarly, detailed assessment of differences between D100 and D200 donor cells, e.g. considering extracellular matrix deposition, could yield additional clues which pathways might help D200 cells to incorporate better and whose manipulation would allow to further improve the incorporation process.

6.6 Cones show preferential survival post grafting

After transplantation, the cellular composition of the grafts was observed to change. At D200, the Crx-mCherry⁺ donor cell population contained ca. 25% rods, yet

after 26 weeks in vivo, only 2% of all Crx-mCherry⁺ were found to be rods. Similarly, staining of the human grafts showed widespread labelling for the cone cytosol marker ARR3, supporting the rod loss.

It is currently unclear why cones show this preferential survival. It could be due to differential vulnerability to the dissociation and sorting process during the transplantation itself. However, in D200+10w samples, roughly 10% of graft cells were still identified as rods according to single cell sequencing, suggesting that some rods do survive until that point and that the decrease in rod number occurs over a more prolonged timeframe than during the transplantation procedure alone.

In the healthy retina, both rods and cones use the canonical visual cycle to recycle pigment. The closely apposed RPE receives all-trans retinol and recycles it to 11-cis retinal, which is shuttled back to the photoreceptors. There is however also an alternative, cone-specific visual cycle, which relies on the close interaction between cones and MG, allowing cones to recover from bleaching in the absence of RPE, while rods do not. Cone recovery is strongly reduced upon physical separation of their inner and outer segment from surrounding cells as well as upon pharmacological disturbance of MG homeostasis and cones require physical association with MG for dark adaptation (J.-S. Wang & Kefalov, 2009). As grafted human cells and endogenous MG are in close contact from an early timepoint on, it is possible that murine MG are able to better support cone than rod function, giving the cones homeostatic advantages over the rods and leading to a gradual loss of the latter.

A close association of MG and cones has also been found in reaction to retinal detachment in cats. Upon subretinal injection of viscous buffer, MG processes positive for intermediate filaments grew into the subretinal space and were always found superimposed on cone sheaths detected by PNA within 3 days (Lewis & Fisher, 2000). While the mechanism of this association is not clear, it is conceivable that cones and MG are in particularly close contact due to cone signaling, surface molecules or cone-specific ECM. With roughly half of the grafted cell mass at D200 consisting of cones, MG outgrowths contacting the graft might also associate easily with the cones, quickly establishing cell support.

6.7 Functional analyses of transplanted animals

The present human PR transplantation into the Cpf1 mouse yielded morphological incorporation, maturation and putative synapse formation, indicative of the grafts' capacity to functionally integrate into the host retinal circuitry. However, these observations alone are no proof of graft-mediated vision, and functional assessment is required. Although mice are nocturnal animals who rely primarily on olfactory and tactile

cues to navigate the world, visual function in mice can nowadays be assessed at various levels: examining the physiology of the relevant cells, analyzing the direct downstream signaling on the tissue level, recording the response in brain activity to a stimulus on the cerebral level and by observing changes in visual-guided behavior. While the first and second currently require post-mortem extraction of the tissue for electrophysiological recordings or Ca^{2+} imaging, the latter two can be performed in live animals. As such, recording of visually-evoked brain activity from the superior colliculus in live animals has been used to detect graft-mediated function in rats (McLelland et al., 2018), yet this method is used rarely, as it is a complex and invasive procedure. Instead, multi-electrode array (MEA) and electroretinogram (ERG) recordings, reflex-based tests like pupillometry and optokinetic tracking, and behavioral assays, such as the light-dark box (LDB) assay or the visual-guided watermaze are more commonly employed.

Here, transplanted Cpfl1 retinal tissue was sampled and submitted to MEA analysis, which measures the RGC activity in response to light stimulation. As Cpfl1 mice have normal rods but degenerating, non-functional cones, any cone-mediated light response could be assumed to be primarily initiated by the grafted cells. Under both mesopic and photopic stimulation conditions, the percentage of responsive RGC was higher in regions containing a transplant compared to those without. Isolation of the cone OFF BC-mediated OFF RGC signal (by illumination with a photopic stimulus while blocking activity of mGluR6 with L-AP4) further showed active RGCs in retinal regions containing a transplant. It is important to note that while OFF RGCs are innervated by cone OFF BC, rods are also able to signal into the cone pathway. Indeed, three rod signaling pathways exist: The primary pathway, which messages via rod BC and All amacrine to the cone circuitry, the secondary pathway, formed by rod/cone gap junctions, and the tertiary pathway, in which rods signal directly to cone OFF BC (Grimes et al., 2018). Therefore, it is theoretically plausible that Cpfl1 rods could have participated in the OFF RGC response. However, under the same conditions as described above (photopic light, mGluR6 inhibited by L-AP4) no response in untransplanted control regions could be detected. This strongly suggests that the OFF RGC response observed in transplanted regions was indeed induced by the grafted human cells, which in turn implies the presence of functional synaptic connections between graft and host as well as the grafts' capacity to mediate visual function after transplantation.

To evaluate whether this tissue-level function also translated to changes in vision-guided behavior, animals were submitted to the LDB assay. As nocturnal animals, mice prefer to avoid brightly lit spaces, and, given the possibility to move freely between a dark and a brightly lit compartment, the time they spend in each portion is the result

of a balance between their light-aversion and exploratory behavior. Naturally, light-aversion behavior relies on visual function. Despite the presence of well-matured transplants in Cpf1 mice and a graft-mediated electrophysiological response as read out by MEA, it was unfortunately not possible to detect changes in light-aversion behavior using the LDB. This was because the baseline light-aversion behavior of Cpf1 animals was found to mirror that of wildtype C57BL/6Jrj animals, with both spending 60-65% of their assay time in the dark. Physiologically, this is due to Cpf1 animals having normal rod morphology and function, which play an important part in light-aversion behavior.

The extent of light-aversion in wildtype animals represents a more general problem with the LDB conditions used. Despite theoretically being sufficient to induce light-aversion behavior (Costall et al., 1989), illumination of the light compartment with 620 lx in the present setup caused C57BL/6Jrj wildtype animals to only spend roughly 60-65% of the assay time in the dark. This value represents the strongest light-aversion behavior that is expectable from previously blind mice on a C57BL/6Jrj background with restored vision – a mere 10-15% above chance. With an assay as inherently variable, detecting changes in such a small range would therefore require higher animal numbers to be assessed. To reduce variability, the application of reflex-based test that do not rely on higher level cognition such as pupillometry might serve beneficial. Irrespectively, in the future, the LDB setup should be adjusted in order to increase the chances of detecting minor improvements within blind treated mice. Changes could include different light intensities to induce stronger baseline light-aversion behavior in seeing and potentially rescued mice, or the use of specific light wavelengths to activate only certain photoreceptor subtypes.

Interestingly, LDB assessment of untransplanted and transplanted animals of the two strongly degenerated mouse lines tgCR and rd1 showed slightly different results. Transplanted tgCR animals remained at baseline, which mirrored the low amount of IS or OS formation observed by immunohistochemical assessment of the animals. Transplanted rd1 animals however continuously showed a trend towards increased light aversion compared to sham-injected controls, albeit mostly statistically not significant. The reason for the visual improvement in rd1 but not tgCR animals is currently not clear. Histologically, transplant survival, distribution and maturation appeared similar in both lines. The grafts in rd1 animals differed only slightly from those in tgCR eyes, in that they appeared “included” into the host retina by GS⁺ MG processes and a ZO1⁺ OLM-like structure above the graft, which was not observed in tgCR eyes.

An alternative explanation for improved visual-guided behavior despite the lack of extensive graft maturation is the support of otherwise degenerating cells through the

transplant. At the time of transplantation, roughly 1-3 rows of photoreceptors still remain in both rd1 and tgCR mice (Santos-Ferreira, Völkner, et al., 2016; M. van Wyk et al., 2015). These residual cells are mostly cones, which in tgCR animals are inherently dysfunctional but do still mediate ganglion cell responses in rd1 until 24 weeks of age (M. van Wyk et al., 2015). Thus, cell support of these cones might provide an alternative explanation for the slight difference in LDB outcome between the two highly degenerated strains.

To properly delineate whether the slight visual function increase is caused by the human grafts themselves or a cell support mechanism, experiments transplanting non-functional but otherwise normal human photoreceptors are the method of choice. As such, Ribeiro et al. showed that despite the complete absence of light-responsiveness in MEA analysis, rd1/Fox^{nu} mice that had subretinally received 500,000 non-functional human cones showed a non-significant but noticeable increase in time spent in the dark (Ribeiro et al., 2021). Further analysis of the relevance of potential cell support effects in rd1 animal transplantations is therefore highly advisable and additional studies using improved testing conditions will be necessary.

6.8 Future clinical translation

Research into human PR transplantations as a potential treatment for retinal degeneration diseases has been taking place for roughly 40 years. Already early on, numerous trials with few patients employed human fetal donor tissue for transplantation. Also today, there is high interest in clinical translation of the research findings, especially given the recent availability of donor material from HRO. Despite important advances, clinical translation however still faces major challenges, particularly considering potential immune responses, the optimal donor material to obtain function and the best timepoint for an intervention.

As with all transplantation studies, there is a risk for the rejection of grafted cells by the host, possibly accompanied by an immune response that further damages the endogenous tissue. Initial human-to-human studies commonly only provided topical immune suppression to mitigate the effects of the surgical procedure, and rarely aimed at a systemic modulation of the host immune system to prevent graft inflammation and rejection. Somewhat surprisingly, the fetal grafts were mostly found to survive in spite of that, supporting the notion of the subretinal space as an immune-privileged compartment and fetal material as hardly immunogenic (Kaplan et al., 1997; Radtke et al., 1999, 2002, 2008).

Since then, research has primarily focused on in vitro-derived material transplanted into rodent hosts, introducing another level of complexity due to inter-

species xenografting. In that setting, and similarly in a recent report grafting into dogs, systemic immune suppression or immune-deficient host animals were widely used, and indeed increased the chances for graft survival (Gonzalez-Cordero et al., 2017; Ribeiro et al., 2021; Ripolles-Garcia et al., 2022). Upon transplantation into non-human primates systemic immune suppression was employed as well, yet without comparing graft survival to the non-immune suppressed condition (Aboualizadeh et al., 2020; Shirai et al., 2016; Tu et al., 2018). In the present thesis, monthly local immune suppression with vitreally applied triamcinolone acetonide was used for the first time in a human-to-mouse PR grafting study and was found sufficient to retain human grafts. While the reduction of the systemic burden and its infrequent application thanks to its depot function are highly beneficial, its use must be carefully titrated, as triamcinolone acetonide can also have detrimental side effects to the visual system (Kumar et al., 2013; Schlichtenbrede et al., 2009). Similarly, further examination of the immune suppressive treatments required upon in vitro-derived human-to-human clinical translation are vital to ensure graft survival at the lowest systemic and local burden possible. In that context, it is also important to consider potential differences arising from the use of diverging material in research and application, such as the widespread presence of reporter proteins in research cell lines, which can induce cytotoxicity and immunogenicity (Ansari et al., 2016).

While the immune response to human grafts differs between varying host species, it is also strongly affected by the transplanted cells themselves. To reduce graft rejection, the use of autologous hiPSC-derived cells would be optimal, yet difficult to achieve at a large scale, as it requires the generation, editing, quality control and differentiation of patient-derived donor cells, which is a cumbersome, expensive and variable process (Wiley et al., 2016). Improvements in the methods and automation used will however make it more efficient and will allow for the possibility to use this personalized medicine approach in selected cases (Mullin et al., 2021).

To instead provide a more general donor cell population, the application of allogeneic, human leukocyte antigen (HLA)-matched cells has been proposed. HLA is the human counterpart to human major histocompatibility complex (MHC) antigens that are present on the cell surface in all mammals and whose recognition as foreign induces an immune response against the HLA-carrying cell. Matching the major MHC/HLA type in donor and host material has been shown to reduce the risk of immune-rejection in central nervous system transplantations (Morizane et al., 2017) and the use of banked HLA lines would provide a consistent donor cell production applicable to a large number of patients. In Japan, it is estimated that cell lines from 70 donors would suffice to cover 80% of Japanese patients (Okita et al., 2011), although it is worth noting that the

required number of banked lines will likely be higher in more heterogeneous populations. In the eye, HLA-matched allogeneic iPSC-derived RPE cells have been reported to survive without systemic immune suppression, and only occasional local immune suppression was required to ensure graft survival for at least one year (Sugita et al., 2020).

Another relevant factor to consider is the immunological capacity of the tissue to be grafted. hESC- and hiPSC-derived retina and RPE have been shown to exhibit low immunogenicity, low expression of HLA cell surface markers and strong immune-suppressing capacities partially mediated by TGF- β secretion in an in vitro assay (Yamasaki et al., 2021). Interestingly, dissociation of retina decreased its immune-suppressing capacity, suggesting that sheet transplantations might have preferable characteristics in that regard, yet it is not yet clear whether those differences play a large role in vivo. Overall, the host immune reaction to ocular transplants and the immunogenicity of the grafts require further research. Given inter-species differences, such efforts would profit from the use of humanized mouse models or larger animal models with a higher resemblance to humans with respect to retinal morphology, pathology and immune system.

With respect to the optimal donor cell population, several questions are not yet answered. It is for example still unclear whether single cell suspension or sheet transplantations are the path forward. Functional rescue could be shown in rodents using both approaches, and recent improvements in sheet transplantations include generation of HRO with a reduced INL (Yamasaki et al., 2022) and quality control of the material to be grafted (Watari et al., 2022).

To progress single cell suspensions to clinical use, a lot more work needs to be done. While enrichment of PR was shown to be beneficial (Gonzalez-Cordero et al., 2017), fluorescent reporters cannot be employed for the use in human patients but only few cell surface marker panels have been proposed for the selection of human cones or PR (Gagliardi et al., 2018; Welby et al., 2017). An alternative and more GMP- (good manufacturing practice) friendly approach to select PRs is sorting by marker-free strategies (Herbig et al., 2022; Stone et al., 2020). Most importantly however, the present work suggests that PR replacement strategies with single cell suspensions might greatly benefit from grafting at a stage when residual PRs are still present. This requires further validation in other intermediate degeneration stages and in other animal models, yet if it holds true, has the potential to greatly impact the choice of possible recipient patients in both clinical studies and ultimately treatment. Crucially, these findings represents encouraging evidence that human photoreceptor transplantation, integration and large-scale maturation might indeed be possible in the long term.

6.9 Major contribution to other work

As mentioned above, there is a need for marker-free sorting strategies to provide an enriched, transplantable PR population for clinical use in the future. In the past, our lab has shown the possibility to detect murine rods in a primary retinal cell suspension by morpho-rheological fingerprinting using real-time deformability cytometry (Santos-Ferreira et al., 2019). Part of my thesis work focused on progressing that approach from cell suspension analysis to cell suspension sorting. In collaboration with Maik Herbig and the lab of Jochen Guck, we could apply label-free flow cytometry to enzymatically dissociated retinal tissues and advance the technology through a series of computational, physical and methodological improvements. This study allowed to successfully enrich and transplant murine rods, providing proof-of-concept that marker-free enrichment of PRs is indeed possible and could in the future potentially be applied to human PRs as well (Herbig et al., 2022).

7 Final Conclusion

Human photoreceptor replacement therapy represents a promising approach to potentially treat blinding diseases that encompass photoreceptor loss. The recent availability of large numbers of donor photoreceptors from human retinal organoid culture enabled extensive assessment of this strategy in pre-clinical research. Indeed, studies have shown maturation and partial rescue of visual function after retinal single cell or sheet grafting into mice, rats and non-human primates. However, most research has targeted models of end-stage degeneration, and little was known so far about the outcome in less degenerated models. On the donor cell side, systematic comparison of optimal graft conditions was not available.

Here, I assessed both these issues by transplanting human retinal organoid derived Crx-mCherry⁺ photoreceptors of different cell ages into the Cpf1 mouse model of cone-only degeneration. Analysis of graft survival, interaction with the host retina, incorporation and maturation concluded that while cells at 100 days of differentiation yielded the largest grafts, cells at 200 days of age exhibited the highest degree of maturation as determined by the number of inner segments formed. As the ultimate goal of photoreceptor replacement is the presence of functionally mature cells that are able to perceive light, inner segment formation is an important step in the process.

Furthermore, my data showed that inner segments were mostly formed in graft regions with close contact to the host retina, and that a high degree of interaction between graft and host took place. The close proximity with host Müller glia in particular and the capacity to form a common outer limiting membrane-like structure appeared vital for inner segment formation. Grafted photoreceptors were found to mature further, additionally generating outer segments and increasing the expression of genes involved in visual transduction characterizing mature photoreceptors, even beyond their age-matched in vitro cultured counterparts. Importantly, the grafts were found to form putative synapses with host bipolar cells, and electrophysiological readout confirmed their functionality, as graft-mediated light responses in retinal ganglion cells could be detected. Comparison with transplantation outcomes in highly degenerated animal models further suggest that an earlier intervention, while more host photoreceptors remain, could be crucial to improved graft incorporation, maturation and function.

Overall, the present work has made valuable contributions to the field of photoreceptor replacement strategies by characterizing important factors to be considered upon grafting human photoreceptors. These insights provide important knowledge to allow a more informed way forward in translating photoreceptor replacement strategies to clinical practice.

8 Materials and Methods

8.1 Study approval

All animal experiments were approved by the ethics committee of the TU Dresden and the Landesdirektion Dresden (approval number: TVV 16/2016 and TVV 38/2019). All regulations from European Union, German laws (Tierschutzgesetz), the ARVO statement for the Use of Animals in Ophthalmic and Vision Research and the NIH Guide for the care and use of laboratory work were strictly followed for all animal work.

8.2 Materials

8.2.1 Materials and Chemicals

The following table contains important Materials used, grouped and in the order they appear within the methods section below.

Table 1. Materials and Chemicals.

	Material	Company	Identifier
Organoid Culture	ReLeSR	StemCell Technologies	05872
	DMEM/F12	Gibco	31331-028
	N2	Gibco	17502-048
	FBS, heat inactivated, origin south america	Thermo Fisher	10500-056
	penicillin/streptomycin	Gibco	15140-122
	GlutaMAX	Gibco	35050-038
	Amphotericin B	Gibco	15290-026
	NEAA	Gibco	11140-035
	B27 without Vitamin	Gibco	12587-010
	B27 with Vitamin	Gibco	17504-044
	Neurobasal A	Gibco	21103-049
	β -mercaptoethanol	Gibco	31350-010
	Matrigel, growth factor reduced	Corning	354230
	Ultra low-attachment 6-well plates	Nunclon Sphera	174932
	6-well plates	Corning	3516
	Dispase	StemCell Technologies	07923
	10 cm low attachment dishes	Greiner	664970
10 cm low attachment dishes, Nunclon Sphera	Thermo Fisher Scientific	174945	
EC23	Tocris	4011	
Dissociation and Transplantation	PBS ^{-/-}	Gibco	10010-023
	DNase I	Thermo	D5025-150KU
	0.22 μ m PVDF filter	Millipore	SLGV033RS
	Papain	Worthington	LK003176
	EBSS	Worthington	LK003188
	Ovomucoid	Worthington	LK003182
	0.2 μ m PES filter	Thermo Scientific	566-0020
	Trypan Blue Stain, 0.4%	Gibco	T10282
	Triamcinolone acetonide suspension, sterile, 80 μ g / μ l in NaCl, preservative-free	University Clinic Pharmacy, Dresden	none
	Ketamin 10%	medistar	04-03-9264/23
	Medetomidin hydrochloride	Orion Pharma	Domitor®
	Medetomidin hydrochloride	CP-Pharma	Cepetor®
	Atipamezole hydrochloride	Orion Pharma	Antisedan®
	0.9% NaCl, sterile	Fresenius Kabi	B306175/03
	Dilating eye drops 2.5% phenylephrine/0.5% tropicamide	University Clinic Pharmacy, Dresden	none
	Moisturizing eye gel	Bausch+Lomb	Vidisis®
	Hamilton Microliter syringe, 5 μ l	Hamilton	065-7634-01

	Material	Company	Identifier
Cell and Eye Assessment	Hamilton Microliter syringe, 10 μ l	Hamilton	065-7635-01
	Hamilton removable needle, blunt, 34-gauge, 12 mm length	Hamilton	special request
	30G needle	BD Biosciences	30400
	Coverslips	Menzel-Gläser	24x50mm#1,5
	Coverslips	Epredia	24x50mm#1,5
	Diamond pen	Roth	1530.1
	Stereotaxic adaptor for mouse head fixation	World Precision Instruments	505242
	Micromanipulator M1 with flat metal base	H. Saur Laborbedarf	M1
	Transplantation microscope	Leica	M651 MSD
	L-AP4, 50 μ M	Tocris	0103
	FlexiPERM micro12	Sarstedt	94.6011.436
	PDL, poly-D-lysine hydrobromide	Sigma-Aldrich	P7280-5MG
	Laminin	Invitrogen	23017-015
	Isoflurane	Isoflurane Baxter	-
	PFA	Electron Microscopy Sciences	15714
	6-well insert, standing	Corning	353090
	NEG-50	Richard-Allan Scientific	6502
	Methylbutane	Sigma-Aldrich	M32631-1L
	Liquid nitrogen	Provided by the CMCB	-
	Aqua Polymount	Polysciences	18606
	Hydrophobic pen	Vector Laboratories	H-4000
	Shandon Plastic Coverplates	Epredia	12766807
	Shandon Sequenza Immunostaining rack	Epredia	73310017
	BSA	Serva	11926
	Normal donkey serum	VWR/Uptima	UPTIUP77719A
	Triton X-100	Serva	37240
	Starfrost Advanced Adhesive Slides	Engelbrecht Medizin- und Labortechnik	11270

8.2.2 Cell Line

The Crx-mCherry cell line was a kind gift from Olivier Goureau. Derived from human retinal Müller glia cells (Slembrouck-Brec et al., 2019), the human induced pluripotent stem cells were edited using CRISPR/Cas9 to harbor the transgene in their AAVS1 locus (Gagliardi et al., 2018). Containing the mCherry gene fused to an H2B histone motif under control of the murine Crx promoter, the transgene thus led to nuclear mCherry expression in photoreceptor cells. All experiments used a homozygous clone.

8.2.3 Mouse Lines

Adult mice of various lines were used as recipients for cell transplantations and are described in more detail below. All mice were maintained in a 12-hour Light/Dark cycle with ad libitum access to food and water.

C57BL/6J – Wildtype: Inbred wildtype mice of the JAX mice strain without known retinal dysfunction were supplied by Charles River (<https://www.criver.com/products-services/find-model/jax-c57bl6j-mice?region=23>). Females of 9-10 weeks were used as recipients.

Cpfl1 – Cone photoreceptor function loss 1: Cpfl1 mice with the official name B6.CXB1-Pde6c^{cpfl1}/J are the result of spontaneous mutations in the Pde6c gene within the CXB1 strain, which were backcrossed onto the C57BL/67J background. Cpfl1 animals are homozygous for a 116 bp insertion between exons 4 and 5 as well as a 1 bp

deletion in exon 7, leading to a frame shift and a premature stop codon. The mutations cause a lack of detectable cone function as well as cone degeneration while both rod structure and function remain normal. At baseline, Cpf1 Müller glia exhibit a slight upregulation of glial fibrillary acidic protein.

Both males and females aged 6-25 w were used as recipients, with 90% of animals younger than 19 w. As males were found to be at a higher risk of unexpected death over the course of the experiments, later experiments were limited to females. All Cpf1 animals originated from the colony maintained at the CRTD animal facility which had been founded from mice kindly provided by Bernd Wissinger (Institute of Ophthalmic Research, Tübingen, Germany).

Rd1 – Retinal degeneration 1: The *Pde6b^{rd1}* mutation is a common mutation in various laboratory and wild-derived inbred strains, containing a murine viral insert as well as a mutation in exon 7 of the *Pde6b* gene. While exact timelines vary depending on further genetic background, *Pde6b^{rd1}* generally causes severe early onset rod degeneration and secondary cone degeneration. Here, C3H/HeOuj mice obtained from Charles River were used, which quickly lose all rods until 3-4 w of age and retain only 2-3 rows of cones at 3 w and 1 row at 23 w. Cone outer segment counts are reduced by roughly half at 12 w and decrease further until 24 w (M. van Wyk et al., 2015). Female rd1 animals aged 7-8 w were used as recipients.

tgCR – cone-rod dystrophic mice: tgCR mice were generated in the animal facility at CRTD by crossing age-matched Cpf1 animals (see above) with *Rho^{-/-}* mice, originally on a 129S2/SvHsd background (Santos-Ferreira, Völkner, et al., 2016). Dysfunctional from birth, the photoreceptors quickly degenerate until at 10-12 w only one row of photoreceptors is retained. tgCR animals of both sexes aged 7-18 w were used as recipients.

Hes5-GFP – Müller glia reporter mice: Hes5-GFP animals express GFP under control of the Hes5 promoter, leading to cytosolic labeling of the Müller glia with an otherwise normal retina (Basak & Taylor, 2007; Nelson et al., 2011). One male at 24 w and females aged 27-32 w were used as recipients

8.2.4 Antibodies

The following table lists all primary antibodies used, sorted alphabetically by the abbreviation used to refer to them within the thesis.

Table 2. Primary Antibody Details.

Abbreviation	Target	Host Species	Catalogue Number	Producer	Dilution	Antigen Retrieval
ARR3	Cone arrestin, human specific	mouse	(Wikler et al., 1997)	Gift from Peter MacLeisch	1:100	no

Abbreviation	Target	Host Species	Catalogue Number	Producer	Dilution	Antigen Retrieval
ARR3	Cone arrestin human specific	goat	NBP1-37003	Novus Biologicals	1:100	no
CRALBP	Retinaldehyde-binding protein 1	mouse	MA1-813	invitrogen	1:100-1:200	no
CRX	Cone-rod homeobox protein	rabbit	(Y. Zhu et al., 2013)	Gift from Elly Tanaka	1:500	no
CRX	Cone-rod homeobox protein	mouse	H00001406-M0	Abnova	1:200	no
CTBP2	C-terminal binding protein 2	mouse	612044	BD	1:2500	EDTA buffer pH 8.0, 30 min at 70°C
GFAP	Glial fibrillary acidic protein	rat	345860	Millipore	1:500	no
GFP	Green fluorescent protein	chicken	ab13970	Abcam	1:500	no
GLAST	Astrocyte cell surface antigen-1 ACSA-1	Mouse	130-095-822	Miltenyi	1:200	no
GS	Glutamine synthetase	mouse	610517	BD Biosciences	1:250	no
hMITO	human mitochondria	mouse	ab92824	abcam	1:500	no
hMITO	human mitochondria	mouse	ab3298	abcam	1:500	no
HUC/HUD	HuC/D biotin-conjugated	mouse	A-21272	Invitrogen	1:100	no
IBA1	Allograft inflammatory factor 1	rabbit	019-19741	Wako	1:500	no
KU80	XRCC5, ATP-dependant DNA helicase II or DNA repair, human specific	mouse	ab119935	abcam	1:500	no
MGLUR6	Metabotropic glutamate receptor 6	rabbit	AGC-026	Alomone	1:2000	EDTA buffer pH 8.0, 30 min at 70°C
NRL	Neural retinal leucine	goat	AF2945	R&D	1:200	no
OPN1L/MW	Long- and medium wave opsin	rabbit	AB5405	Millipore	1:1000	no
OPN1SW	Short wave opsin	goat	sc-14363	Santa Cruz	1:200	no
PKCA	Protein kinase C alpha type	rabbit	sc-208	Santa Cruz	1:300	no
PNA	Carbohydrates in cone-specific IPM	biotinylated	B-1075	Vector Laboratories	1:1000	no
PRPH2	Peripherin, PRPH2	rabbit	18109-1-AP	Thermo fisher	1:200	no
RCVRN	Recoverin	rabbit	AB5585	Millipore	1: 1500	no
RHO	Rhodopsin (opsin RET-P1)	mouse	O4886	Sigma	1:1000	no
SCGN	Secretagogen	sheep	RD184120100	Biovendor	1:300	no
SOX2	Transcription factor SOX-2	goat	sc-17320	santa cruz	1:200	no
ZO1	Tight junction protein ZO-1	rabbit	617300	invitrogen	1:200	no

The following table lists all secondary antibodies used. All secondary antibodies were produced by Jackson ImmunoResearch Europe Ltd, raised in donkey and diluted 1:1000.

Table 3. Secondary Antibody Details.

Target	Fluorophore	Identifier
Chicken IgY	Cy3	703-165-155
Goat IgG	Cy2	705-225-147
Goat IgG	Cy3	705-165-147
Goat IgG	Cy5	705-175-147

Target	Fluorophore	Identifier
Mouse IgG	AF488	715-545-151
Mouse IgG	Cy2	715-225-150
Mouse IgG	Cy3	715-165-150
Mouse IgG	Cy5	715-175-150
Rabbit IgG	Cy2	711-225-152
Rabbit IgG	Cy3	711-165-152
Rabbit IgG	Cy5	711-175-152
Rat IgG	AF488	712-545-153
Rat IgG	Cy2	712-225-153
Rat IgG	Cy3	712-165-153
Rat IgG	AF647	712-605-153
Sheep IgG	Cy2	713-225-147

8.3 Methods

8.3.1 Cell culture

8.3.1.1 Human iPSC culture

The Crx-mCherry iPSC line was cultured by the Stem Cell Engineering Facility at CMCB, Dresden, using Matrigel-coated plates, mTeSR1 medium and splitting after incubation with room temperature ReleSR.

8.3.1.2 Human retinal organoid generation

For human retinal organoid (HRO) generation, at day 0 (D0) Crx-mCherry iPSC cultures at 60-80% confluence were briefly washed with 1 ml PBS and detached from the 6-well culture dish for ca. 3 min at 37°C using a thin film of ReLeSR. Usually, 8 wells of iPSCs were used per round. Small colony clumps were collected in DMEM/F-12 and centrifuged for 3 min at 88 rcf at room temperature. The supernatant was removed and clumps were carefully resuspended, first by delicately tapping the tube, then by slowly mixing in 10 µl N2B27 medium (1:1 DMEM/F-12:Neurobasal A media, 1% B27 with VitaminA, 0.5% N2, 1% penicillin/streptomycin, 1% GlutaMAX, 0.1 mM β-mercaptoethanol) per starting well. The cooled clumps were embedded in 150 µl Matrigel, growth factor reduced, per starting well, by adding the Matrigel, carefully mixing and then allowing the mix to become viscous at room temperature for 4-7 min. After breaking up the gel into smaller chunks by pipetting up and down with an additional 12 ml N2B27 medium, the chunks were transferred to 12 wells of low-attachment 6-well plates already containing 1 ml N2B27 medium each. Cells were fed by adding 2 ml N2B27 medium on D2.

Within 5 days, the cell clusters inside the Matrigel chunks developed into cysts. The chunks were then collected, the medium replaced completely with fresh N2B27 medium and the chunks were distributed into double the amount of 6-wells coated with Matrigel. After distributing the chunks in the wells, they were allowed to settle and attach

to the dish. Until D13, the medium was completely replaced with fresh N2B27 medium every second day without disturbing the cells.

At D13, attached cysts were lifted from the dishes: they were washed with prewarmed DMEM/F-12, incubated with 1 ml Dispase per well for 10-15 min at 37°C and collected in DMEM/F-12. The aggregates were again washed carefully with DMEM/F-12 and then distributed in B27 medium (DMEM/F-12, 1% B27 without Vitamin A, 1% penicillin/streptomycin, 1% GlutaMAX, 1% NEAA, 0.1% Amphotericin B) into 10 cm low attachment dishes. From now on, B27 medium was renewed by half-media changes on Mondays, Wednesdays and Fridays. At D25, floating aggregates were changed from B27 to B27/FBS medium (B27 medium, 10% FBS) containing 0.3 µM EC23, a photostable synthetic analog of all-trans retinoic acid.

Around D30, once bright neuroepithelial regions became visible, organoids were cut into smaller organoids, retaining those containing neuroepithelial regions. Until D100, the organoids were kept in B27/FBS medium containing 0.3 mM EC23. Then, the medium was changed to RM2 (DMEM/F12, 1% N2, 10% FBS, 1% penicillin/streptomycin, 1% GlutaMAX, 0.1% Amphotericin B) with 0.3 mM EC23 until D120, after which the organoids were cultured in RM2 only.

8.3.2 Transplantations

8.3.2.1 Dissociation of HRO

All following steps were carried out in a sterile environment. HRO were collected and washed three times in 37°C PBS^{-/-} to remove excess protein. Up to ten HRO at once were transferred to 1 ml 37°C Papain at 20 U/ml in EBSS (Papain reconstituted in fresh sterile EBSS to 20 U/ml with heating 5 min at 37°C, used fresh or aliquoted and stored at -20°C for up to 3 months) and samples were enzymatically dissociated for 1.5-2 h on a horizontal shaker at 70-100 rpm, 37°C. Afterwards, 50 µl DNase I solution (DNase I dissolved in 0.15 M NaCl in H₂O to an activity of >10.000 KU/ml at a concentration of 5 mg/ml, sterile filtered through 0.22 µm PVDF, used fresh or aliquoted and stored at -20°C) were added to a final activity of >480 KU/ml, samples were inverted once and incubated at RT for 5 min. To each ml of HRO/Papain, wash mix containing 520 µl EBSS, 60 µl Ovomuroid solution (Ovomucoid resuspended in 32 ml sterile EBSS per bottle, stored at 4°C) and 60 µl DNase I solution was added and HRO were manually triturated carefully by slowly pipetting up and down ca. 10x using a narrow Pasteur pipette. Separate vials of dissociated HRO were combined at this point and the mixture was overlaid on top of 1 ml Ovomuroid solution at RT per ml Papain used. After centrifugation for 6 min at 600 g, RT, the supernatant was removed, and the tube

carefully flicked to loosen up the pellet before resuspension of the cells in MACS buffer/DNaseI (MACS buffer: PBS^{-/-}, 2 mM EDTA, 0.5% w/v BSA, sterile filtered through 0.2 µm PES; MACS/DNaseI: MACS buffer with 2% DNase I solution yielding a final activity of >200 KU/ml) to ca. 4-6x10⁶ cells/ml. From then on, cells were kept on ice in the dark.

8.3.2.2 Sorting of HRO-derived photoreceptors

Human Crx-mCherry expressing photoreceptors were sorted on Aria II or Aria III cell sorters (BD Biosciences) with support from the CMCB Flow Cytometry Core Facility.

Before sorting, the HRO cell suspension was filtered through a 35 µm mesh and dead cell marker DAPI was added (final concentration 0.02 µg/ml). Then, the sample was loaded onto the pre-cooled sample holder and a small sample volume was assessed. The gating hierarchy was defined as follows: 1) FSC-A vs SSC-A was used to gate for cells and exclude debris. 2) Doublets were removed by gating for singlets using FSC-A versus FSC-H and SSC-H versus SSC-W sequentially. 3) Live cells were selected through absence of DAPI signal in the FSC-A versus DAPI plot. 4) Finally, the mCherry^{high}/GFP^{low} target cell population was selected in the mCherry versus GFP view.

Human photoreceptors were sorted cold using a 100 µm nozzle into 15 ml Falcon tubes containing pre-cooled MACS buffer. The flow rate was set to 1-2. For sorting quality control, a small volume of sorted cells was removed from the collection tube and re-analysed in the FACS machine.

8.3.2.3 Preparation of sorted photoreceptors for transplantation

Sorted cells were centrifuged 6 min at 600 g, RT, resuspended carefully in circa 300 µl MACS/DNaseI and transferred to a 500 µl tube. Live and dead cell numbers were quickly counted in a Neubauer chamber using Trypan exclusion (2 µl cell suspension, 13 µl PBS, 5 µl 0.4% Trypan Blue). Cells were centrifuged again as before and resuspended in MACS/DNaseI to 1.5x10⁵ cells/µl. For easier access during transplantation, the cell suspension was transferred to the tube lid, the tube closed and placed on a tissue on ice, protected from light. Transplantation was performed immediately afterwards.

8.3.2.4 Subretinal injection

The materials and methods used to dissociate, sort and subretinally inject HRO-derived photoreceptors are described in detail in the book chapter “Micromanipulator-assisted subretinal transplantation of human photoreceptor reporter cell suspensions into mice”, which is accepted for publication as of now (Tessmer et al., 2022).

Briefly, host mice were anesthetized by intraperitoneal injection of anesthesia mix (C57BL/6JRj background: 1 mg/kg bw medetomidine hydrochloride and 30 mg/kg bw ketamine; 129 background: 1 mg/kg bw medetomidine hydrochloride and 80 mg/kg bw ketamine). Upon movement loss, pupils were dilated by application of 1 drop of dilating eye drops. After 2-5 min, the drop was taken off and replaced by Vidisic eye gel to keep the cornea moist. Once the mouse was fully anesthetized, it was secured in a stereotaxic head holder, placed under the transplantation microscope and oriented with the eye facing up. A small piece of a glass coverslip was placed on top of the Vidisic gel as a window. Using a 30G needle, an incision was made into the ora serrata in the temporal portion of the globe. The cell suspension was mixed carefully by slowly pipetting up and down and 1 μ l of cell suspension then 0.2 μ l of air were loaded into a 5 μ l Hamilton syringe with a blunt 34-gauge needle. The Hamilton syringe was mounted onto a Micromanipulator, its needle inserted through the hole and carefully, using the micromanipulator controls, steered to very lightly touch the retina on the site opposite of the incision. There, the retina was pierced with the blunt needle and the 0.2 μ l air were inserted into the subretinal space, creating a pre-bleb, followed by the cell suspension. The syringe was carefully retracted, with the injection site sealing itself. The successfully delivered cell volume was estimated and potential bleedings – vitreal bleeding from a disruption of the inner plexus or subretinal bleeding from disruption of the blood-retina barrier on the RPE side – were noted. The needle was flushed with sterile distilled H₂O and PBS^{-/-}.

Directly after transplantation, triamcinolone acetonide filtered through a 35 μ m mesh was resuspended and 1 μ l was drawn up in a 10 μ l Hamilton syringe with a blunt end needle. The needle was inserted handheld through the incision site and triamcinolone acetonide was deposited in the temporal portion of the vitreous. The needle was cleaned with sterile PBS^{-/-}. The animal was released and anesthesia was reversed by intraperitoneal injection of anesthesia reversal compound (10 mg/kg bw atipamezole). Until waking up, the animal was placed in a warm cage and monitored carefully. Usually, triamcinolone acetonide was re-applied every four weeks using anesthesia as described above.

8.3.3 Functional analyses

8.3.3.1 *Light-Dark Box*

For light-aversion testing, animals were submitted to the Light-Dark Box (LDB) assay (TSE Systems, Bad Homburg). The LDB setup consists of two chambers, one brightly lit with 620 lx at its bottom, and one dark, connected by a doorway. Upon doorway opening, the dark chamber is illuminated by incident light of 2.5-6 lux. For

assessment, the animals were placed in the lit chamber with the doorway closed for 30 s before actual trial start. Then, the doorway was opened and the animal allowed to roam for 10 min, freely choosing between both sides. The percentage of time spent in the dark chamber after doorway opening was used as a measure of light aversion. Animals that took >5 min until the first cross into the dark compartment or that made fewer than 3 crosses in total were excluded from analysis. Except for the longitudinal study using rd1 mice, animals were tested once without prior training.

8.3.3.2 Electrophysiology with multi-electrode array

All multi-electrode array (MEA) recordings were performed by Miriam Reh at NMI Tübingen, in the laboratory of Günther Zeck. For full methods and analyses see (Gasparini et al., 2022).

MEA setup

Experimental mice were euthanized, enucleated and the eyes were transferred to carbonated (95% O₂, 5% CO₂) Ames' medium. After incision with a small needle, the lens was removed and the globe cut in half. A Leica M80 stereomicroscope with a fluorescent illumination unit was used to locate the human cells, then the retina was trimmed and isolated carefully from the remaining RPE, sclera and vitreous. The retina was transiently placed on a filter paper (RGC layer facing up) and from there transferred to the pre-coated Glass MEA, RGC layer facing down. The Glass MEA contained 256 recording electrodes (256MEA100/30iR-ITO, Multi Channel Systems MCS) situated in an array of 3 mm x 3 mm, spaced 200 µm apart with an electrode diameter of 30 µm. With the retina located on top of the electrodes, the MEA was placed into a recording headstage (MEA256-System, Multi Channel Systems MCS), located below an objective for light stimulation. The MEA chamber was kept at 36°C during the entire RGC activity recording and perfused with 36°C carbonated Ames' solution at a rate of 2-4 ml/min.

MEA light stimulation and recording

To evoke retinal activity, the explant was stimulated with green light (peak wavelength 550 nm, Figure 43) binary checkerboard white noise, generated by an oLED display controlled by the GEARS software (Szécsi et al., 2017). The stimulation paradigm, a pseudo-random binary checkerboard of 30 x 30 green and black pixels, lasted 25 min with a temporal frequency of 38 Hz and a total illuminated area of 3.2 mm x 4.2 mm. The stimulation was repeated with light intensities increasing from scotopic via mesopic to photopic (full-field illumination equivalent to $P=0.7 \times 10^{-2}$ µW, $P=0.7 \times 10^{-1}$ µW and $P=0.7$ µW respectively, with $P=0.7$ µW yielding photoisomerizations on the level of ca. 1×10^5 R*/photoreceptor/s for both rods and m-cones). Then the

metabotropic glutamate receptor blocker L-AP4 was added at 50 μM to the Ames' buffer to isolate OFF RGC responses and recording was repeated under photopic conditions.

The MCRack software was used to record extracellular voltages, which were then filtered with a 2nd order Butterworth highpass filter (300Hz) before spike detection.

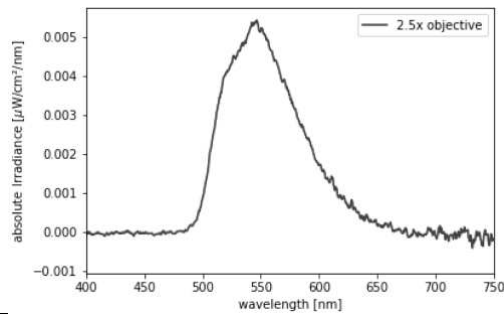


Figure 43. Absolute Irradiance and Full Spectrum of Light used during MEA Stimulation.
Figure reproduced from (Reh, 2021) with permission.

Further processing of MEA samples

After recording, samples were detached from the glass MEA, fixed in 4% PFA, and shipped back in PBS for embedding, cryosectioning and immunohistochemistry as described above.

MEA spike detection, spike triggered average and receptive field calculations

For detailed methods on spike detection, spike triggered average and receptive field calculations, see (Gasparini et al., 2022).

In summary, a threshold was calculated from the first 10 seconds of spontaneous activity and used to determine true spike events upon light stimulation. The spikes were then clustered to identify single cell activities. Spike-triggered averages (STAs) were calculated by averaging all stimuli that induced a spike within 600 ms before spiking, allowing to determine the type of stimulus that the RGC responded to. STAs were further filtered to ensure they represent a stimulus resulting in a robust cell response. Additionally, fitting and averaging of the recorded STA images 80-24 ms before spiking allowed to determine the receptive field of the reacting RGC.

8.3.4 Immunohistochemistry and Immunocytochemistry

8.3.4.1 Tissue collection for cryosectioning

Experimental animals were deeply anesthetized by isoflurane inhalation and decapitated. Eyes were enucleated and placed in 4% PFA/PBS for 1 h at 4°C. Then, cornea, iris, lens and excess muscles were carefully dissected away in PBS and the remaining eye cup was placed in 30% sucrose/PBS at 4°C over night. For freezing, sucrose solution was removed and replaced with cryoprotectant by swirling the eyecup

in NEG-50, also ensuring replacement of the solution within. Eyecups were then embedded in moulds filled with NEG-50 and frozen over a methylbutane bath in liquid nitrogen. Frozen blocks were stored in sealed bags at -80°C. Before cutting, blocks were allowed to come to -20°C for at least 1 h and cut into 12 µm or 20 µm thick sections using an Eprelia™ CryoStar™ NX70. Sections were collected on Starfrost Advanced Adhesive slides in four series (A-D), and every new slide per series was considered a new level marked by numbers. As such, a section was placed in the first row of slide 1A, then 1B, 1C, 1D then in the second row on 1A, 1B, 1C, 1D, and so on until the slide was full, then collection was continued on the next level, in this case 2A, 2B, 2C, 2D, and so forth. As a consequence, each series contained every fourth section of the entire eyecup. Slides were air dried for 20-30 min at 37°C and either directly stained or stored at -80°C.

8.3.4.2 Tissue collection for retinal flatmounts

Animals were anesthetized, killed and enucleated as for retinal cryosectioning. The globes were fixed in 4% PFA/PBS for 20 min at 4°C. Then, the cornea, lens and ciliary muscle were dissected away in PBS after a circumferential cut right below the ora serrata. The RPE and choroid was carefully torn with two tweezers and the retina was incised in a cloverleaf fashion. The retina was transferred to a standing 6-well insert using a wide cut plastic Pasteur pipette, and any residual liquid was carefully removed, flattening the retina in the process with the inner retina facing the membrane. If necessary, the flattening was helped with a thin brush. The retina flatmount was further fixed for 20 min through the addition of 4% PFA below the membrane, so that the retina was touched but not covered by the liquid. Flatmounts were stored at 4°C in PBS until staining.

8.3.4.3 Cell collection for immunocytochemistry

Single cell suspensions for immunocytochemistry were either spotted onto microscopy slides before or after fixation. For spotting after fixation, samples were fixed in dilution by addition of 4x volume 4% PFA/PBS and incubation for 15-25 min at room temperature. Cells were washed by filling the vial with PBS and centrifuging 10 min at 600 g. The cell pellet was resuspended in ddH₂O, small drops placed onto microscopy slides and allowed to dry overnight. Samples were circled with a hydrophobic pen and submitted to staining as described below.

Spotting cells before fixation first required the preparation of microscopy slides. Slides were equipped with sterile-treated FlexiPERM micro12 and resulting wells were precoated with PDL at 50 µg/ml for 2 h at 37°C, which was then washed away with

sterile water. The cells were centrifuged 6 min at 600 g and resuspended in 100 µl RM2 (see organoid culture protocol) per well. Laminin was added to a final concentration of 5 µg/ml and the mix placed in the well. After 30-120 min in the cell culture incubator, 200 µl 4% PFA/PBS were added to each well, fixing the cells for 15 min at RT. The wells were washed by very slowly removing 200 µl volume and adding 200 µl PBS and stored in a sealed container at 4°C until staining in the wells as described below. For staining, it was crucial to never pipette fast, as cells were easily dislodged. After staining, the silicone mould was removed and the slides mounted as described.

8.3.4.4 Immunofluorescent staining

Immunohistochemistry samples were rehydrated in PBS and where necessary (see *Table 2. Primary Antibody Details.*), antigen retrieval was performed. Samples were then permeabilized and blocked in blocking solution for 1 h at room temperature and incubated with primary antibodies diluted in blocking buffer at 4°C over night. See *Table 1* for primary antibody dilutions and details. After 3 washes with PBS, secondary antibodies diluted in PBS containing 0.2 µg/ml DAPI were added to the slides and allowed to incubate for 1-1.5 h at room temperature. See *Table 3* for details on secondary antibodies used. Samples were washed with PBS as before, rinsed with ddH₂O and mounted between the microscopic slide and a coverslip using AquaPolyMount. Mounting medium was allowed to harden over night at room temperature before storage at 4°C.

Mostly, cryosectioned samples were stained using the Eprelia Shandon Coverplate system. Here, coverplates were positioned on the slide after rehydration and dissolution of NEG-50 or antigen retrieval and installed in the Eprelia Shandon Sequenza Immunostaining rack. Correct positioning was ensured by inspecting the flow-through speed of PBS. Then sections were permeabilized, blocked and stained as described above, by adding 300 µl PBS for washing and 120 µl antibody suspensions into the reservoir. After the final washing step in ddH₂O, the assembly was removed from the rack, coverplates were carefully detached and the slides mounted as described.

Occasionally, samples were stained lying flat. In that case, samples were rehydrated, excess liquid removed and the sections isolated by circling with a hydrophobic pen. After allowing the hydrophobic seal to dry, slides were placed in a moist chamber and staining was performed as above. To reduce the risk of spillage, liquid volumes were adjusted so that the samples were fully covered without creating a large dome. Washes were carried out 5 instead of 3 times.

Staining of flatmounts was performed in 24-well plates on a horizontal shaker at 80-100 rpm. Incubation times were extended as follows to allow full penetration of the tissue: 1 h permeabilization/blocking, 2-4 d primary antibody incubation, 1 d secondary antibody incubation, 1 h per wash step. For mounting, flatmounts were placed on a coverplate with the outer retina facing the coverplate and flattened carefully with a very thin brush. AquaPolyMount and the microscope slide added on top, facing the inner retina.

8.3.4.5 Antigen retrieval

Where antigen retrieval was necessary, slides were washed in PBS to dissolve NEG-50 and rehydrate the sections. Slides were then slowly inserted into chambers containing the respective 70°C antigen retrieval solution and incubated for 30 min in a waterbath of the same temperature. Afterwards, containers and slides were allowed to cool to RT for ca. 20 min, washed in PBS and stained as described above. Antigen retrieval solutions and antibodies requiring antigen retrieval can be found in *Table 2*.

8.3.5 Imaging and image processing

8.3.5.1 Imaging

Immunohistochemistry samples were generally imaged on an Axio Imager.Z1 with ApoTome.2 enabled using an HXP120 lamp as light source (all Zeiss). For quantifications, the A-series of each cryosectioned block, i.e. every fourth serial section traversing the entire eye, was first assessed for human graft presence using the Imager.Z1 microscope. All graft-containing sections were then imaged with an AxioScanZ.1 by the Light Microcopy Facility at CMCB, Dresden. In both cases images were usually taken as z-stacks and presented as a maximum intensity projection.

Images were processed using Zen Blue Software (Zeiss), FIJI Version 2.3.0/1.53q (Schindelin et al., 2012) and Affinity Designer (Serif Europe Ltd.).

8.3.5.2 Image quantifications

Graft-containing sections imaged with the AxioScan.Z1 were quantified using the ZEN Blue Software and its image analysis wizard or manual measurements in the Measure tab. Data was processed and visualized using Microsoft Excel for Mac and RStudio.

Graft volume quantification

Graft volumes were determined based on RCVRN staining using the Image Analysis Wizard of the ZEN Blue software, with a new image analysis setup for each image. Briefly, a manual region of interest (ROI) was drawn closely around the strongly RCVRN⁺ human cells. Then, foreground and background pixel intensity cutoffs were

adjusted manually to best reflect RCVRN⁺ area. Erroneous segmentation, e.g. due to fluorescence intensity differences within slides, was manually corrected through deletion or addition of areas where necessary. RCVRN⁺ areas were exported and summarized per eye. To infer graft volumes, the measured areas were multiplied by the section thickness and by 4, correcting for only every fourth section being quantified. Values from unquantifiable, e.g. missing or folded, sections were extrapolated by averaging the values from the neighboring sections.

Quantification of incorporation

Extent of incorporation was quantified based on RCVRN staining using the polygon contour tool in the Measure tab of the ZEN Blue Software where human graft cells were present amongst host photoreceptors. The human cell clusters were traced, with the apical border represented by an assumed OLM, i.e. the place where the OLM would be if no human cells were present. As described above, the resulting area was summarized per eye, multiplied by 4 and the section thickness and missing values were imputed. The total incorporated volume per eye was expressed as percentage of the total graft volume in the respective eye. Note that this approach on one hand potentially underestimates the incorporated volume, as it disregards human cellular structures such as inner segments that oftentimes extend beyond the assumed OLM. On the other hand in cases of loosely packed grafts the incorporated volume is likely overestimated, as small holes within the graft were included in the measurement of incorporation area, but excluded during total graft volume quantification.

Quantification of inner segment formation

Presumptive inner segments (IS) in the shape of bulbous, hMITO⁺ outgrowths were manually counted using the number tool in the Measure tab of the ZEN Blue Software. IS were further characterized based on the graft type they were associated with: isolated (IS present in a graft cluster without contact to host retina nuclei in this section), touchFar (IS in a graft cluster with contact to host retina nuclei but more than 50 µm away from the contact site), contact (IS in a graft present in the subretinal space within 50 µm of graft cell contact to host nuclei or IS directly neighbouring host ONL nuclei without a visible cell body) and incorporated (IS sprouting from an incorporated cluster). IS of the contact and incorporated type were both considered to be interacting with the host retina, while IS of the isolated and touchFar were both considered isolated.

IS counts per eye were summarized and multiplied by 4 to approximate the total number of IS per eye. As above, values for unquantifiable sections were imputed by averaging the neighbouring sections.

8.3.5.3 *Electron microscopy*

Electron microscopy sample preparation and imaging was carried out by the Electron Microscopy Facility at CMCB, Dresden.

Transmission electron Microscopy (TEM)

TEM was performed as previously described (Völkner et al., 2019, 2021). Briefly, eyes were retrieved from the animals as described above for cryosectioning. Globes were fixed in 4% PFA/PB (PFA diluted in 100 mM phosphate buffer) at 4°C for 20-24 h, with the cornea punctured after the first hour. Then, cornea, iris, lens and muscles were dissected away as described above. The region of interest (ROI) was detected by human cell reporter fluorescence and cut out under a Leica MZ10F fluorescence stereomicroscope. Samples for epon embedding and TEM were postfixed in Modified Karnovsky's Fixative (2% glutaraldehyde, 2% paraformaldehyde in 50 mM HEPES) at least overnight at 4°C and samples for CLEM were directly stored in 1% PFA/PBS, 4°C until further preparation.

For TEM, the ROI was then postfixed in a 2% OsO₄ solution (2% OsO₄, 1.5% potassium ferrocyanide, 2 mM CaCl₂ in water), followed by incubation in 1% aqueous thiocarbohydrazide, another contrasting step in 2% aqueous OsO₄, en-bloc contrasting with 1% uranyl acetate in water, dehydration in a graded ethanol series from 30% to 100% (on molecular sieve) and stepwise infiltration in the epon substitute EMBED 812. Samples were washed with water in between all steps until dehydration and were cured at 65°C overnight after embedding. The Z-plane of the ROIs in the blocks were identified by scoring semithin sections stained with toluidine blue/borax. Subsequently, ultrathin sections of 70 nm thickness were cut using a Leica UC6 ultramicrotome and a diamond knife (Diatome). Sections were collected on formvar-coated slot grids followed by staining with lead citrate (Venable & Coggeshall, 1965) and uranyl acetate. TEM imaging was performed with a Jeol JEM1400 Plus transmission electron microscope (camera: Ruby, Jeol) running at 80 kV acceleration voltage.

Correlative light and electron microscopy (CLEM)

For CLEM, the selected ROIs in 1% PFA/PBS were dehydrated in a graded series of ethanol, before infiltration and embedding in Lowicryl K4M at progressively lower temperatures, from 4°C to -35°C (Carlemalm et al., 1982). Lowicryl K4M was polymerized for 48 h by UV-irradiation at -35°C. Ultrathin sections were cut with a diamond knife (Diatome) and mounted onto formvar-coated mesh grids. CLEM of immunolabeled sections was performed as described previously (Eberle et al., 2012; Fabig et al., 2012). The sections were then labelled by sequential blocking with 1% BSA/PBS, incubation with the primary antibody, a bridging antibody, protein A

10 nm gold for immunogold labelling, and a fluorophore-conjugated secondary antibody for immunofluorescence. DAPI was used for nuclear counterstain and samples were washed with PBS or water in between all steps. Finally, the labeled grids were mounted in glycerol-water (1:1). A Keyence Biozero 8000 fluorescence microscope was used for fluorescent imaging and selection of ROIs for TEM. The chosen grids were then demounted and washed in water before contrasting with uranyl acetate and drying for electron microscopy.

8.3.6 Statistics

The below table details all statistical tests used to compare quantitative results, ordered by the figure they relate to.

Table 4. Statistical Analyses

Figure 12. Assessment of D200 Sorting for Crx-mCherry by ICC.	
Comparing percentages of subpopulations for each staining, with samples from the same dissociation round matched:	Mixed-effects analysis with Geisser-Greenhouse correction plus Tukey's multiple comparisons test with individual variances computed for each comparison.
Figure 14. Graft Volumes in D100, D200 and D300 Transplants. Figure 16. Quantification of Graft Subtypes by Positioning. Figure 20. Inner Segments in IHC and EM and Their Quantification in D100, D200 and D300 Grafts.	
Comparing D100-derived means, acknowledging experimental round:	Ordinary 2-way ANOVA with main effects only plus Šidák's multiple comparisons test with individual variances computed for each comparison.
Comparing D100-derived means, irrespective of experimental round:	Brown-Forsythe and Welch ANOVA tests plus Dunnett's T3 multiple comparison test with individual variances computed for each comparison.
Comparing D100-derived means one by one, irrespective of experimental round:	Unpaired t-test with Welch's correction.
Comparing D200-derived means, acknowledging experimental round:	Ordinary 2-way ANOVA with main effects only plus Šidák's multiple comparisons test with individual variances computed for each comparison.
Comparing D200-derived means, irrespective of experimental round:	Unpaired parametric t-test.
Comparing between D370 means, irrespective of experimental round:	Brown-Forsythe and Welch ANOVA tests plus Dunnett's T3 multiple comparisons test, with individual variances computed for each comparison.
Figure 21. Inner Segment Development in Proximal and Distal Grafts.	
Comparing proximal and distal IS counts within each timepoint, acknowledging experimental round:	Ordinary two-way ANOVA plus Šidák's multiple comparisons test with individual variances computed for each comparison.
Comparing proximal and distal IS counts (values paired per eye) within each timepoint, irrespective of experimental round:	Paired t-test, parametric.
Figure 26. Graft Size and Positioning in D200 Early Timeline Samples.	
Comparing between timepoints, acknowledging experimental round:	Ordinary two-way ANOVA with main effects only plus Tukey's multiple comparisons test with individual variances computed for each comparison.
Comparing timepoints separately, irrespective of experimental rounds (only for B: Incorporated Area)	Unpaired Mann-Whitney test for each sequential comparison (4 v 6, 6 v 8, 8 wpt v 10 wpt).
Figure 39. Light-Dark Box Results of C57BL/6Jrj and Cpf1 Animals Figure 40. Light-Dark Box Results of Strongly Degenerated Animals., A: tgCR animals	

Comparing all means with the control:	Ordinary one-way ANOVA plus Dunnett's multiple comparisons test with single pooled variance.
Comparing +10w with +26w means within the same donor cell age:	Ordinary one-way ANOVA with Šidák's multiple comparison with single pooled variance.
Figure 40. Light-Dark Box Results of Strongly Degenerated Animals., B: rd1 animals	
Comparing all means with matching repeated measures of the same animals:	Mixed-effects model plus Šidák's multiple comparisons test with single pooled variance

8.3.7 Single cell sequencing

8.3.7.1 Dissociation and sorting of samples for sequencing

In vitro HRO samples were dissociated as described above (section 8.3.2.1 *Dissociation of HRO*). For recollection of the ex vivo samples, i.e. human cells from transplanted murine eyes, animals were deeply anesthetized by isoflurane inhalation, decapitated and enucleated. Globes were kept on ice in the dark. Cornea, iris, lens, excess muscles and the optic nerve were quickly dissected away in PBS. After transfer to the lid of a 1.5 ml tube containing 1 ml 37°C Papain at 2 U/ml in EBSS with 20 µl DNaseI solution, the eye cups were roughly chopped with microscissors. The tube was briefly inverted to mix and incubated at 37°C for 20 min in the dark, inverting once every 5 min. After dissociation, samples were carefully triturated, washed, overlaid onto Ovomuroid, centrifuged, resuspended and filtered as described above (section 8.3.2.1 *Dissociation of HRO*).

Cells of interest of both in vitro and ex vivo samples were sorted directly into 384-well plates containing 0.5 µl lysis buffer (nuclease free water, 0.2% Triton-X 100, 4 U murine RNase Inhibitor (NEB)), otherwise using the same FACS conditions and gating strategy as described above (8.3.2.2 Sorting of HRO-derived photoreceptors).

Single cell cDNA and library preparation

Single cell processing from cell lysis until provision of read count matrices was performed by the Dresden concept Genome Center at CMCB, Dresden, according to the SmartSeq2 protocol as described in (Willenborg et al., 2022).

Briefly, following cell lysis, 0.5 µl dT-buffer (5 mM dNTP (Invitrogen), 0.5 µM dT-primer¹), was added to each well and RNA was denatured by 3 min incubation at 72°C. RNA was reverse transcribed by addition of 1.5 µl Reverse Transcription Buffer (Final concentration: 1 U RNase Inhibitor (NEB), 1x superscript II buffer (Invitrogen), 1 M betaine, 5 mM DTT, 6 mM MgCl₂, 1 µM TSO-primer², 9 U RNase Inhibitor, 90 U

¹ C6-aminolinker-AAGCAGTGGTATCAACGCAGAGTCGACTTTTTTTTTTTTTTTTTTTTTTTTTTTTTTTTTTTTTV

² AAGCAGTGGTATCAACGCAGAGTACATrGrGrG

Superscript II) and incubation at 42°C for 90 min, after which the enzyme was heat inactivated for 15 min at 70°C.

The cDNA was amplified by cycling using Kapa HiFi HotStart Readymix (Peqlab; 1x final concentration) and 0.1 µM UP-primer³ (Program: 98°C, 3 min; 23x [98°C, 20 sec; 67°C, 15 sec; 72°C, 6 min]; 72°C, 5 min), bead-purified and eluted in 12 µl nuclease free water. cDNA concentration was measured with a Tecan plate reader Infinite 200 using AccuBlue Broas range chemistry (Biotium).

Tagmentation for library preparation was done by desiccating and rehydrating up to 700 pg cDNA in 1 µl Tagmentation mix (Tagmentation Buffer and BLT transposome from the Illumina DNA BLT library prep), incubating for 5 min at 55°C. Barcoding during library amplification used 1x concentrated KAPA Hifi HotStart Ready Mix and 300 nM dual indexing primers (72°C, 3 min; 98°C, 30 sec; 13x [98°C, 10 sec; 63°C, 20 sec; 72°C, 1 min], 72°C 5 min).

Libraries were quantified with the AccuBlue Broad range chemistry, equimolarly pooled and bead-purified twice. Sequencing was done on the NovaSeq 6000 with 1.5 mio paired-end 100 bp reads per cell.

8.3.8 Bioinformatic analysis

8.3.8.1 Pre-processing

Data pre-processing, alignment and count matrix generation were carried out by the bioinformatics team at Dresden concept Genome Center at CMCB, Dresden.

Basic quality control of the resulting sequence data was done with FastQC (v0.11.6, <https://www.bioinformatics.babraham.ac.uk/projects/fastqc/>) and the degree of mouse contamination was assessed with FastQ-Screen (v0.9.3, https://www.bioinformatics.babraham.ac.uk/projects/fastq_screen). Reads originating from mouse were removed with xengsort (v2021-05-27) (Zentgraf & Rahmann, 2021). Reads were aligned to the human reference genome hg38 using the aligner gsnap (v2021-05-08) (Wu & Nacu, 2010) with Ensembl 104 human splice sites as support. Uniquely mapped reads were compared based on their overlap to Ensembl 104 human gene annotations using featureCounts (v2.0.1) (Liao et al., 2014) to create a table of fragments per human gene and cell.

³ AAGCAGTGGTATCAACGCAGAGT

8.3.8.2 Analysis

Single cell sequencing data was analysed running R using the Seurat pipeline in a jupyterlab notebook run on the High Performance Computing Cluster at ZIH, TU Dresden (Butler et al., 2018; Hao et al., 2021; Satija et al., 2015; Stuart et al., 2019).

Filtering, normalization and clustering

All read counts were combined in one table and a Seurat object created, with `min.cells = 3`, `min.features = 50`. During initial quality control, cells with `>25%` mitochondrial read content and `>25%` ERCC read content were removed to retain only viable cells. Further, an outlier sample (cells from one of four organoids from in vitro D270) was removed as it continuously generated a separate UMAP cluster later on, without showing any cell-type specific gene expression. After filtering for the experimental conditions of interest, the reads were normalized and scaled (`normalization.method = "LogNormalize"`, `scale.factor = 1e4`). Then, variable feature detection (`selection.method = 'vst'`, `nfeatures = 2000`), principal component analysis and visualization using ElbowPlot with `ndims = 50` was used to pre-select dimensions for uniform manifold approximation and projection for dimension reduction (UMAP). UMAP clustering was repeated with various combinations of parameters for dimensions, resolution and number of neighbors, and the resulting clustering was manually evaluated for reproducibility across different conditions, as well as the possibility to identify cell types in the resulting clusters. Ultimately, organoid-derived samples only were clustered using `dim = 20`, `resolution = 1.2`, `n.neighbors = 20`. For comparison of in vitro D200, D270 and D370 samples with age-matched ex vivo samples (D200+10w and D200+26w) the parameters were set to `dim = 20`, `resolution = 0.7`, `n.neighbors = 30`.

Following quality control of UMAP clustering, clusters were manually annotated based on marker gene expression as detected by Seurat (`only.pos = FALSE`, `min.pct = 0.25`, `logfc.threshold = 0.25`) shown in a heatmap, as well as plotting of additional known marker gene expression levels on the UMAP plot. While cone subclusters were identified with the clustering conditions used, they were addressed combined for simplification as analysis could not yet be completed and hence the implications of the subclusters were not yet clear.

Differential gene expression between D370 in vitro and ex vivo samples

For detection of differentially expressed genes between cones of D370 in vitro and ex vivo samples, the Seurat object was subset to only contain cells assigned to cone clusters. The `active.ident` was set to the experimental condition and marker genes of the respective conditions were identified using the FindMarker function (`min.pct = 0.25`). Differentially expressed genes with an adjusted p value $p_{\text{adj}} < 0.001$ were used as

input to gprofiler (Raudvere et al., 2019) and panther (Mi et al., 2021) for gene enrichment analysis using the statistical overrepresentation Fisher's exact test corrected with calculated false discovery rate in an ordered query based on increasing p_{adj} (lowest p_{adj} = highest importance). GO terms reported here were of the first hierarchy level only to reduce repetitive pathway findings, filtered for a fold enrichment > 10 as displayed by panther and used only if they were detected with both gprofiler and panther. Dot plots and violin plots were generated with the respective Seurat functions using a selection of differentially expressed marker genes that were found to contribute to the GO term detection as shown by gprofiler, as well other as genes found to be differentially expressed under similar conditions with a different, cone-specific reporter cell line (Gasparini et al., 2022).

9 Bibliography

- Aboualizadeh, E., Phillips, M. J., McGregor, J. E., DiLoreto, D. A., Strazzeri, J. M., Dhakal, K. R., Bateman, B., Jager, L. D., Nilles, K. L., Stuedemann, S. A., Ludwig, A. L., Hunter, J. J., Merigan, W. H., Gamm, D. M., & Williams, D. R. (2020). Imaging Transplanted Photoreceptors in Living Nonhuman Primates with Single-Cell Resolution. *Stem Cell Reports*, *15*(2), 482–497. <https://doi.org/10.1016/j.stemcr.2020.06.019>
- Ansari, A. M., Ahmed, A. K., Matsangos, A. E., Lay, F., Born, L. J., Marti, G., Harmon, J. W., & Sun, Z. (2016). Cellular GFP Toxicity and Immunogenicity: Potential Confounders in in Vivo Cell Tracking Experiments. *Stem Cell Reviews*, *12*(5), 553–559. <https://doi.org/10.1007/s12015-016-9670-8>
- Aramant, R., Seiler, M., Ehinger, B., Bergström, A., Gustavii, B., Brundin, P., & Adolph, A. R. (1990). Transplantation of human embryonic retina to adult rat retina. *Restorative Neurology and Neuroscience*, *2*(1), 9–22. <https://doi.org/10.3233/RNN-1990-2102>
- Awatramani, G. B., & Slaughter, M. M. (2000). Origin of Transient and Sustained Responses in Ganglion Cells of the Retina. *Journal of Neuroscience*, *20*(18), 7087–7095. <https://doi.org/10.1523/JNEUROSCI.20-18-07087.2000>
- Baccus, S. A. (2007). Timing and Computation in Inner Retinal Circuitry. *Annual Review of Physiology*, *69*(1), 271–290. <https://doi.org/10.1146/annurev.physiol.69.120205.124451>
- Bainbridge, J. W. B., Mehat, M. S., Sundaram, V., Robbie, S. J., Barker, S. E., Ripamonti, C., Georgiadis, A., Mowat, F. M., Beattie, S. G., Gardner, P. J., Feathers, K. L., Luong, V. A., Yzer, S., Balaggan, K., Viswanathan, A., De Ravel, T. J. L., Casteels, I., Holder, G. E., Tyler, N., ... Ali, R. R. (2015). Long-term effect of gene therapy on Leber's congenital amaurosis. *New England Journal of Medicine*, *372*(20), 1887–1897. Scopus. <https://doi.org/10.1056/NEJMoa1414221>
- Baker, S. A., & Kerov, V. (2013). Chapter Seven—Photoreceptor Inner and Outer Segments. In V. Bennett (Ed.), *Current Topics in Membranes* (Vol. 72, pp. 231–265). Academic Press. <https://doi.org/10.1016/B978-0-12-417027-8.00007-6>
- Banin, E., Obolensky, A., Idelson, M., Hemo, I., Reinhardt, E., Pikarsky, E., Ben-Hur, T., & Reubinoff, B. (2006). Retinal Incorporation and Differentiation of Neural Precursors Derived from Human Embryonic Stem Cells. *Stem Cells*, *24*(2), 246–257. <https://doi.org/10.1634/stemcells.2005-0009>
- Barber, A. C., Hippert, C., Duran, Y., West, E. L., Bainbridge, J. W. B., Warre-Cornish, K., Luhmann, U. F. O., Lakowski, J., Sowden, J. C., Ali, R. R., & Pearson, R. A. (2013). Repair of the degenerate retina by photoreceptor transplantation. *Proceedings of the National Academy of Sciences*, *110*(1), 354–359. <https://doi.org/10.1073/pnas.1212677110>
- Barnea-Cramer, A. O., Wang, W., Lu, S.-J., Singh, M. S., Luo, C., Huo, H., McClements, M. E., Barnard, A. R., MacLaren, R. E., & Lanza, R. (2016). Function of human pluripotent stem cell-derived photoreceptor progenitors in blind mice. *Scientific Reports*, *6*(1), 29784. <https://doi.org/10.1038/srep29784>
- Basak, O., & Taylor, V. (2007). Identification of self-replicating multipotent progenitors in the embryonic nervous system by high Notch activity and Hes5 expression: Subdividing CNS progenitor populations. *European Journal of Neuroscience*, *25*(4), 1006–1022. <https://doi.org/10.1111/j.1460-9568.2007.05370.x>
- Battu, R., Ratra, D., & Gopal, L. (2022). Newer therapeutic options for inherited retinal diseases: Gene and cell replacement therapy. *Indian Journal of Ophthalmology*, *70*(7), 2316–2325. https://doi.org/10.4103/ijo.IJO_82_22

- Ben M'Barek, K., Habeler, W., Regent, F., & Monville, C. (2019). Developing Cell-Based Therapies for RPE-Associated Degenerative Eye Diseases. In K. Bharti (Ed.), *Pluripotent Stem Cells in Eye Disease Therapy* (pp. 55–97). Springer International Publishing. https://doi.org/10.1007/978-3-030-28471-8_3
- Berber, P., Milenkovic, A., Michaelis, L., & Weber, B. H. F. (2021). Retinal organoid differentiation methods determine organoid cellular composition. *Journal of Translational Genetics and Genomics*, 5(3), 292–303. <https://doi.org/10.20517/jtgg.2021.35>
- Botto, C., Rucli, M., Tekinsoy, M. D., Pulman, J., Sahel, J.-A., & Dalkara, D. (2022). Early and late stage gene therapy interventions for inherited retinal degenerations. *Progress in Retinal and Eye Research*, 86, 100975. <https://doi.org/10.1016/j.preteyeres.2021.100975>
- Bowmaker, J. K., & Dartnall, H. J. (1980). Visual pigments of rods and cones in a human retina. *The Journal of Physiology*, 298(1), 501–511. <https://doi.org/10.1113/jphysiol.1980.sp013097>
- Bringmann, A., Grosche, A., Pannicke, T., & Reichenbach, A. (2013). GABA and Glutamate Uptake and Metabolism in Retinal Glial (Müller) Cells. *Frontiers in Endocrinology*, 4. <https://www.frontiersin.org/articles/10.3389/fendo.2013.00048>
- Burger, C. A., Jiang, D., Mackin, R. D., & Samuel, M. A. (2021). Development and maintenance of vision's first synapse. *Developmental Biology*, 476, 218–239. <https://doi.org/10.1016/j.ydbio.2021.04.001>
- Burgoyne, T., Meschede, I. P., Burden, J. J., Bailly, M., Seabra, M. C., & Futter, C. E. (2015). Rod disc renewal occurs by evagination of the ciliary plasma membrane that makes cadherin-based contacts with the inner segment. *Proceedings of the National Academy of Sciences*, 112(52), 15922–15927. <https://doi.org/10.1073/pnas.1509285113>
- Buskamp, V., Duebel, J., Balya, D., Fradot, M., Viney, T. J., Siebert, S., Groner, A. C., Cabuy, E., Forster, V., Seeliger, M., Biel, M., Humphries, P., Paques, M., Mohand-Said, S., Trono, D., Deisseroth, K., Sahel, J. A., Picaud, S., & Roska, B. (2010). Genetic Reactivation of Cone Photoreceptors Restores Visual Responses in Retinitis Pigmentosa. *Science*, 329(5990), 413–417. <https://doi.org/10.1126/science.1190897>
- Butler, A., Hoffman, P., Smibert, P., Papalexi, E., & Satija, R. (2018). Integrating single-cell transcriptomic data across different conditions, technologies, and species. *Nature Biotechnology*, 36(5), 411–420. <https://doi.org/10.1038/nbt.4096>
- Capowski, E. E., Samimi, K., Mayerl, S. J., Phillips, M. J., Pinilla, I., Howden, S. E., Saha, J., Jansen, A. D., Edwards, K. L., Jager, L. D., Barlow, K., Valiauga, R., Erlichman, Z., Hagstrom, A., Sinha, D., Sluch, V. M., Chamling, X., Zack, D. J., Skala, M. C., & Gamm, D. M. (2018). Reproducibility and staging of 3D human retinal organoids across multiple pluripotent stem cell lines. *Development*, dev.171686. <https://doi.org/10.1242/dev.171686>
- Carlemalm, E., Garavito, R. M., & Villiger, W. (1982). Resin development for electron microscopy and an analysis of embedding at low temperature*. *Journal of Microscopy*, 126(2), 123–143. <https://doi.org/10.1111/j.1365-2818.1982.tb00362.x>
- Cebrián, C., Loike, J. D., & Sulzer, D. (2014). Neuronal MHC-I expression and its implications in synaptic function, axonal regeneration and Parkinson's and other brain diseases. *Frontiers in Neuroanatomy*, 8. <https://www.frontiersin.org/articles/10.3389/fnana.2014.00114>
- Chenais, N. A. L., Airaghi Leccardi, M. J. I., & Ghezzi, D. (2021). Photovoltaic retinal prosthesis restores high-resolution responses to single-pixel stimulation in blind retinas. *Communications Materials*, 2(1), 1–16. <https://doi.org/10.1038/s43246-021-00133-2>

- Collin, J., Zerti, D., Queen, R., Santos-Ferreira, T., Bauer, R., Coxhead, J., Hussain, R., Steel, D., Mellough, C., Ader, M., Sernagor, E., Armstrong, L., & Lako, M. (2019). CRX Expression in Pluripotent Stem Cell-Derived Photoreceptors Marks a Transplantable Subpopulation of Early Cones. *STEM CELLS*, *0*(0). <https://doi.org/10.1002/stem.2974>
- Costall, B., Jones, B. J., Kelly, M. E., Naylor, R. J., & Tomkins, D. M. (1989). Exploration of mice in a black and white test box: Validation as a model of anxiety. *Pharmacology Biochemistry and Behavior*, *32*(3), 777–785. [https://doi.org/10.1016/0091-3057\(89\)90033-6](https://doi.org/10.1016/0091-3057(89)90033-6)
- Cowan, C. S., Renner, M., De Gennaro, M., Gross-Scherf, B., Goldblum, D., Hou, Y., Munz, M., Rodrigues, T. M., Krol, J., Szikra, T., Cuttat, R., Waldt, A., Papasaikas, P., Diggelmann, R., Patino-Alvarez, C. P., Galliker, P., Spirig, S. E., Pavlinic, D., Gerber-Hollbach, N., ... Roska, B. (2020). Cell Types of the Human Retina and Its Organoids at Single-Cell Resolution. *Cell*, *182*(6), 1623-1640.e34. <https://doi.org/10.1016/j.cell.2020.08.013>
- Curcio, C. A., & Hendrickson, A. E. (1991). Chapter 5 Organization and development of the primate photoreceptor mosaic. *Progress in Retinal Research*, *10*, 89–120. [https://doi.org/10.1016/0278-4327\(91\)90010-Y](https://doi.org/10.1016/0278-4327(91)90010-Y)
- Dartnall, H. J. A., Bowmaker, James. K., Mollon, J. D., & Barlow, H. B. (1983). Human visual pigments: Microspectrophotometric results from the eyes of seven persons. *Proceedings of the Royal Society of London. Series B. Biological Sciences*, *220*(1218), 115–130. <https://doi.org/10.1098/rspb.1983.0091>
- Das, T., del Cerro, M., Jalali, S., Rao, V. S., Gullapalli, V. K., Little, C., Loreto, D. A. D., Sharma, S., Sreedharan, A., del Cerro, C., & Rao, G. N. (1999). The Transplantation of Human Fetal Neuroretinal Cells in Advanced Retinitis Pigmentosa Patients: Results of a Long-Term Safety Study. *Experimental Neurology*, *157*(1), 58–68. <https://doi.org/10.1006/exnr.1998.6992>
- De Silva, S. R., & Moore, A. T. (2022). Optogenetic approaches to therapy for inherited retinal degenerations. *The Journal of Physiology*, *n/a*(n/a). <https://doi.org/10.1113/JP282076>
- del Cerro, M., Gash, D. M., Rao, G. N., Notter, M. F., Wiegand, S. J., & Gupta, M. (1985). Intraocular retinal transplants. *Investigative Ophthalmology & Visual Science*, *26*(8), 1182–1185.
- del Cerro, M., Ison, J. R., Bowen, G. P., Lazar, E., & del Cerro, C. (1991). Intraretinal grafting restores visual function in light-blinded rats. *Neuroreport: An International Journal for the Rapid Communication of Research in Neuroscience*, *2*(9), 529–532. <https://doi.org/10.1097/00001756-199109000-00008>
- Deng, W.-T., Kolandaivelu, S., Dinculescu, A., Li, J., Zhu, P., Chiodo, V. A., Ramamurthy, V., & Hauswirth, W. W. (2018). Cone Phosphodiesterase-6γ Subunit Augments Cone PDE6 Holoenzyme Assembly and Stability in a Mouse Model Lacking Both Rod and Cone PDE6 Catalytic Subunits. *Frontiers in Molecular Neuroscience*, *11*. <https://www.frontiersin.org/articles/10.3389/fnmol.2018.00233>
- Derouiche, A., Pannicke, T., Haseleu, J., Blaess, S., Grosche, J., & Reichenbach, A. (2012). Beyond Polarity: Functional Membrane Domains in Astrocytes and Müller Cells. *Neurochemical Research*, *37*(11), 2513–2523. <https://doi.org/10.1007/s11064-012-0824-z>
- Duncan, J. L., Pierce, E. A., Laster, A. M., Daiger, S. P., Birch, D. G., Ash, J. D., Iannaccone, A., Flannery, J. G., Sahel, J. A., Zack, D. J., & Zarbin, M. A. (2018). Inherited Retinal Degenerations: Current Landscape and Knowledge Gaps. *Translational Vision Science & Technology*, *7*(4), 6–6. <https://doi.org/10.1167/tvst.7.4.6>
- Eberle, D., Kurth, T., Santos-Ferreira, T., Wilson, J., Corbeil, D., & Ader, M. (2012). Outer Segment Formation of Transplanted Photoreceptor Precursor Cells. *PLoS ONE*, *7*(9), e46305. <https://doi.org/10.1371/journal.pone.0046305>

- Ehinger, B., Bergström, A., Seiler, M., Aramant, R. B., Zucker, C. L., Gustavi, B., & Adolph, A. R. (1991). Ultrastructure of human retinal cell transplants with long survival times in rats. *Experimental Eye Research*, 53(4), 447–460. [https://doi.org/10.1016/0014-4835\(91\)90162-8](https://doi.org/10.1016/0014-4835(91)90162-8)
- Ehlken, C., Jungmann, S., Böhringer, D., Agostini, H. T., Junker, B., & Pielen, A. (2014). Switch of anti-VEGF agents is an option for nonresponders in the treatment of AMD. *Eye*, 28(5), 538–545. <https://doi.org/10.1038/eye.2014.64>
- Eiraku, M., & Sasai, Y. (2011). Mouse embryonic stem cell culture for generation of three-dimensional retinal and cortical tissues. *Nature Protocols*, 7(1), 69–79. <https://doi.org/10.1038/nprot.2011.429>
- Euler, T., Haverkamp, S., Schubert, T., & Baden, T. (2014). Retinal bipolar cells: Elementary building blocks of vision. *Nature Reviews Neuroscience*, 15(8), 507–519. <https://doi.org/10.1038/nrn3783>
- Fabig, G., Kretschmar, S., Weiche, S., Eberle, D., Ader, M., & Kurth, T. (2012). Chapter 5—Labeling of Ultrathin Resin Sections for Correlative Light and Electron Microscopy. In T. Müller-Reichert & P. Verkade (Eds.), *Methods in Cell Biology* (Vol. 111, pp. 75–93). Academic Press. <https://doi.org/10.1016/B978-0-12-416026-2.00005-4>
- FDA. (2017, December 18). *FDA approves novel gene therapy to treat patients with a rare form of inherited vision loss*. FDA; FDA. <https://www.fda.gov/news-events/press-announcements/fda-approves-novel-gene-therapy-treat-patients-rare-form-inherited-vision-loss>
- Fischer, A. J., & Reh, T. A. (2003). Potential of Müller glia to become neurogenic retinal progenitor cells. *Glia*, 43(1), 70–76. <https://doi.org/10.1002/glia.10218>
- Franze, K., Grosche, J., Skatchkov, S. N., Schinkinger, S., Foja, C., Schild, D., Uckermann, O., Travis, K., Reichenbach, A., & Guck, J. (2007). Müller cells are living optical fibers in the vertebrate retina. *Proceedings of the National Academy of Sciences*, 104(20), 8287–8292. <https://doi.org/10.1073/pnas.0611180104>
- Fritsche, L. G., Fariss, R. N., Stambolian, D., Abecasis, G. R., Curcio, C. A., & Swaroop, A. (2014). Age-Related Macular Degeneration: Genetics and Biology Coming Together. *Annual Review of Genomics and Human Genetics*, 15, 151–171. <https://doi.org/10.1146/annurev-genom-090413-025610>
- Gagliardi, G., Ben M'Barek, K., Chaffiol, A., Slembrouck-Brec, A., Conart, J.-B., Nanteau, C., Rabesandratana, O., Sahel, J.-A., Duebel, J., Orioux, G., Reichman, S., & Goureau, O. (2018). Characterization and Transplantation of CD73-Positive Photoreceptors Isolated from Human iPSC-Derived Retinal Organoids. *Stem Cell Reports*, 11(3), 665–680. <https://doi.org/10.1016/j.stemcr.2018.07.005>
- Gasparini, S. J., Llonch, S., Borsch, O., & Ader, M. (2018). Transplantation of photoreceptors into the degenerative retina: Current state and future perspectives. *Progress in Retinal and Eye Research*. <https://doi.org/10.1016/j.preteyeres.2018.11.001>
- Gasparini, S. J., Tessmer, K., Reh, M., Wieneke, S., Carido, M., Völkner, M., Borsch, O., Swiersy, A., Zuzic, M., Goureau, O., Kurth, T., Buskamp, V., Zeck, G., Karl, M. O., & Ader, M. (2022). Transplanted human cones incorporate into the retina and function in a murine cone degeneration model. *The Journal of Clinical Investigation*, 132(12). <https://doi.org/10.1172/JCI154619>
- Gonzalez-Cordero, A., Kruczek, K., Naeem, A., Fernando, M., Kloc, M., Ribeiro, J., Goh, D., Duran, Y., Blackford, S. J. I., Abelleira-Hervas, L., Sampson, R. D., Shum, I. O., Branch, M. J., Gardner, P. J., Sowden, J. C., Bainbridge, J. W. B., Smith, A. J., West, E. L., Pearson, R. A., & Ali, R. R. (2017). Recapitulation of Human Retinal Development from Human Pluripotent Stem Cells Generates Transplantable Populations of Cone

- Photoreceptors. *Stem Cell Reports*, 9(3), 820–837.
<https://doi.org/10.1016/j.stemcr.2017.07.022>
- Gouras, P., Du, J., Kjeldbye, H., Kwun, R., Lopez, R., & Zack, D. J. (1991). Transplanted photoreceptors identified in dystrophic mouse retina by a transgenic reporter gene. *Investigative Ophthalmology & Visual Science*, 32(13), 3167–3174.
- Grimes, W. N., Songco-Aguas, A., & Rieke, F. (2018). Parallel Processing of Rod and Cone Signals: Retinal Function and Human Perception. *Annual Review of Vision Science*, 4(1), 123–141. <https://doi.org/10.1146/annurev-vision-091517-034055>
- Gurevich, V. V., & Gurevich, E. V. (2014). Overview of Different Mechanisms of Arrestin-Mediated Signaling. *Current Protocols in Pharmacology*, 67(1), 2.10.1-2.10.9. <https://doi.org/10.1002/0471141755.ph0210s67>
- Hanany, M., Rivolta, C., & Sharon, D. (2020). Worldwide carrier frequency and genetic prevalence of autosomal recessive inherited retinal diseases. *Proceedings of the National Academy of Sciences*, 117(5), 2710–2716. <https://doi.org/10.1073/pnas.1913179117>
- Hao, Y., Hao, S., Andersen-Nissen, E., Mauck, W. M., Zheng, S., Butler, A., Lee, M. J., Wilk, A. J., Darby, C., Zager, M., Hoffman, P., Stoeckius, M., Papalexi, E., Mimitou, E. P., Jain, J., Srivastava, A., Stuart, T., Fleming, L. M., Yeung, B., ... Satija, R. (2021). Integrated analysis of multimodal single-cell data. *Cell*, 184(13), 3573-3587.e29. <https://doi.org/10.1016/j.cell.2021.04.048>
- Hartong, D. T., Berson, E. L., & Dryja, T. P. (2006). Retinitis pigmentosa. *The Lancet*, 368(9549), 1795–1809. [https://doi.org/10.1016/S0140-6736\(06\)69740-7](https://doi.org/10.1016/S0140-6736(06)69740-7)
- Heidelberger, R. (2007). Mechanisms of tonic, graded release: Lessons from the vertebrate photoreceptor. *The Journal of Physiology*, 585(Pt 3), 663–667. <https://doi.org/10.1113/jphysiol.2007.137927>
- Heisterkamp, P., Borsch, O., Lezama, N. D., Gasparini, S., Fathima, A., Carvalho, L. S., Wagner, F., Karl, M. O., Schlierf, M., & Ader, M. (2022). Evidence for endogenous exchange of cytoplasmic material between a subset of cone and rod photoreceptors within the adult mammalian retina via direct cell-cell connections. *Experimental Eye Research*, 219, 109033. <https://doi.org/10.1016/j.exer.2022.109033>
- Herbig, M., Tessmer, K., Nötzel, M., Nawaz, A. A., Santos-Ferreira, T., Borsch, O., Gasparini, S. J., Guck, J., & Ader, M. (2022). Label-free imaging flow cytometry for analysis and sorting of enzymatically dissociated tissues. *Scientific Reports*, 12(1), 1–17. <https://doi.org/10.1038/s41598-022-05007-2>
- Higenell, V., & Ruthazer, E. S. (2010). Layers upon Layers: MHC Class I Acts in the Retina to Influence Thalamic Segregation. *Neuron*, 65(4), 439–441. <https://doi.org/10.1016/j.neuron.2010.02.008>
- Holcman, D., & Korenbrot, J. I. (2005). The Limit of Photoreceptor Sensitivity: Molecular Mechanisms of Dark Noise in Retinal Cones. *Journal of General Physiology*, 125(6), 641–660. <https://doi.org/10.1085/jgp.200509277>
- Ingram, N. T., Fain, G. L., & Sampath, A. P. (2020). Elevated energy requirement of cone photoreceptors. *Proceedings of the National Academy of Sciences*, 117(32), 19599–19603. <https://doi.org/10.1073/pnas.2001776117>
- Iraha, S., Tu, H.-Y., Yamasaki, S., Kagawa, T., Goto, M., Takahashi, R., Watanabe, T., Sugita, S., Yonemura, S., Sunagawa, G. A., Matsuyama, T., Fujii, M., Kuwahara, A., Kishino, A., Koide, N., Eiraku, M., Tanihara, H., Takahashi, M., & Mandai, M. (2018). Establishment of Immunodeficient Retinal Degeneration Model Mice and Functional Maturation of Human ESC-Derived Retinal Sheets after Transplantation. *Stem Cell Reports*, 10(3), 1059–1074. <https://doi.org/10.1016/j.stemcr.2018.01.032>

- Izaddoost, S., Nam, S.-C., Bhat, M. A., Bellen, H. J., & Choi, K.-W. (2002). Drosophila Crumbs is a positional cue in photoreceptor adherens junctions and rhabdomeres. *Nature*, *416*(6877), 178–183. <https://doi.org/10.1038/nature720>
- Jacobson, S. G., Cideciyan, A. V., Roman, A. J., Sumaroka, A., Schwartz, S. B., Heon, E., & Hauswirth, W. W. (2015). Improvement and Decline in Vision with Gene Therapy in Childhood Blindness. *New England Journal of Medicine*, *372*(20), 1920–1926. <https://doi.org/10.1056/NEJMoa1412965>
- Jones, B. W., Watt, C. B., Frederick, J. M., Baehr, W., Chen, C.-K., Levine, E. M., Milam, A. H., Lavail, M. M., & Marc, R. E. (2003). Retinal remodeling triggered by photoreceptor degenerations. *Journal of Comparative Neurology*, *464*(1), 1–16. <https://doi.org/10.1002/cne.10703>
- Kalargyrou, A., Basche, M., Hare, A., West, E. L., Smith, A. J., Ali, R. R., & Pearson, R. A. (2021). Nanotube-like processes facilitate material transfer between photoreceptors. *EMBO Reports*, *n/a*(n/a), e53732. <https://doi.org/10.15252/embr.202153732>
- Kaplan, H. J., Tezel, T. H., Berger, A. S., Wolf, M. L., & Del Priore, L. V. (1997). Human Photoreceptor Transplantation in Retinitis Pigmentosa: A Safety Study. *Archives of Ophthalmology*, *115*(9), 1168–1172. <https://doi.org/10.1001/archophth.1997.01100160338012>
- Kevany, B. M., & Palczewski, K. (2010). Phagocytosis of Retinal Rod and Cone Photoreceptors. *Physiology*, *25*(1), 8–15. <https://doi.org/10.1152/physiol.00038.2009>
- Kim, S., Lowe, A., Dharmat, R., Lee, S., Owen, L. A., Wang, J., Shakoob, A., Li, Y., Morgan, D. J., Hejazi, A. A., Cvekl, A., DeAngelis, M. M., Zhou, Z. J., Chen, R., & Liu, W. (2019). Generation, transcriptome profiling, and functional validation of cone-rich human retinal organoids. *Proceedings of the National Academy of Sciences of the United States of America*, *116*(22), 10824–10833. <https://doi.org/10.1073/pnas.1901572116>
- Kostic, C., & Arsenijevic, Y. (2016). Animal modelling for inherited central vision loss. *The Journal of Pathology*, *238*(2), 300–310. <https://doi.org/10.1002/path.4641>
- Kruczek, K., & Swaroop, A. (2020). Pluripotent stem cell-derived retinal organoids for disease modeling and development of therapies. *Stem Cells (Dayton, Ohio)*. <https://doi.org/10.1002/stem.3239>
- Kumar, S., Shah, S., Deutsch, E. R., Tang, H. M., & Danias, J. (2013). Triamcinolone Acetonide Decreases Outflow Facility in C57BL/6 Mouse Eyes. *Investigative Ophthalmology & Visual Science*, *54*(2), 1280–1287. <https://doi.org/10.1167/iovs.12-11223>
- Lakkaraju, A., Umapathy, A., Tan, L. X., Daniele, L., Philp, N. J., Boesze-Battaglia, K., & Williams, D. S. (2020). The cell biology of the retinal pigment epithelium. *Progress in Retinal and Eye Research*, *78*, 100846. <https://doi.org/10.1016/j.preteyeres.2020.100846>
- Lakowski, J., Han, Y.-T., Pearson, R. A., Gonzalez-Cordero, A., West, E. L., Gualdoni, S., Barber, A. C., Hubank, M., Ali, R. R., & Sowden, J. C. (2011). Effective Transplantation of Photoreceptor Precursor Cells Selected via Cell Surface Antigen Expression. *STEM CELLS*, *29*(9), 1391–1404. <https://doi.org/10.1002/stem.694>
- Lakowski, J., Welby, E., Budinger, D., Di Marco, F., Di Foggia, V., Bainbridge, J. W. B., Wallace, K., Gamm, D. M., Ali, R. R., & Sowden, J. C. (2018). Isolation of Human Photoreceptor Precursors via a Cell Surface Marker Panel from Stem Cell-Derived Retinal Organoids and Fetal Retinae: Human Stem Cell-Derived Photoreceptor Purification. *STEM CELLS*, *36*(5), 709–722. <https://doi.org/10.1002/stem.2775>
- Lamb, T. D. (2022). Photoreceptor physiology and evolution: Cellular and molecular basis of rod and cone phototransduction. *The Journal of Physiology*, *n/a*(n/a). <https://doi.org/10.1113/JP282058>

- Lamba, D. A., Gust, J., & Reh, T. A. (2009). Transplantation of Human Embryonic Stem Cell-Derived Photoreceptors Restores Some Visual Function in Crx-Deficient Mice. *Cell Stem Cell*, 4(1), 73–79. <https://doi.org/10.1016/j.stem.2008.10.015>
- Lamba, D. A., Karl, M. O., Ware, C. B., & Reh, T. A. (2006). Efficient generation of retinal progenitor cells from human embryonic stem cells. *Proceedings of the National Academy of Sciences*, 103(34), 12769–12774. <https://doi.org/10.1073/pnas.0601990103>
- Leskov, I. B., Klenchin, V. A., Handy, J. W., Whitlock, G. G., Govardovskii, V. I., Bownds, M. D., Lamb, T. D., Pugh, E. N., & Arshavsky, V. Y. (2000). The Gain of Rod Phototransduction: Reconciliation of Biochemical and Electrophysiological Measurements. *Neuron*, 27(3), 525–537. [https://doi.org/10.1016/S0896-6273\(00\)00063-5](https://doi.org/10.1016/S0896-6273(00)00063-5)
- Lewis, G. P., & Fisher, S. K. (2000). Müller Cell Outgrowth after Retinal Detachment: Association with Cone Photoreceptors. *Investigative Ophthalmology & Visual Science*, 41(6), 1542–1545.
- Liao, Y., Smyth, G. K., & Shi, W. (2014). featureCounts: An efficient general purpose program for assigning sequence reads to genomic features. *Bioinformatics*, 30(7), 923–930. <https://doi.org/10.1093/bioinformatics/btt656>
- Lin, B., McLelland, B. T., Mathur, A., Aramant, R. B., & Seiler, M. J. (2018). Sheets of human retinal progenitor transplants improve vision in rats with severe retinal degeneration. *Experimental Eye Research*, 174, 13–28. <https://doi.org/10.1016/j.exer.2018.05.017>
- Lindqvist, N., Liu, Q., Zajadacz, J., Franze, K., & Reichenbach, A. (2010). Retinal Glial (Müller) Cells: Sensing and Responding to Tissue Stretch. *Investigative Ophthalmology & Visual Science*, 51(3), 1683–1690. <https://doi.org/10.1167/iovs.09-4159>
- Llonch Armengol, S. (2018). *Photoreceptor transplantation into the mammalian retina – new perspectives in donor-host interaction* [Thesis]. Technische Universität Dresden.
- Llonch, S., Carido, M., & Ader, M. (2018). Organoid technology for retinal repair. *Developmental Biology*, 433(2), 132–143. <https://doi.org/10.1016/j.ydbio.2017.09.028>
- Lowe, A., Harris, R., Bhansali, P., Cvekl, A., & Liu, W. (2016). Intercellular Adhesion-Dependent Cell Survival and ROCK-Regulated Actomyosin-Driven Forces Mediate Self-Formation of a Retinal Organoid. *Stem Cell Reports*, 6(5), 743–756. <https://doi.org/10.1016/j.stemcr.2016.03.011>
- Lu, Y., Shiau, F., Yi, W., Lu, S., Wu, Q., Pearson, J. D., Kallman, A., Zhong, S., Hoang, T., Zuo, Z., Zhao, F., Zhang, M., Tsai, N., Zhuo, Y., He, S., Zhang, J., Stein-O'Brien, G. L., Sherman, T. D., Duan, X., ... Clark, B. S. (2020). Single-Cell Analysis of Human Retina Identifies Evolutionarily Conserved and Species-Specific Mechanisms Controlling Development. *Developmental Cell*, 53(4), 473–491.e9. <https://doi.org/10.1016/j.devcel.2020.04.009>
- MacLaren, R. E., Pearson, R. A., MacNeil, A., Douglas, R. H., Salt, T. E., Akimoto, M., Swaroop, A., Sowden, J. C., & Ali, R. R. (2006). Retinal repair by transplantation of photoreceptor precursors. *Nature*, 444(7116), 203–207. <https://doi.org/pear>
- Mahroo, O. a. R., & Lamb, T. D. (2004). Recovery of the human photopic electroretinogram after bleaching exposures: Estimation of pigment regeneration kinetics. *The Journal of Physiology*, 554(2), 417–437. <https://doi.org/10.1113/jphysiol.2003.051250>
- Malhotra, H., Barnes, C. L., & Calvert, P. D. (2021). Functional compartmentalization of photoreceptor neurons. *Pflügers Archiv - European Journal of Physiology*, 473(9), 1493–1516. <https://doi.org/10.1007/s00424-021-02558-7>
- Mao, W., Miyagishima, K. J., Yao, Y., Soreghan, B., Sampath, A. P., & Chen, J. (2013). Functional Comparison of Rod and Cone G_{at} on the Regulation of Light Sensitivity. *The Journal of Biological Chemistry*, 288(8), 5257–5267. <https://doi.org/10.1074/jbc.M112.430058>

- Marc, R. E., Jones, B. W., Watt, C. B., & Strettoi, E. (2003). Neural remodeling in retinal degeneration. *Progress in Retinal and Eye Research*, 22(5), 607–655. [https://doi.org/10.1016/S1350-9462\(03\)00039-9](https://doi.org/10.1016/S1350-9462(03)00039-9)
- Masland, R. H. (2012). The Neuronal Organization of the Retina. *Neuron*, 76(2), 266–280. <https://doi.org/10.1016/j.neuron.2012.10.002>
- Matsuyama, T., Tu, H.-Y., Sun, J., Hashiguchi, T., Akiba, R., Sho, J., Fujii, M., Onishi, A., Takahashi, M., & Mandai, M. (2021). Genetically engineered stem cell-derived retinal grafts for improved retinal reconstruction after transplantation. *iScience*, 24(8), 102866. <https://doi.org/10.1016/j.isci.2021.102866>
- Matthews, G., & Fuchs, P. (2010). The diverse roles of ribbon synapses in sensory neurotransmission. *Nature Reviews Neuroscience*, 11(12), 812–822. <https://doi.org/10.1038/nrn2924>
- McClements, M. E., Staurengi, F., MacLaren, R. E., & Cehajic-Kapetanovic, J. (2020). Optogenetic Gene Therapy for the Degenerate Retina: Recent Advances. *Frontiers in Neuroscience*, 14. <https://www.frontiersin.org/articles/10.3389/fnins.2020.570909>
- McLelland, B. T., Lin, B., Mathur, A., Aramant, R. B., Thomas, B. B., Nistor, G., Keirstead, H. S., & Seiler, M. J. (2018). Transplanted hESC-Derived Retina Organoid Sheets Differentiate, Integrate, and Improve Visual Function in Retinal Degenerate Rats. *Investigative Ophthalmology & Visual Science*, 59(6), 2586. <https://doi.org/10.1167/iovs.17-23646>
- Mehalow, A. K., Kameya, S., Smith, R. S., Hawes, N. L., Denegre, J. M., Young, J. A., Bechtold, L., Haider, N. B., Tepass, U., Heckenlively, J. R., Chang, B., Naggert, J. K., & Nishina, P. M. (2003). CRB1 is essential for external limiting membrane integrity and photoreceptor morphogenesis in the mammalian retina. *Human Molecular Genetics*, 12(17), 2179–2189. <https://doi.org/10.1093/hmg/ddg232>
- Mellough, C. B., Collin, J., Queen, R., Hilgen, G., Dorgau, B., Zerti, D., Felemban, M., White, K., Sernagor, E., & Lako, M. (2019). Systematic Comparison of Retinal Organoid Differentiation from Human Pluripotent Stem Cells Reveals Stage Specific, Cell Line, and Methodological Differences. *STEM CELLS Translational Medicine*, 0(0). <https://doi.org/10.1002/sctm.18-0267>
- Mi, H., Ebert, D., Muruganujan, A., Mills, C., Albu, L.-P., Mushayamaha, T., & Thomas, P. D. (2021). PANTHER version 16: A revised family classification, tree-based classification tool, enhancer regions and extensive API. *Nucleic Acids Research*, 49(D1), D394–D403. <https://doi.org/10.1093/nar/gkaa1106>
- Milam, A. H., Li, Z. Y., & Fariss, R. N. (1998). Histopathology of the human retina in retinitis pigmentosa. *Progress in Retinal and Eye Research*, 17(2), 175–205. [https://doi.org/10.1016/s1350-9462\(97\)00012-8](https://doi.org/10.1016/s1350-9462(97)00012-8)
- Mochizuki, M., Sugita, S., & Kamoi, K. (2013). Immunological homeostasis of the eye. *Progress in Retinal and Eye Research*, 33, 10–27. <https://doi.org/10.1016/j.preteyeres.2012.10.002>
- Molday, R. S., & Moritz, O. L. (2015). Photoreceptors at a glance. *Journal of Cell Science*, 128(22), 4039–4045. <https://doi.org/10.1242/jcs.175687>
- Morizane, A., Kikuchi, T., Hayashi, T., Mizuma, H., Takara, S., Doi, H., Mawatari, A., Glasser, M. F., Shiina, T., Ishigaki, H., Itoh, Y., Okita, K., Yamasaki, E., Doi, D., Onoe, H., Ogasawara, K., Yamanaka, S., & Takahashi, J. (2017). MHC matching improves engraftment of iPSC-derived neurons in non-human primates. *Nature Communications*, 8(1), 385. <https://doi.org/10.1038/s41467-017-00926-5>
- Morshedian, A., Kaylor, J. J., Ng, S. Y., Tsan, A., Frederiksen, R., Xu, T., Yuan, L., Sampath, A. P., Radu, R. A., Fain, G. L., & Travis, G. H. (2019). Light-Driven Regeneration of Cone

- Visual Pigments through a Mechanism Involving RGR Opsin in Müller Glial Cells. *Neuron*, 102(6), 1172–1183.e5. <https://doi.org/10.1016/j.neuron.2019.04.004>
- Mullin, N. K., Voigt, A. P., Cooke, J. A., Bohrer, L. R., Burnight, E. R., Stone, E. M., Mullins, R. F., & Tucker, B. A. (2021). Patient derived stem cells for discovery and validation of novel pathogenic variants in inherited retinal disease. *Progress in Retinal and Eye Research*, 83, 100918. <https://doi.org/10.1016/j.preteyeres.2020.100918>
- Nakano, T., Ando, S., Takata, N., Kawada, M., Muguruma, K., Sekiguchi, K., Saito, K., Yonemura, S., Eiraku, M., & Sasai, Y. (2012). Self-Formation of Optic Cups and Storable Stratified Neural Retina from Human ESCs. *Cell Stem Cell*, 10(6), 771–785. <https://doi.org/10.1016/j.stem.2012.05.009>
- Nelson, B. R., Ueki, Y., Reardon, S., Karl, M. O., Georgi, S., Hartman, B. H., Lamba, D. A., & Reh, T. A. (2011). Genome-Wide Analysis of Müller Glial Differentiation Reveals a Requirement for Notch Signaling in Postmitotic Cells to Maintain the Glial Fate. *PLOS ONE*, 6(8), e22817. <https://doi.org/10.1371/journal.pone.0022817>
- Newman, E., & Reichenbach, A. (1996). The Müller cell: A functional element of the retina. *Trends in Neurosciences*, 19(8), 307–312. [https://doi.org/10.1016/0166-2236\(96\)10040-0](https://doi.org/10.1016/0166-2236(96)10040-0)
- Ohlemacher, S. K., Iglesias, C. L., Sridhar, A., Gamm, D. M., & Meyer, J. S. (2015). Generation of Highly Enriched Populations of Optic Vesicle-Like Retinal Cells from Human Pluripotent Stem Cells. *Current Protocols in Stem Cell Biology*, 32(1), 1H.8.1-1H.8.20. <https://doi.org/10.1002/9780470151808.sc01h08s32>
- Okita, K., Matsumura, Y., Sato, Y., Okada, A., Morizane, A., Okamoto, S., Hong, H., Nakagawa, M., Tanabe, K., Tezuka, K., Shibata, T., Kunisada, T., Takahashi, M., Takahashi, J., Saji, H., & Yamanaka, S. (2011). A more efficient method to generate integration-free human iPS cells. *Nature Methods*, 8(5), 409–412. <https://doi.org/10.1038/nmeth.1591>
- Omri, S., Omri, B., Savoldelli, M., Jonet, L., Thillaye-Goldenberg, B., Thuret, G., Gain, P., Jeanny, J. C., Crisanti, P., & Behar-Cohen, F. (2010). The outer limiting membrane (OLM) revisited: Clinical implications. *Clinical Ophthalmology*, 4, 183–195. <https://doi.org/10.2147/OPHTH.S5901>
- Ortin-Martinez, A., Tsai, E. L. S., Nickerson, P. E., Bergeret, M., Lu, Y., Smiley, S., Comanita, L., & Wallace, V. A. (2017). A Reinterpretation of Cell Transplantation: GFP Transfer From Donor to Host Photoreceptors: GFP Transfer to Recipient Photoreceptors. *STEM CELLS*, 35(4), 932–939. <https://doi.org/10.1002/stem.2552>
- Ortin-Martinez, A., Yan, N., Tsai, E. L. S., Comanita, L., Gurdita, A., Tachibana, N., Liu, Z. C., Lu, S., Dolati, P., Pokrajac, N. T., El-Sehemy, A., Nickerson, P. E. B., Schuurmans, C., Bremner, R., & Wallace, V. A. (2021). Photoreceptor nanotubes mediate the in vivo exchange of intracellular material. *The EMBO Journal*, n/a(n/a), e107264. <https://doi.org/10.15252/embj.2020107264>
- Osakada, F., Ikeda, H., Mandai, M., Wataya, T., Watanabe, K., Yoshimura, N., Akaike, A., Sasai, Y., & Takahashi, M. (2008). Toward the generation of rod and cone photoreceptors from mouse, monkey and human embryonic stem cells. *Nature Biotechnology*, 26(2), 215–224. <https://doi.org/10.1038/nbt1384>
- Ostad-Ahmadi, Z., Daemi, A., Modabberi, M.-R., & Mostafaie, A. (2021). Safety, effectiveness, and cost-effectiveness of Argus II in patients with retinitis pigmentosa: A systematic review. *International Journal of Ophthalmology*, 14(2), 310–316. <https://doi.org/10.18240/ijo.2021.02.20>
- Pearson, R. A., Barber, A. C., Rizzi, M., Hippert, C., Xue, T., West, E. L., Duran, Y., Smith, A. J., Chuang, J. Z., Azam, S. A., Luhmann, U. F. O., Benucci, A., Sung, C. H., Bainbridge, J. W., Carandini, M., Yau, K.-W., Sowden, J. C., & Ali, R. R. (2012). Restoration of vision

- after transplantation of photoreceptors. *Nature*, 485(7396), 99–103. <https://doi.org/10.1038/nature10997>
- Pearson, R. A., Barber, A. C., West, E. L., Maclaren, R. E., Duran, Y., Bainbridge, J. W., Sowden, J. C., & Ali, R. R. (2010). Targeted Disruption of Outer Limiting Membrane Junctional Proteins (Crb1 and ZO-1) Increases Integration of Transplanted Photoreceptor Precursors into the Adult Wild-Type and Degenerating Retina. *Cell Transplantation*, 19(4), 487–503. <https://doi.org/10.3727/096368909X486057>
- Peirson, S. N., Brown, L. A., Pothecary, C. A., Benson, L. A., & Fisk, A. S. (2018). Light and the laboratory mouse. *Journal of Neuroscience Methods*, 300, 26–36. <https://doi.org/10.1016/j.jneumeth.2017.04.007>
- Pelikka, M., Tanentzapf, G., Pinto, M., Smith, C., McGlade, C. J., Ready, D. F., & Tepass, U. (2002). Crumbs, the Drosophila homologue of human CRB1/RP12, is essential for photoreceptor morphogenesis. *Nature*, 416(6877), 143–149. <https://doi.org/10.1038/nature721>
- Petit, L., Ma, S., Cipi, J., Cheng, S.-Y., Zieger, M., Hay, N., & Punzo, C. (2018). Aerobic Glycolysis Is Essential for Normal Rod Function and Controls Secondary Cone Death in Retinitis Pigmentosa. *Cell Reports*, 23(9), 2629–2642. <https://doi.org/10.1016/j.celrep.2018.04.111>
- Radtke, N. D., Aramant, R. B., Petry, H. M., Green, P. T., Pidwell, D. J., & Seiler, M. J. (2008). Vision Improvement in Retinal Degeneration Patients by Implantation of Retina Together with Retinal Pigment Epithelium. *American Journal of Ophthalmology*, 146(2), 172–182.e1. <https://doi.org/10.1016/j.ajo.2008.04.009>
- Radtke, N. D., Aramant, R. B., Seiler, M. J., Petry, H. M., & Pidwell, D. (2004). Vision Change After Sheet Transplant of Fetal Retina With Retinal Pigment Epithelium to a Patient With Retinitis Pigmentosa. *Archives of Ophthalmology*, 122(8), 1159–1165. <https://doi.org/10.1001/archoph.122.8.1159>
- Radtke, N. D., Aramant, R. B., Seiler, M., & Petry, H. M. (1999). Preliminary report: Indications of improved visual function after retinal sheet transplantation in retinitis pigmentosa patients. Norman D. Radtke, MD, Robert B. Aramant, PhD, and Magdalene Seiler, PhD, have a proprietary interest in the instrument and method (patent pending) discussed. *American Journal of Ophthalmology*, 128(3), 384–387. [https://doi.org/10.1016/S0002-9394\(99\)00250-0](https://doi.org/10.1016/S0002-9394(99)00250-0)
- Radtke, N. D., Seiler, M. J., Aramant, R. B., Petry, H. M., & Pidwell, D. J. (2002). Transplantation of intact sheets of fetal neural retina with its retinal pigment epithelium in retinitis pigmentosa patients. *American Journal of Ophthalmology*, 133(4), 544–550. [https://doi.org/10.1016/S0002-9394\(02\)01322-3](https://doi.org/10.1016/S0002-9394(02)01322-3)
- Raudvere, U., Kolberg, L., Kuzmin, I., Arak, T., Adler, P., Peterson, H., & Vilo, J. (2019). g:Profiler: A web server for functional enrichment analysis and conversions of gene lists (2019 update). *Nucleic Acids Research*, 47(W1), W191–W198. <https://doi.org/10.1093/nar/gkz369>
- Reh, M. (2021). *Functional assessment of optogenetics and cell transplantation as strategies for vision restoration* [Dissertation, Tübingen]. <https://publikationen.uni-tuebingen.de/xmlui/handle/10900/126177>
- Reichenbach, A., & Bringmann, A. (2020). Glia of the human retina. *Glia*, 68(4), 768–796. <https://doi.org/10.1002/glia.23727>
- Reingruber, J., Ingram, N. T., Griffis, K. G., & Fain, G. L. (2020). A kinetic analysis of mouse rod and cone photoreceptor responses. *The Journal of Physiology*, 598(17), 3747–3763. <https://doi.org/10.1113/JP279524>

- RetNet: Summaries of Genes and Loci Causing Retinal Diseases*. (2022, June 9). Summaries of Genes and Loci Causing Retinal Diseases. <https://sph.uth.edu/RetNet/sum-dis.htm#A-genes>
- Ribeiro, J., Procyk, C. A., West, E. L., O'Hara-Wright, M., Martins, M. F., Khorasani, M. M., Hare, A., Basche, M., Fernando, M., Goh, D., Jumbo, N., Rizzi, M., Powell, K., Tariq, M., Michaelides, M., Bainbridge, J. W. B., Smith, A. J., Pearson, R. A., Gonzalez-Cordero, A., & Ali, R. R. (2021). Restoration of visual function in advanced disease after transplantation of purified human pluripotent stem cell-derived cone photoreceptors. *Cell Reports*, 35(3), 109022. <https://doi.org/10.1016/j.celrep.2021.109022>
- Ripolles-Garcia, A., Dolgova, N., Phillips, M. J., Savina, S., Ludwig, A. L., Stuedemann, S. A., Nlebedum, U., Wolfe, J. H., Garden, O. A., Maminishkis, A., Amaral, J., Bharti, K., Gamm, D. M., Aguirre, G. D., & Beltran, W. A. (2022). Systemic immunosuppression promotes survival and integration of subretinally implanted human ESC-derived photoreceptor precursors in dogs. *Stem Cell Reports*, 0(0). <https://doi.org/10.1016/j.stemcr.2022.06.009>
- Robertson, C. (1998). *The Wordsworth Dictionary of Quotations*. Wordsworth Editions.
- Rossi, E. A., & Roorda, A. (2010). The relationship between visual resolution and cone spacing in the human fovea. *Nature Neuroscience*, 13(2), 156–157. <https://doi.org/10.1038/nn.2465>
- Saha, A., Capowski, E., Fernandez Zepeda, M. A., Nelson, E. C., Gamm, D. M., & Sinha, R. (2022). Cone photoreceptors in human stem cell-derived retinal organoids demonstrate intrinsic light responses that mimic those of primate fovea. *Cell Stem Cell*. <https://doi.org/10.1016/j.stem.2022.01.002>
- Sahel, J.-A., & Roska, B. (2013). Gene Therapy for Blindness. *Annual Review of Neuroscience*, 36(1), 467–488. <https://doi.org/10.1146/annurev-neuro-062012-170304>
- Santos-Ferreira, T., Herbig, M., Otto, O., Carido, M., Karl, M. O., Michalakis, S., Guck, J., & Ader, M. (2019). Morpho-Rheological Fingerprinting of Rod Photoreceptors Using Real-Time Deformability Cytometry. *Cytometry Part A*, 0(0). <https://doi.org/10.1002/cyto.a.23798>
- Santos-Ferreira, T., Llonch, S., Borsch, O., Postel, K., Haas, J., & Ader, M. (2016). Retinal transplantation of photoreceptors results in donor–host cytoplasmic exchange. *Nature Communications*, 7, 13028. <https://doi.org/10.1038/ncomms13028>
- Santos-Ferreira, T., Völkner, M., Borsch, O., Haas, J., Cimalla, P., Vasudevan, P., Carmeliet, P., Corbeil, D., Michalakis, S., Koch, E., Karl, M. O., & Ader, M. (2016). Stem Cell–Derived Photoreceptor Transplants Differentially Integrate Into Mouse Models of Cone-Rod Dystrophy. *Investigative Ophthalmology & Visual Science*, 57(7), 3509. <https://doi.org/10.1167/iops.16-19087>
- Satija, R., Farrell, J. A., Gennert, D., Schier, A. F., & Regev, A. (2015). Spatial reconstruction of single-cell gene expression data. *Nature Biotechnology*, 33(5), 495–502. <https://doi.org/10.1038/nbt.3192>
- Schindelin, J., Arganda-Carreras, I., Frise, E., Kaynig, V., Longair, M., Pietzsch, T., Preibisch, S., Rueden, C., Saalfeld, S., Schmid, B., Tinevez, J.-Y., White, D. J., Hartenstein, V., Eliceiri, K., Tomancak, P., & Cardona, A. (2012). Fiji: An open-source platform for biological-image analysis. *Nature Methods*, 9(7), 676–682. <https://doi.org/10.1038/nmeth.2019>
- Schlichtenbrede, F. C., Mittmann, W., Rensch, F., Hagen, F. vom, Jonas, J. B., & Euler, T. (2009). Toxicity Assessment of Intravitreal Triamcinolone and Bevacizumab in a Retinal Explant Mouse Model Using Two-Photon Microscopy. *Investigative Ophthalmology & Visual Science*, 50(12), 5880–5887. <https://doi.org/10.1167/iops.08-3078>

- Seiler, M. J., & Aramant, R. B. (1998). Intact sheets of fetal retina transplanted to restore damaged rat retinas. *Investigative Ophthalmology & Visual Science*, 39(11), 2121–2131.
- Sethi, C. S., Lewis, G. P., Fisher, S. K., Leitner, W. P., Mann, D. L., Luthert, P. J., & Charteris, D. G. (2005). Glial Remodeling and Neural Plasticity in Human Retinal Detachment with Proliferative Vitreoretinopathy. *Investigative Ophthalmology & Visual Science*, 46(1), 329–342. <https://doi.org/10.1167/iovs.03-0518>
- Shastry, S. P. (2020). *Cellular Composition of Retinal Organoids During Differentiation from a Photoreceptor-Specific iPSC Reporter Line* [Master's thesis]. TU Dresden.
- Shirai, H., Mandai, M., Matsushita, K., Kuwahara, A., Yonemura, S., Nakano, T., Assawachananont, J., Kimura, T., Saito, K., Terasaki, H., Eiraku, M., Sasai, Y., & Takahashi, M. (2016). Transplantation of human embryonic stem cell-derived retinal tissue in two primate models of retinal degeneration. *Proceedings of the National Academy of Sciences*, 113(1), E81–E90. <https://doi.org/10.1073/pnas.1512590113>
- Silverman, M. S., & Hughes, S. E. (1989). Transplantation of photoreceptors to light-damaged retina. *Investigative Ophthalmology & Visual Science*, 30(8), 1684–1690.
- Singh, M. S., Balmer, J., Barnard, A. R., Aslam, S. A., Moralli, D., Green, C. M., Barnea-Cramer, A., Duncan, I., & MacLaren, R. E. (2016). Transplanted photoreceptor precursors transfer proteins to host photoreceptors by a mechanism of cytoplasmic fusion. *Nature Communications*, 7, 13537. <https://doi.org/10.1038/ncomms13537>
- Singh, M. S., Charbel Issa, P., Butler, R., Martin, C., Lipinski, D. M., Sekaran, S., Barnard, A. R., & MacLaren, R. E. (2013). Reversal of end-stage retinal degeneration and restoration of visual function by photoreceptor transplantation. *Proceedings of the National Academy of Sciences*, 110(3), 1101–1106. <https://doi.org/10.1073/pnas.1119416110>
- Singh, R. K., Winkler, P. A., Binette, F., Petersen-Jones, S. M., & Nasonkin, I. O. (2021). Comparison of Developmental Dynamics in Human Fetal Retina and Human Pluripotent Stem Cell-Derived Retinal Tissue. *Stem Cells and Development*, 30(8), 399–417. <https://doi.org/10.1089/scd.2020.0085>
- Slembrouck-Brec, A., Rodrigues, A., Rabesandratana, O., Gagliardi, G., Nanteau, C., Fouquet, S., Thuret, G., Reichman, S., Orioux, G., & Goureau, O. (2019). Reprogramming of Adult Retinal Müller Glial Cells into Human-Induced Pluripotent Stem Cells as an Efficient Source of Retinal Cells. *Stem Cells International*, 2019, e7858796. <https://doi.org/10.1155/2019/7858796>
- Solovei, I., Kreysing, M., Lanctôt, C., Kösem, S., Peichl, L., Cremer, T., Guck, J., & Joffe, B. (2009). Nuclear Architecture of Rod Photoreceptor Cells Adapts to Vision in Mammalian Evolution. *Cell*, 137(2), 356–368. <https://doi.org/10.1016/j.cell.2009.01.052>
- Soucy, E., Wang, Y., Nirenberg, S., Nathans, J., & Meister, M. (1998). A Novel Signaling Pathway from Rod Photoreceptors to Ganglion Cells in Mammalian Retina. *Neuron*, 21(3), 481–493. [https://doi.org/10.1016/S0896-6273\(00\)80560-7](https://doi.org/10.1016/S0896-6273(00)80560-7)
- Stone, N. E., Voigt, A. P., Cooke, J. A., Giacalone, J. C., Hanasoge, S., Mullins, R. F., Tucker, B. A., & Sulchek, T. (2020). Label-free microfluidic enrichment of photoreceptor cells. *Experimental Eye Research*, 199, 108166. <https://doi.org/10.1016/j.exer.2020.108166>
- Stuart, T., Butler, A., Hoffman, P., Hafemeister, C., Papalexi, E., Mauck, W. M., Hao, Y., Stoekius, M., Smibert, P., & Satija, R. (2019). Comprehensive Integration of Single-Cell Data. *Cell*, 177(7), 1888–1902.e21. <https://doi.org/10.1016/j.cell.2019.05.031>
- Sugita, S., Mandai, M., Hirami, Y., Takagi, S., Maeda, T., Fujihara, M., Matsuzaki, M., Yamamoto, M., Iseki, K., Hayashi, N., Hono, A., Fujino, S., Koide, N., Sakai, N., Shibata, Y., Terada, M., Nishida, M., Dohi, H., Nomura, M., ... Takahashi, M. (2020). HLA-Matched Allogeneic iPSC Cells-Derived RPE Transplantation for Macular Degeneration. *Journal of Clinical Medicine*, 9(7), 2217. <https://doi.org/10.3390/jcm9072217>

- Szécsi, L., Kacsó, Á., Zeck, G., & Hantz, P. (2017). Interactive Light Stimulus Generation with High Performance Real-Time Image Processing and Simple Scripting. *Frontiers in Neuroinformatics*, *11*. <https://www.frontiersin.org/articles/10.3389/fninf.2017.00070>
- Takahashi, K., Tanabe, K., Ohnuki, M., Narita, M., Ichisaka, T., Tomoda, K., & Yamanaka, S. (2007). Induction of Pluripotent Stem Cells from Adult Human Fibroblasts by Defined Factors. *Cell*, *131*(5), 861–872. <https://doi.org/10.1016/j.cell.2007.11.019>
- Tessmer, K., Borsch, O., Ader, M., & Gasparini, S. J. (2022). Micromanipulator-Assisted Subretinal Transplantation of Human Photoreceptor Reporter Cell Suspensions into Mice. In *Brain Organoid Research* (Vol. 189). SPRINGER NATURE.
- Thomson, J. A., Itskovitz-Eldor, J., Shapiro, S. S., Waknitz, M. A., Swiergiel, J. J., Marshall, V. S., & Jones, J. M. (1998). Embryonic Stem Cell Lines Derived from Human Blastocysts. *Science*, *282*(5391), 1145–1147. <https://doi.org/10.1126/science.282.5391.1145>
- Tsin, A., Betts-Obregon, B., & Grigsby, J. (2018). Visual cycle proteins: Structure, function, and roles in human retinal disease. *Journal of Biological Chemistry*, *293*(34), 13016–13021. <https://doi.org/10.1074/jbc.AW118.003228>
- Tsukamoto, Y., & Omi, N. (2014). Some OFF bipolar cell types make contact with both rods and cones in macaque and mouse retinas. *Frontiers in Neuroanatomy*, *8*. <https://www.frontiersin.org/articles/10.3389/fnana.2014.00105>
- Tu, H.-Y., Watanabe, T., Shirai, H., Yamasaki, S., Kinoshita, M., Matsushita, K., Hashiguchi, T., Onoe, H., Matsuyama, T., Kuwahara, A., Kishino, A., Kimura, T., Eiraku, M., Suzuma, K., Kitaoka, T., Takahashi, M., & Mandai, M. (2018). Medium- to long-term survival and functional examination of human iPSC-derived retinas in rat and primate models of retinal degeneration. *EBioMedicine*. <https://doi.org/10.1016/j.ebiom.2018.11.028>
- Tucker, B. A., Mullins, R. F., Streb, L. M., Anfinson, K., Eyestone, M. E., Kaalberg, E., Riker, M. J., Drack, A. V., Braun, T. A., & Stone, E. M. (2013). Patient-specific iPSC-derived photoreceptor precursor cells as a means to investigate retinitis pigmentosa. *ELife*, *2*, e00824. <https://doi.org/10.7554/eLife.00824>
- Van Gelder, R. N., Chiang, M. F., Dyer, M. A., Greenwell, T. N., Levin, L. A., Wong, R. O., & Svendsen, C. N. (2022). Regenerative and restorative medicine for eye disease. *Nature Medicine*, *28*(6), 1149–1156. <https://doi.org/10.1038/s41591-022-01862-8>
- van Wyk, M., Schneider, S., & Kleinlogel, S. (2015). Variable phenotypic expressivity in inbred retinal degeneration mouse lines: A comparative study of C3H/HeOu and FVB/N rd1 mice. *Molecular Vision*, *21*, 811–827.
- Vecino, E., Rodriguez, F. D., Ruzafa, N., Pereiro, X., & Sharma, S. C. (2016). Glia–neuron interactions in the mammalian retina. *Progress in Retinal and Eye Research*, *51*, 1–40. <https://doi.org/10.1016/j.preteyeres.2015.06.003>
- Veleri, S., Lazar, C. H., Chang, B., Sieving, P. A., Banin, E., & Swaroop, A. (2015). Biology and therapy of inherited retinal degenerative disease: Insights from mouse models. *Disease Models & Mechanisms*, *8*(2), 109–129. <https://doi.org/10.1242/dmm.017913>
- Venable, J. H., & Coggeshall, R. (1965). A simplified lead citrate stain for use in electron microscopy. *The Journal of Cell Biology*, *25*, 407–408. <https://doi.org/10.1083/jcb.25.2.407>
- Vlasits, A. L., Euler, T., & Franke, K. (2019). Function first: Classifying cell types and circuits of the retina. *Current Opinion in Neurobiology*, *56*, 8–15. <https://doi.org/10.1016/j.conb.2018.10.011>
- Voigt, A. P., Whitmore, S. S., Flamme-Wiese, M. J., Riker, M. J., Wiley, L. A., Tucker, B. A., Stone, E. M., Mullins, R. F., & Scheetz, T. E. (2019). Molecular characterization of foveal versus peripheral human retina by single-cell RNA sequencing. *Experimental Eye Research*, *184*, 234–242. <https://doi.org/10.1016/j.exer.2019.05.001>

- Völkner, M., Kurth, T., & Karl, M. O. (2019). The Mouse Retinal Organoid Trisection Recipe: Efficient Generation of 3D Retinal Tissue from Mouse Embryonic Stem Cells. In B. H. F. Weber & T. Langmann (Eds.), *Retinal Degeneration: Methods and Protocols* (pp. 119–141). Springer. https://doi.org/10.1007/978-1-4939-8669-9_9
- Völkner, M., Kurth, T., Schor, J., Ebner, L. J. A., Bardtke, L., Kavak, C., Hackermüller, J., & Karl, M. O. (2021). Mouse Retinal Organoid Growth and Maintenance in Longer-Term Culture. *Frontiers in Cell and Developmental Biology*, 9. <https://www.frontiersin.org/articles/10.3389/fcell.2021.645704>
- Waldron, P. V., Di Marco, F., Kruczek, K., Ribeiro, J., Graca, A. B., Hippert, C., Aghaizu, N. D., Kalargyrou, A. A., Barber, A. C., Grimaldi, G., Duran, Y., Blackford, S. J. I., Kloc, M., Goh, D., Zabala Aldunate, E., Sampson, R. D., Bainbridge, J. W. B., Smith, A. J., Gonzalez-Cordero, A., ... Pearson, R. A. (2018). Transplanted Donor- or Stem Cell-Derived Cone Photoreceptors Can Both Integrate and Undergo Material Transfer in an Environment-Dependent Manner. *Stem Cell Reports*, 10(2), 406–421. <https://doi.org/10.1016/j.stemcr.2017.12.008>
- Wang, J.-S., & Kefalov, V. J. (2009). An Alternative Pathway Mediates the Mouse and Human Cone Visual Cycle. *Current Biology*, 19(19), 1665–1669. <https://doi.org/10.1016/j.cub.2009.07.054>
- Wang, Y., Wang, V. M., & Chan, C.-C. (2011). The role of anti-inflammatory agents in age-related macular degeneration (AMD) treatment. *Eye*, 25(2), 127–139. <https://doi.org/10.1038/eye.2010.196>
- Wässle, H., Haverkamp, S., Grünert, U., & Morgans, C. W. (2003). The Cone Pedicle, the First Synapse in the Retina. In A. Kaneko (Ed.), *The Neural Basis of Early Vision* (pp. 19–38). Springer Japan. https://doi.org/10.1007/978-4-431-68447-3_6
- Wässle, H., Puller, C., Müller, F., & Haverkamp, S. (2009). Cone Contacts, Mosaics, and Territories of Bipolar Cells in the Mouse Retina. *Journal of Neuroscience*, 29(1), 106–117. <https://doi.org/10.1523/JNEUROSCI.4442-08.2009>
- Watari, K., Yamasaki, S., Tu, H.-Y., Shikamura, M., Kamei, T., Adachi, H., Tochitani, T., Kita, Y., Nakamura, A., Ueyama, K., Ono, K., Morinaga, C., Matsuyama, T., Sho, J., Nakamura, M., Fujiwara, M., Hori, Y., Tanabe, A., Hirai, R., ... Kuwahara, A. (2022). Self-organization, quality control, and preclinical studies of human iPSC-derived retinal sheets for tissue-transplantation therapy. In *BioRxiv* (p. 2022.02.18.480968). <https://doi.org/10.1101/2022.02.18.480968>
- Welby, E., Lakowski, J., Di Foggia, V., Budinger, D., Gonzalez-Cordero, A., Lun, A. T. L., Epstein, M., Patel, A., Cuevas, E., Kruczek, K., Naeem, A., Minneci, F., Hubank, M., Jones, D. T., Marioni, J. C., Ali, R. R., & Sowden, J. C. (2017). Isolation and Comparative Transcriptome Analysis of Human Fetal and iPSC-Derived Cone Photoreceptor Cells. *Stem Cell Reports*, 9(6), 1898–1915. <https://doi.org/10.1016/j.stemcr.2017.10.018>
- Wensel, T. G., Potter, V. L., Moye, A., Zhang, Z., & Robichaux, M. A. (2021). Structure and dynamics of photoreceptor sensory cilia. *Pflügers Archiv - European Journal of Physiology*, 473(9), 1517–1537. <https://doi.org/10.1007/s00424-021-02564-9>
- Wert, K. J., Lin, J. H., & Tsang, S. H. (2014). General Pathophysiology in Retinal Degeneration. *Cell-Based Therapy for Retinal Degenerative Disease*, 53, 33–43. <https://doi.org/10.1159/000357294>
- West, E. L., Majumder, P., Naeem, A., Fernando, M., O'Hara-Wright, M., Lanning, E., Kloc, M., Ribeiro, J., Ovando-Roche, P., Shum, I. O., Jumbu, N., Sampson, R., Hayes, M., Bainbridge, J. W. B., Georgiadis, A., Smith, A. J., Gonzalez-Cordero, A., & Ali, R. R. (2022). Antioxidant and lipid supplementation improve the development of photoreceptor outer segments in pluripotent stem cell-derived retinal organoids. *Stem Cell Reports*. <https://doi.org/10.1016/j.stemcr.2022.02.019>

- Wikler, K. c., Rakic, P., Bhattacharyya, N., & Macleish, P. r. (1997). Early emergence of photoreceptor mosaicism in the primate retina revealed by a novel cone-specific monoclonal antibody. *Journal of Comparative Neurology*, 377(4), 500–508. [https://doi.org/10.1002/\(SICI\)1096-9861\(19970127\)377:4<500::AID-CNE2>3.0.CO;2-6](https://doi.org/10.1002/(SICI)1096-9861(19970127)377:4<500::AID-CNE2>3.0.CO;2-6)
- Wiley, L. A., Burnight, E. R., DeLuca, A. P., Anfinson, K. R., Cranston, C. M., Kaalberg, E. E., Penticoff, J. A., Affatigato, L. M., Mullins, R. F., Stone, E. M., & Tucker, B. A. (2016). CGMP production of patient-specific iPSCs and photoreceptor precursor cells to treat retinal degenerative blindness. *Scientific Reports*, 6, 30742. <https://doi.org/10.1038/srep30742>
- Willenborg, S., Roscito, J. G., Gerbault, A., Roers, A., Dahl, A., Eming, S. A., & Reinhardt, S. (2022). Isolation of macrophages from mouse skin wounds for single-cell RNA sequencing. *STAR Protocols*, 3(2), 101337. <https://doi.org/10.1016/j.xpro.2022.101337>
- World Health Organization. (2019). *World report on vision*. World Health Organization. <https://apps.who.int/iris/handle/10665/328717>
- Wu, T. D., & Nacu, S. (2010). Fast and SNP-tolerant detection of complex variants and splicing in short reads. *Bioinformatics*, 26(7), 873–881. <https://doi.org/10.1093/bioinformatics/btq057>
- Wyk, M. V., Wässle, H., & Taylor, W. R. (2009). Receptive field properties of ON- and OFF-ganglion cells in the mouse retina. *Visual Neuroscience*, 26(3), 297–308. <https://doi.org/10.1017/S0952523809990137>
- Yamasaki, S., Sugita, S., Horiuchi, M., Masuda, T., Fujii, S., Makabe, K., Kawasaki, A., Hayashi, T., Kuwahara, A., Kishino, A., Kimura, T., Takahashi, M., & Mandai, M. (2021). Low Immunogenicity and Immunosuppressive Properties of Human ESC- and iPSC-Derived Retinas. *Stem Cell Reports*, 16(4), 851–867. <https://doi.org/10.1016/j.stemcr.2021.02.021>
- Yamasaki, S., Tu, H.-Y., Matsuyama, T., Horiuchi, M., Hashiguchi, T., Sho, J., Kuwahara, A., Kishino, A., Kimura, T., Takahashi, M., & Mandai, M. (2022). A Genetic modification that reduces ON-bipolar cells in hESC-derived retinas enhances functional integration after transplantation. *iScience*, 25(1), 103657. <https://doi.org/10.1016/j.isci.2021.103657>
- Yan, W., Peng, Y.-R., van Zyl, T., Regev, A., Shekhar, K., Juric, D., & Sanes, J. R. (2020). Cell Atlas of The Human Fovea and Peripheral Retina. *Scientific Reports*, 10(1), 9802. <https://doi.org/10.1038/s41598-020-66092-9>
- Young, M. J., Ray, J., Whiteley, S. J. O., Klassen, H., & Gage, F. H. (2000). Neuronal Differentiation and Morphological Integration of Hippocampal Progenitor Cells Transplanted to the Retina of Immature and Mature Dystrophic Rats. *Molecular and Cellular Neuroscience*, 16(3), 197–205. <https://doi.org/10.1006/mcne.2000.0869>
- Zentgraf, J., & Rahmann, S. (2021). Fast lightweight accurate xenograft sorting. *Algorithms for Molecular Biology*, 16(1), 2. <https://doi.org/10.1186/s13015-021-00181-w>
- Zerti, D., Dorgau, B., Felemban, M., Ghareeb, A. E., Yu, M., Ding, Y., Krasnogor, N., & Lako, M. (2020). Developing a simple method to enhance the generation of cone and rod photoreceptors in pluripotent stem cell-derived retinal organoids. *STEM CELLS*, 38(1), 45–51. <https://doi.org/10.1002/stem.3082>
- Zerti, D., Hilgen, G., Dorgau, B., Collin, J., Ader, M., Armstrong, L., Sernagor, E., & Lako, M. (2021). Transplanted pluripotent stem cell-derived photoreceptor precursors elicit conventional and unusual light responses in mice with advanced retinal degeneration. *STEM CELLS*, n/a(n/a). <https://doi.org/10.1002/stem.3365>
- Zhong, X., Gutierrez, C., Xue, T., Hampton, C., Vergara, M. N., Cao, L.-H., Peters, A., Park, T. S., Zambidis, E. T., Meyer, J. S., Gamm, D. M., Yau, K.-W., & Canto-Soler, M. V. (2014).

- Generation of three-dimensional retinal tissue with functional photoreceptors from human iPSCs. *Nature Communications*, 5, 4047. <https://doi.org/10.1038/ncomms5047>
- Zhu, J., Cifuentes, H., Reynolds, J., & Lamba, D. A. (2017). Immunosuppression via Loss of IL2 γ Enhances Long-Term Functional Integration of hESC-Derived Photoreceptors in the Mouse Retina. *Cell Stem Cell*, 20(3), 374-384.e5. <https://doi.org/10.1016/j.stem.2016.11.019>
- Zhu, Y., Carido, M., Meinhardt, A., Kurth, T., Karl, M. O., Ader, M., & Tanaka, E. M. (2013). Three-Dimensional Neuroepithelial Culture from Human Embryonic Stem Cells and Its Use for Quantitative Conversion to Retinal Pigment Epithelium. *PLOS ONE*, 8(1), e54552. <https://doi.org/10.1371/journal.pone.0054552>
- Zweifel, S. A., Engelbert, M., Laud, K., Margolis, R., Spaide, R. F., & Freund, K. B. (2009). Outer Retinal Tubulation: A Novel Optical Coherence Tomography Finding. *Archives of Ophthalmology*, 127(12), 1596–1602. <https://doi.org/10.1001/archophthalmol.2009.326>

10 Appendix

10.1 Appendix 1: Erklärungen zur Eröffnung des Promotionsverfahrens

Erklärungen zur Eröffnung des Promotionsverfahrens

Technische Universität Dresden

Medizinische Fakultät Carl Gustav Carus

1. Hiermit versichere ich, dass ich die vorliegende Arbeit ohne unzulässige Hilfe Dritter und ohne Benutzung anderer als der angegebenen Hilfsmittel angefertigt habe; die aus fremden Quellen direkt oder indirekt übernommenen Gedanken sind als solche kenntlich gemacht.

2. Bei der Auswahl und Auswertung des Materials sowie bei der Erstellung des Manuskripts habe ich Unterstützungsleistungen von folgenden Personen erhalten:

3. Weitere Personen waren an der geistigen Herstellung der vorliegenden Arbeit nicht beteiligt. Insbesondere habe ich nicht die Hilfe eines kommerziellen Promotionsberaters bzw. einer kommerziellen Promotionsberaterin in Anspruch genommen. Dritte haben von mir weder unmittelbar noch mittelbar geldwerte Leistungen für Arbeiten erhalten, die im Zusammenhang mit dem Inhalt der vorgelegten Dissertation stehen.

4. Die Arbeit wurde bisher weder im Inland noch im Ausland in gleicher oder ähnlicher Form einer anderen Prüfungsbehörde vorgelegt.

5. Die Inhalte dieser Dissertation wurden in folgender Form veröffentlicht:

Gasparini*, S. J., Tessmer*, K., et al. (2022). Transplanted human cones incorporate into the retina and function in a murine cone degeneration model. *The Journal of Clinical Investigation*, 132(12). <https://doi.org/10.1172/JCI1154619>

6. Ich bestätige, dass es keine zurückliegenden erfolglosen Promotionsverfahren gab.

7. Ich bestätige, dass ich die Promotionsordnung der Medizinischen Fakultät der Technischen Universität Dresden anerkenne.

8. Ich habe die Zitierrichtlinien für Dissertationen an der Medizinischen Fakultät der Technischen Universität Dresden zur Kenntnis genommen und befolgt.

9. Ich bin mit den an der Technischen Universität Dresden geltenden „Richtlinien zur Sicherung guter wissenschaftlicher Praxis, zur Vermeidung wissenschaftlichen Fehlverhaltens und für den Umgang mit Verstößen“ einverstanden.

Ort, Datum

Unterschrift der Promovierenden

10.2 Appendix 2: Bestätigung über Einhaltung der aktuellen gesetzlichen Vorgaben

Hiermit bestätige ich die Einhaltung der folgenden aktuellen gesetzlichen Vorgaben im Rahmen meiner Dissertation:

- das zustimmende Votum der Ethikkommission bei Klinischen Studien, epidemiologischen Untersuchungen mit Personenbezug oder Sachverhalten, die das Medizinproduktegesetz betreffen
Aktenzeichen der zuständigen Ethikkommission: _____
- die Einhaltung der Bestimmungen des Tierschutzgesetzes
Aktenzeichen der Genehmigungsbehörde: _____
- die Einhaltung des Gentechnikgesetzes
Projektnummer: _____
- die Einhaltung von Datenschutzbestimmungen der Medizinischen Fakultät Carl Gustav Carus und des Universitätsklinikums Carl Gustav Carus.

Ort, Datum

Unterschrift der Promovierenden